FROM THE END TO THE MIDDLE: REGULATION OF TELOMERE LENGTH AND KINETOCHORE ASSEMBLY BY THE RNR INHIBITOR SML1

Amitabha Gupta

Submitted in partial fulfillment of the
requirements for the degree of
Doctor of Philosophy
in the Graduate School of Arts and Sciences

COLUMBIA UNIVERSITY
2012

ABSTRACT

FROM THE END TO THE MIDDLE: REGULATION OF TELOMERE LENGTH AND KINETOCHORE ASSEMBLY BY THE RNR INHIBITOR SML1

Amitabha Gupta

Accurate DNA replication is essential for proper cellular growth and requires an adequate and balanced supply of dNTPs. In *Saccharomyces cerevisiae*, *de novo* dNTP synthesis through nucleotide reduction by the Ribonucleotide reductase (RNR) enzyme is the sole method of production. Hence, RNR activitity is highly regulated via allosteric control, transcriptional control, differential localization of subunits, and direct inhibition of the large subunit, Rnr1, by Sml1. Loss of RNR regulation results in increased mutation due to an imbalance or an absolute change in the dNTP levels in cells. In this study, I describe how mutants in dNTP regulation, including *sml1*Δ, play a role in telomere length homeostasis. Reduction in total dNTP concentration results in a modest decrease in telomere length, while altering the ratios between the four dNTPs has a much more pronounced effect. The altered telomere lengths correlate with the relative amount of dGTP and are dependent on telomerase. At reduced levels of relative dGTP, telomerase repeatedly stalls and dissociates from telomeres, thereby leading to shorter telomeres. Conversely, with elevated relative dGTP levels, telomerase is able to processively add nucleotides and even shows low levels of repeat addition processivity. The correlation between telomerase activity and dGTP is conserved in human telomerase, which shows increased repeat addition processivity at increased dGTP concentrations. Thus, telomere

length homeostasis is also sensitive to dNTP regulation in the cell via a conserved dependence on dGTP.

RNR regulation is, however, relaxed in the cell following DNA damage to allow for an increase in dNTP levels to repair the damage. In response to various forms of damage, Rad53 and Dun1 are activated and then phosphorylate numerous downstream targets, including the Rnr1 inhibitor Sml1. In this study, it was shown that the phosphorylation of Sml1 triggers its ubiquitylation by the Rad6-Ubr2-Mub1 ubiquitin ligase complex and subsequent degradation by the 26S proteasome. Furthermore, I was able to identify novel genes involved in the degradation of Sml1. Of the genes identified, many are involved in the spindle assembly checkpoint (SAC), cohesin establishment, and kinetochore integrity. The loss of *SML1* in mutants of these genes resulted in synthetic growth defects that were not due to the loss of dNTP regulation, indicating a second dNTP-independent function for Sml1. Analysis of the double mutants revealed elevated chromosome loss and aberrant spindle dynamics, pointing to a role for Sml1 in the spindle/kinetochore. Through analysis of kinetochore assembly kinetics, Sml1 was found to be the functional human Mis18α ortholog involved in timely establishment of the kinetochore. Thus, Sml1 has a novel structural function at the kinetochore in addition to its role in dNTP regulation.

TABLE OF CONTENTS

LIST OF FIGURES

CHAPTER 1

CHAPTER 2

CHAPTER 3

CHAPTER 4

LIST OF TABLES

CHAPTER 2

CHAPTER 3

LIST OF ABBREVIATIONS

dNTP	Deoxynucleotide triphosphate
dA/T/G/CTP	Deoxyadenosine/thymidine/guanosine/cytidine triphosphate
NDP	Nucleoside diphosphate
A/U/G/CDP	Adenosine/Uridine/Guanosine/Cytidine diphosphate
dN/CDP	Deoxynucleoside/Deoxycytidine diphosphate
ATP	Adenosine triphosphate
RNR	Ribonucleotide reductase
MBF	Mlu1-box binding factor
HMG	High-mobility group
TFIID	Transcription factor II D
SWI/SNF	Switch/Sucrose nonfermentable
DDR	DNA damage response
DSB	Double-strand break
MRX	Mre11-Rad50-Xrs2 complex
ssDNA	Single-stranded DNA
RPA	Replication protein A
9-1-1	Rad9-Hus1-Rad1 (humans)/ Ddc1-Rad17-Mec3 (yeast)
ATM	Ataxia telangiectasia, mutated
ATR	ATM and Rad3-related
PCNA	Proliferating cell nuclear antigen
RFC	Replication factor C
SAC	Spindle assembly checkpoint
APC/C	Anaphase promoting complex/cyclosome
SPB	Spindle pole body
HU	Hydroxyurea
KMN	KNL-1/Mis12 complex/Ndc80 complex
DAM/DASH	Dam1-Dad1-Dad2-Dad3-Dad4-Duo1-Ask1-Spc19-Spc34-Hsk3 complex
COMA	Ctf19-Okp1-Mcm21-Ame1 complex
WT	wild-type

ACKNOWLEDGEMENTS

First, I must thank my advisor, Rodney Rothstein, for accepting me into his laboratory. His patience and support over the course of my studies have allowed me to find my feet and develop my own way of doing science. That development has also been shaped by Rodney's insistence on accuracy over speed as well as his desire to keep things simple and understandable. These traits, allied with his uncontrollable enthusiasm for science, are things that I hope to carry with me going forward.

Thanks also to my thesis committee members: Fred Chang, for chairing my numerous thesis committee members and always insisting on asking the simplest next question; Jean Gautier, for pushing me to think beyond yeast and look at the broader picture; Lorraine Symington, for assisting me every step of the way from my qualifying exam through to the end and pointing me to the right papers thanks to your encyclopaedic knowledge of all things DNA; and Xiaolan Zhao, for showing a constant interest in Sml1 and suggesting experiments – your presence on this committee brings the project full circle and means a lot to me.

Additional thanks must also go to my previous mentors in science who encouraged my development. KJ Myung mentored me in my first project and gave me a start in yeast biology for which I am grateful. My undergrad advisor, Ken Belanger, was a great influence and his example is something that I continue to aspire to. Additionally, Patricia Jue and Julie Chanatry in the Chemistry department at Colgate University made being in lab a joy and helped me realize my love for all manner of science.

I would also like to thank all members of the Rothstein lab, past and present. I could not imagine working with a better, smarter group of people who are as motivated to do good science as they are to enjoy themselves while doing so. Special thanks must go to Michael Chang who helped me learn how to construct a paper. Additional thanks to Kara Bernstein, Peter Thorpe, John Dittmar, and Sake van Wageningen for reviewing my thesis and providing helpful suggestions.

To Nii Noi, 'The 7', Jen and Steve, you have all been instrumental in helping me through. While many of you are in far-flung places and we rarely see each other, you still provide the laughter and memories that keep things in perspective. To my friends at Columbia – Danny, Nsikan, Ian, Joe, Katie, Sabrina – it has been great to have friends such as you and I cherish the poker games and brunches at Coogans where we all acted like the children we really are at heart.

To my family - my mother, father, brother, and cousins – thank you for all your support over the years. Having the constant backing and encouragement I have had over the years has really helped. Thanks for being friends in addition to family.

And finally, I must thank my wife and anchor, Ashley Nagle. The extreme stability and joy you have provided over the years cannot be overstated. Thank you also for keeping me on an even keel – bringing me down a notch or two when I get too full of myself and raising me up when I get too down. This whole process would have been well nigh impossible with you so, THANKS!

CHAPTER 1:

INTRODUCTION

OVERVIEW

DNA is the essential component of all life and thus the accurate replication and segregation of DNA is required for propagation of a species. In order to allow for this, the cell utilizes numerous specialized checkpoints to monitor the fidelity of the DNA (Paulovich et al., 1997). These checkpoints ensure that the DNA is accurately replicated (DNA replication checkpoint) and properly aligned at the time of division to allow the correct number of chromosomes to be segregated into both the mother and daughter cells (spindle assembly checkpoint). Inability of the cell to replicate the DNA or construct specialized structures (kinetochores) that allow microtubules to connect to chromosomes triggers these two checkpoint responses. Furthermore, the DNA of all organisms is under constant assault from various exogenous and endogenous factors that need to be repaired before the DNA can be segregated necessitating a third checkpoint (DNA damage checkpoint/response). Interestingly, the DNA damage checkpoint is also activated in the absence of a break when specialized structures that protect the ends of the chromosomes (telomeres) are exposed. The damage checkpoint is able to cross-talk with both the replication and spindle checkpoint to arrest the cells thereby allowing the DNA to be repaired without the cell progressing through the cell cycle. Failure to arrest the cell and repair DNA results in a variety of chromosomal defects including aneuploidy. Therefore, the timely and accurate activation of checkpoints is essential to survival of a cell. However, equally important is the prevention of activation of the checkpoints by the proper functioning of the different cellular processes such as dNTP regulation, telomere length maintenance and protection, as well as timely kinetochore assembly.

dNTP REGULATION IN THE CELL

The accurate replication of DNA is essential for propagation of a species, thereby necessitating the proper production and regulation of the building blocks - deoxynucleotide triphosphates (dNTPs). The regulation of these molecules has been extensively studied in multiple organisms, and while the mechanisms are divergent, the requirement for balanced dNTP pools is conserved.

Importance of dNTP pool size and ratios

During the course of the cell cycle, there is an inherent fluctuation in the levels of dNTPs, particularly with an increase seen during S-phase to accommodate the increased need during DNA replication (Chabes et al., 2003a; Hakansson et al., 2006). However, an unchecked increase in dNTP pools can lead to a concomitant increase in the mutation rates seen in the cell (Chabes et al., 2003a; Reichard, 1988). Furthermore, in cells with constitutively high dNTP pools, both cell cycle progression and checkpoint activation are inhibited (Chabes and Stillman, 2007). In fact, an increase in mutation rates caused by defects in replication or repair can also lead to a significant increase in dNTP pool sizes, which in turn leads to further mutation (Davidson et al., 2012). This vicious circle of mutagenesis is an extreme example but successfully highlights the need for tight regulation of the dNTP levels in the cell.

While absolute levels of dNTPs are important, recent studies have begun to highlight a similar need to maintain a proper balance between the dNTPs. Both yeast and mammalian cells exhibit a similar ratio of the four dNTPs – dATP, dTTP, dCTP, and dGTP – with dTTP being the most abundant and dGTP being the least (Nick McElhinny

et al., 2010b; Sabouri et al., 2008; Traut, 1994). However, this ratio can be unbalanced, leading to an increase in mutagenesis. The spectrum of mutagenesis is directly related to which dNTP is increased relative to the others (Kumar et al., 2011). Furthermore, an imbalance can trigger the replication checkpoint if any of the four dNTPs are reduced below physiological levels (Kumar et al., 2010).

Production of dNTPs by ribonucleotide reduction

dNTP pools in cells are produced by slightly different mechanisms in mammalian cells and in yeast. Mammalian cells primarily obtain dNTPs by *de novo* dNTP synthesis. However, they are also able to obtain dNTPs by utilizing four different kinases - thymidine kinase 1 and 2, deoxyguanosine kinase, and deoxycytidine kinase - to salvage deodyribonucleosides (Sandrini and Piskur, 2005). Yeast, on the other hand, can only produce dNTPs by *de novo* dNTP synthesis, and this process is conserved with the one seen in mammals. ADP, GDP, and CDP are reduced to their respective deoxy forms, which are then converted to dATP, dGTP, and dCTP. dTTP is obtained by the further processing of the dCDP product (Reichard, 1988; Toussaint et al., 2005) (Figure 1-1). The reduction of the NDPs to their respective dNDPs is the rate-limiting step in this process and is performed by the holoenzyme, ribonucleotide reductase (RNR) (Reichard, 1988).

Both yeast and human RNR is comprised of a large catalytic subunit, R1, and a small subunit, R2, which supplies both the tyrosyl radical and the cysteinyl group for the reduction reaction. The R1 and R2 are in an $\alpha_2\beta_2$ configuration; i.e., both R1 and R2 are dimers. In humans there is one R1 protein and two small R2 subunit proteins, R2 and

p53R2. p53R2 is 80-90% identical to R2, but lacks 33 amino-terminal residues, including a KEN box domain that is important for degradation during mitosis (Chabes et al., 2003b). While R1 and R2 levels are increased in the cell upon entry into S-phase or upon treatment with DNA damage, p53R2 levels are only increased following damage (Hakansson et al., 2006). Indeed, p53R2 was first identified as a downstream target of p53 (Tanaka et al., 2000).

Yeast RNR differs from mammalian RNR in that there are four genes that encode the different subunits. The large subunit – equivalent to mammalian R1 – is encoded by *RNR1* and *RNR3.* While *RNR1* is essential in both YNN402 and W303 backgrounds, *RNR3* is not essential (Elledge and Davis, 1990). This result is due to the fact that in undamaged conditions, Rnr1 homodimerizes to function as the α_2 without Rnr3. However, following DNA damage, Rnr3 is upregulated and substitutes for one of the Rnr1 subunits. Interestingly, while the catalytic activity of Rnr3 is much lower than that of Rnr1 *in vitro*, the Rnr1-Rnr3 heterodimer has higher catalytic activity compared to the Rnr1 homodimer (Domkin et al., 2002). The equivalent R2 subunit in yeast is encoded by both *RNR2* and *RNR4*, both of which are essential in the W303 background (Elledge and Davis, 1987; Huang and Elledge, 1997). Rnr2 and Rnr4 function together as a heterodimer and are unable to form a functional RNR without one another. This is due, in part, to the fact that Rnr4 lacks an iron binding pocket in comparison to the other R2s, rendering it unable to supply the tyrosyl radical for RNR catalysis. However, it is thought that it provides necessary structural support, allowing for proper assembly of the subunits into a functional holoenzyme (Chabes et al., 2000; Ge et al., 2001).

Regulation of RNR in *Saccharomyces cerevisiae*

The importance of regulation of dNTPs in the cell is highlighted by the multifaceted regulation of RNR. In an intact holoenzyme, the sole mechanism of regulation is through negative feedback. This allosteric regulation, which was first identified in RNR (Reichard, 1988), is monitored in two different ways. Firstly, there is a specificity site on Rnr1 that can bind to any of the four dNTPs. The specificity site regulates the affinity of RNR for different substrates, thereby maintaining the ratios between the different nucleotides (Kumar et al., 2010). Furthermore, Rnr1 contains an activity site that monitors the ratio of dATP to ATP and thus regulates the overall activity of the enzyme. Mutation of this site leads to a 2-fold increase in dNTP levels in the cell (Chabes et al., 2003a).

In addition to regulation of the holoenzyme, the individual components of RNR are controlled by three distinct transcription factors. The MBF heterodimeric transcription factor, comprising Swi6 and Mbp1, functions in the transcription initiation of over 200 different G1-specific genes. During a normal cell cycle, MBF serves to transcriptionally regulate the levels of Rnr1 (de Bruin et al., 2006). Additionally, the HMG-box protein, Ixr1 also plays a minor role in transcription regulation of Rnr1 in undamaged cells (Tsaponina et al., 2011). However, following DNA damage, Ixr1 assumes the role of primary transcription factor, and, in its absence, Rnr1 levels are significantly reduced (Figure 1-2) (Tsaponina et al., 2011). By coordination of these two transcriptional regulators, the cell is able to maintain Rnr1 levels in the cell.

Transcription is also a key mechanism of regulation for *RNR2*, *RNR3*, and *RNR4*. The upstream sequences of these genes contain binding sites for Crt1, Rox1, and Mot3,

which serve to recruit the Ssn6/Tup1general repression complex, thus inhibiting transcription of these *RNR* genes (Huang et al., 1998; Klinkenberg et al., 2006). Furthermore, the simultaneous binding of Crt1, Rox1, and Mot3 induces a synergistic recruitment of Ssn6/Tup1. This leads to a strong repression of transcription of *RNR2*, *RNR3*, and *RNR4*. However, removal of any one of these recruitment factors allows robust induction of transcription from the promoters (Klinkenberg et al., 2006). Following DNA damage, Crt1 is phosphorylated and removed from the upstream regions, thus increasing the levels of *RNR2*, *RNR3*, and *RNR4* (Figure 1-2) (Huang et al., 1998). Interestingly, Crt1 also acts as an activator at the same sites by recruiting TFIID and the SWI/SNF chromatin-remodeling complex (Zhang and Reese, 2005). It is possible that the duality of function for Crt1 may be dependent upon its phosphorylation following DNA damage. Thus, Crt1 plays a crucial role in both repression and, following DNA damage, expression of *RNR2*, *RNR3*, and *RNR4*.

In addition to regulation of RNR by transcriptional control, the subunits of RNR are differentially localized to prevent formation of the holoenzyme. In the absence of DNA damage, Rnr1 is present in the cytoplasm while both Rnr2 and Rnr4 are sequestered in the nucleus (Yao et al., 2003). This is achieved by the actions of Dif1 and Wtm1 (Figure 1-2). Dif1 localizes to the cytoplasm where it binds Rnr2 and Rnr4 and aids in their import into the nucleus (Lee et al., 2008; Wu and Huang, 2008). Once in the nucleus, the Rnr2/Rnr4 dimer is prevented from exiting by Wtm1, which serves as an anchor (Lee and Elledge, 2006; Zhang et al., 2006). Following entry into S-phase or DNA damage, the interaction between Wtm1 and Rnr2/Rnr4 is weakened, allowing the dimer to translocate into the cytoplasm (Figure 1-2) (Lee and Elledge, 2006).

Furthermore, Dif1 is degraded, thus allowing Rnr2 and Rnr4 to remain in the cytoplasm where they interact with Rnr1 to form a functional holoenzyme (Figure 1-2) (Wu and Huang, 2008). However, the binding of Rnr1 with Rnr2 and Rnr4 can still be prevented by the direct inhibition of Rnr1 by Sml1.

Sml1 is a specific inhibitor of Rnr1

S. cerevisiae RNR is also inhibited by a direct 1:1 interaction between Rnr1 and Sml1 (Figure 1-2). In the presence of Sml1, Rnr2 and Rnr4 are unable to bind Rnr1, and thus the assembly of the holoenzyme is inhibited. This is not due to disassembly of the Rnr1 dimer but exclusively due to the interaction with Sml1 (Chabes et al., 1999). Interestingly, although no Sml1 homolog has been identified in higher eukaryotes, human R1 has been shown to interact with Sml1 by yeast two-hybrid (Zhao et al., 2000). Furthermore, mouse R1 is also inhibited by Sml1, albeit slightly differently than by the regulation seen with yeast Rnr1 (Chabes et al., 1999). One possibility is that the structural differences account for the altered regulation observed in mouse and *S. cerevisiae* Rnr1.

While mouse Rnr1 has not been crystallized yet, the structure of *S. cerevisiae* Rnr1 has been identified, and comprises a helical domain and an α/β domain closer to the N terminus, with the active site of Rnr1 located in between. Alternatively, the C terminus is largely unstructured (Xu et al., 2006a; Xu et al., 2006b). However, yeast two-hybrid studies show that the unstructured C terminus does play an important role in regulation of the active site at the N terminus of Rnr1. Interestingly, the binding pocket in the N terminus of Rnr1 where the C terminus binds is the same site where Sml1 can bind (Zhang et al., 2007). Therefore, Sml1 in effect inhibits RNR in two ways – preventing

reactivation of Rnr1 and inhibiting formation of the holoenzyme. Study of the mechanism of interaction between Sml1 and Rnr1 is, therefore, of great interest in the field.

Previous work has elucidated the secondary structure of Sml1, as well as the residues important for interaction with Rnr1. Sml1 is a 104 amino acid protein that exists in solution as an intrinsically disordered protein. However, three regions of the protein exhibit some secondary structure. Amino acids 4-14 and 60-85 display alpha helical structure, while there is also a high degree of backbone order between amino acids 20 to 35. This results in a loose three-dimensional structure whereby the protein folds on itself due to an interaction between the two alpha helices (Zhao et al., 2000). At a higher local concentration, amino acids 60-80, within the previously implicated alpha helix, trigger a dimerization of Sml1. Both the dimerization and the loose folding are important for the stabilization of Sml1. This is due to the fact that degradation of Sml1 occurs from the N terminus, and these two three-dimensional structures serve to cap the protein and thus inhibit degradation (Danielsson et al., 2008). The end capping appears to be the principal role for the N terminus as mutations in this region have no effect on Sml1-Rnr1 interaction. All the amino acids that are important for the binding between these two proteins are clustered in the C terminal region (Zhao et al., 2000).

In summary, dNTP regulation in *S. cerevisiae* is a multifaceted process, which helps maintain both the levels and the ratios between the four dNTPs to prevent mutations during DNA replication. However, while duplication of the DNA is the most widely studied output of dNTP misregulation, very little work thus far has focused on the

effect on telomeres. Such a study is interesting, as telomeres are regulated not by DNA polymerase, but by an independent reverse-transcriptase, telomerase.

TELOMERE LENGTH REGULATION

DNA replication is semi-conservative in nature proceeding in a 5' to 3' direction. The directionality necessitates discontinuous duplication of the lagging strand in addition to the continuous leading-strand synthesis. This process involves the synthesis of short (180–200 bp in eukaryotic cells) DNA fragments known as Okazaki fragments (Okazaki et al., 1968). Furthermore, to prime the replication of these fragments, a short RNA fragment is required. Removal of these RNA fragments leads to the loss of DNA sequence (Olovnikov, 1973; Watson, 1972). Furthermore, there is nucleolytic processing of both the leading and lagging strand following replication, leading to 3' overhang at both ends of the chromosome (Chai et al., 2006; Jacob et al., 2003; Larrivee et al., 2004; Sfeir et al., 2005). This also leads to the loss of sequence from the end of the DNA. To prevent the loss of coding sequence as a consequence of these processes, all linear chromosomes possess repetitive sequences at their ends called telomeres. Additionally, telomeres also prevent the ends of DNA from being incorrectly recognized as breaks in the DNA (de Lange, 2009).

The sequence of telomeric repeats differs across species but is often between 6-8 nucleotides long and rich in dGTP and dTTP (Greider, 1996). In some species, the sequence is constant from one repeat to the next. For example, vertebrates contain tandem repeats of TTAGGG (Meyne et al., 1989), while ciliated protozoa such as *Tetrahymena thermophila* and *Euplotes aediculatus* contain multiple copies of TTGGGG

and TTTTGGGG, respectively (Greider, 1996). However, some other organisms contain degenerate repeats. Most notably, in *Saccharomyces cerevisiae* the telomeric repeats have a consensus sequence of $(TG)_{0-6}TGGGTGTG(G)_{0-1}$ (Forstemann and Lingner, 2001). Furthermore, the number of these repeats is not fixed from organism to organism or even from telomere to telomere in each cell. This leads to a range in sizes of the telomeres when resolved on a DNA blot (Greider, 1996). However, the length of the telomere needs to be maintained against the erosion that naturally occurs, as this may result in short telomeres. Consequently, short telomeres can no longer be bound by the proteins that distinguish them from DNA breaks. The unprotected telomeres trigger a Rad9-mediated cell cycle arrest (Garvik et al., 1995). In extreme cases of telomere shortening, the cells senesce (Harley et al., 1990; Lundblad and Szostak, 1989; Yu et al., 1990), thus highlighting the need for maintenance of telomere lengths.

Telomerase structure, function, and regulation

Telomere lengths are maintained in all organisms by the enzyme telomerase. Discovered first in *Tetrahymena* (Greider and Blackburn, 1985), telomerase is a specialized reverse transcriptase that uses an RNA template to extend DNA (Yu et al., 1990). The RNA moiety (hTR in humans and TLC1 in *S. cerevisiae*) acquires a secondary structure and is bound by a catalytic protein subunit (hTERT in humans and Est2 in *S. cerevisiae)* to create the functional enzyme (Feng et al., 1995; Lingner et al., 1997b; Nakamura et al., 1997; Singer and Gottschling, 1994). While other proteins interact with the individual components as well as the holoenzyme to assist in assembly

and recruitment to the telomere, they do not affect the processivity of the enzyme (Collins, 2006; DeZwaan and Freeman, 2010; Hug and Lingner, 2006).

The RNA component of telomerase ranges between 159 bp in *Tetrahymena* (Greider and Blackburn, 1989) and ~1300 bp in *S. cerevisiae* (Singer and Gottschling, 1994). However, the template that is passively utilized in these organisms for extension of telomeres is only between 9 and 16 bp, respectively (Greider and Blackburn, 1989; Singer and Gottschling, 1994). Upon recruitment to the telomere, base pairing occurs between the 3' overhang of DNA and the template region of the RNA component, and the telomere is extended. However, the efficacy of telomere extension is dependent on two different translocation reactions: (i) the simultaneous movement of the RNA-DNA duplex relative to the active site after addition of each nucleotide (termed nucleotide addition processivity or type I processivity) and (ii) the ability to add multiple telomeric repeats before dissociation of the DNA-telomerase hybrid (termed repeat addition processivity or type II processivity) (Figure 1-3) (Lue, 2004).

Type I processivity has not been well studied due to the fact that it is only extensively seen in *S. cerevisiae*. One factor that has been found to affect type I processivity *in vitro* has been the levels of dGTP in the reaction. There is a positive correlation between dGTP concentration and type I processing, resulting in an increase in telomere lengths (Bosoy and Lue, 2004; Peng et al., 2001). Additionally, the reverse transcriptase motifs that are present in the catalytic protein subunit of telomerase also play a significant role in type I processivity (Haering et al., 2000; Harrington et al., 1997; Lingner et al., 1997b). Mutations in this region have been shown to affect nucleotide addition processivity *in vitro* using *S. cerevisiae* extracts (Peng et al., 2001). Furthermore,

using the same system, it was determined that different mutations within the same region can shift the balance of telomerase function away from type II processivity towards type I processivity (Lue et al., 2003).

Type II processivity, on the other hand, has been extensively studied. However, there is a difference from organism to organism with respect to the ability to perform type II processivity. Telomerase isolated from human cells and ciliated protozoa are capable of adding multiple repeats *in vitro* (Greider, 1991; Morin, 1989), while those from fungi add maximally one repeat per binding event *in vitro* (Cohn and Blackburn, 1995; Fulton and Blackburn, 1998; Lue and Peng, 1997). Despite this difference in processivity, *Tetrahymena*, *Euplotes*, and S. *cerevisiae* all show a dependence on dGTP for repeat addition processivity. In all three organisms, *in vitro* experiments using purified telomerase showed increased type II processivity upon increase in dGTP levels (Bosoy and Lue, 2004; Hammond and Cech, 1998; Hammond et al., 1997; Hardy et al., 2001). In fact, in *Euplotes*, increased concentrations of dGTP increased the rate of dissociation of the telomerase-DNA hybrid and changed the site for re-annealing, leading to different telomeric intermediates as resolved on an acrylamide gel (Hammond and Cech, 1998; Hammond et al., 1997).

In summary, telomerase is a ribonucleoprotein that catalyzes a reverse transcription reaction to elongate telomeres. This is done processively, leading to type II processivity seen in most organisms. In *S. cerevisiae*, however, telomerase processivity is low, resulting in type I processivity being the primary mode of elongation.

Mechanism of telomere sequence divergence in *Saccharomyces cerevisiae*

One drawback of the findings enumerated thus far with regards to *S. cerevisiae*, however, is the fact that they are all *in vitro* experiments that are performed using only dTTP and dGTP. Extending these results to an *in vivo* situation is difficult as three factors that are essential for telomere maintenance are dispensable in an *in vitro* situation (Cohn and Blackburn, 1995; Lingner et al., 1997a). Indeed, type I processivity is lower *in vitro* than *in vivo* (Forstemann and Lingner, 2001). Furthermore, despite *S. cerevisiae* telomerase showing lack of type II processivity *in vitro*, *in vivo* studies have shown that yeast telomeres can add repeats processively at critically short telomeres (Chang et al., 2007). However, during the normal course of telomere extension, telomerase has been shown to dissociate and re-associate with the telomeric sequence within one round of replication (Chang et al., 2007). Once telomerase has dissociated from the telomere, it can reanneal at a different site before starting another cycle of extension by nucleotide addition (Forstemann and Lingner, 2001). Multiple dissociation-reannealing-extension cycles lead to the divergence of the telomere sequence from that predicted exclusively by the TLC1 RNA sequence seen in *S. cerevisiae*. Crucially, the mechanism leading to these repeated cycles has not been elucidated yet and is an open question in the field. Understanding this feature will explain the mechanisms by which telomere shortening can be controlled, thus preventing recognition of the DNA ends as damaged DNA.

The DNA damage response in *Saccharomyces cerevisiae*

The DNA of all organisms is frequently damaged by both exogenous and endogenous factors, including altered dNTPs and uncapped telomeres (Chabes and Stillman, 2007;

Garvik et al., 1995). To protect the genome, these insults must be rapidly and accurately detected. The DNA damage response (DDR) serves to locate and rapidly transduce and amplify the response to genotoxic stress. The most severe of these stresses is the DNA double strand break (DSB), which can be lethal for the haploid genome (Resnick and Martin, 1976).

In response to DSBs, the first proteins to arrive at the site of damage are the members of the MRX complex – Mre11, Rad50, and Xrs2 (Nbs1 in humans) (Lisby et al., 2004). The MRX complex plays a role in preventing binding of the ends by the Ku complex, thus inhibiting non-homologous end joining (Shim et al., 2010). Additionally, Mre11 possesses nuclease functions and, in conjunction with Sae2, removes a small oligonucleotide from the exposed ends (Mimitou and Symington, 2008). The MRX complex also recruits other nucleases, Dna2 and Exo1, which further resect the DNA to reveal 3' single-stranded DNA (Shim et al., 2010). The ssDNA is subsequently coated by the heterotrimeric complex, RPA, (Alani et al., 1992; Kim et al., 1992; Lisby et al., 2004). This RPA-coated ssDNA plays a critical role in the DDR by recruiting two different groups of proteins that serve to amplify the response.

The first set of proteins is the 9-1-1 complex comprised of Ddc1, Rad17, and Mec3 and named for the human homologues RAD9-RAD1-HUS1 (Figure 1-2). Absence of any component of this complex leads to an abrogation of the damage signal (Kondo et al., 1999; Majka et al., 2006a; Melo et al., 2001). The 9-1-1 complex forms a heterotrimeric clamp that structurally resembles the replication clamp PCNA and similarly needs to be loaded onto DNA. The clamp loader that loads the 9-1-1 complex onto DNA is Rad24 in conjunction with the heteropentameric complex, RFC (Majka et

al., 2006b). The clamp loader is recruited to the site of damage by its interaction with RPA (Majka et al., 2006a). Interestingly, one of the components of the 9-1-1 complex, Rad17, also interacts with RPA and is similarly recruited to sites of damage along with its binding partners (Zou et al., 2003). It is thought that the recruitment of both the clamp loader and the 9-1-1 complex by RPA serves to stabilize all three proteins at the sites of damage and facilitate loading of the 9-1-1 complex onto DNA.

Additionally, RPA promotes the recruitment of the principal kinase, Mec1 (ATR in humans), involved in DNA damage signaling (Lydall and Weinert, 1995), via its association with Ddc2 (ATRIP in humans), which is the binding partner of Mec1 (Figure 1-2)(Ball et al., 2007). It was initially thought that the recruitment of Mec1 and the 9-1-1 complex were independent of one another (Melo et al., 2001); however, formation of Mec1 foci is seen to be dependent on the 9-1-1 complex in both G1 and S phase (Barlow et al., 2008). Furthermore, dependency of Mec1 on the 9-1-1 complex is highlighted by the fact that Mec1 has a low basal activity (Paciotti et al., 2000) and requires recruitment of the 9-1-1 complex to attain full activation (Majka et al., 2006b). Once activated, Mec1 has numerous downstream phosphorylation targets, including some of the components that helped recruit it to the site of damage (Chen et al., 2010; Smolka et al., 2007). One of the principal downstream targets of Mec1 is Rad53 (Sanchez et al., 1996; Sun et al., 1996).

Rad53 is the yeast homolog of mammalian Chk2 and serves to transduce the damage signal (Sun et al., 1996). To facilitate phosphorylation of Rad53, Mec1 utilizes another one of its downstream targets, Rad9 (Emili, 1998), which serves as a scaffold. Hyperphosphorylated Rad9 functions as an adaptor that concentrates Rad53 at the sites of

damage, allowing phosphorylation of Rad53 by Mec1 (Figure 1-2) (Schwartz et al., 2002; Sweeney et al., 2005). Following the initial Rad53 phosphorylation, Rad53 undergoes autophosphorylation (Pellicioli et al., 1999). Appearance of hyperphosphorylated Rad53 is used as an indicator of an active DDR. Following activation, Rad53 is released from Rad9 in an ATP dependent manner (Gilbert et al., 2001).

Dun1 is one of the potentially 42 targets of activated Rad53 (Figure 1-2) (Chen et al., 2010; Chen et al., 2007; Zhou and Elledge, 1993). It possesses a kinase domain that is 40% similar to Chk2 and is essential for function of Dun1 (Bashkirov et al., 2003; Chen et al., 2007). Furthermore, like Chk2 and Rad53, Dun1 contains an FHA domain that is a phosphopeptide specific binding domain (Li et al., 2000). This domain is essential for binding of Dun1 to Rad53 and its subsequent activation (Bashkirov et al., 2003; Chen et al., 2007). As no other kinase is involved in Dun1 activation, this interaction is essential for Dun1 activity in regulating the further downstream targets in response to DNA damage. In fact, one of the key sets of targets for Dun1 is the group of proteins involved in dNTP regulation: Crt1, Dif1, Wtm1, and Sml1 (Figure 1-2).

Sml1 regulation following DNA damage

Dun1 plays a major role in regulation of RNR activity following DNA damage. The importance of Dun1 is illustrated by the fact that in *dun1*Δ cells, dNTP levels are reduced two-fold compared to wild-type (Fasullo et al., 2010). In addition to phosphorylation of Crt1, Dif1, and Wtm1 as explained previously, Dun1 also phosphorylates Sml1 (Zhao and Rothstein, 2002).

By mass-spectrometry, the serines at position 56, 58, and 60 were identified as sites on Sml1 that are phosphorylated by Dun1 *in vitro* (Uchiki et al., 2004). Previous work from this lab found that converting these three serines as well as the serine at position 61 to alanines (*sml1-SA$_1$*) blocks phosphorylation of Sml1 (Andreson et al., 2010). Conversion of the same sites to aspartic acids to create phospho-mimics (*sml1-SD$_1$*) results in disruption of the interaction between Sml1 and Rnr1. However, this mutant also unveiled the presence of another three serines at positions 50, 53, and 54 on Sml1 that are also phosphorylated by Dun1 a second time. Modifications of these serines to alanines (*sml1-SA$_2$*) also result in stabilization of Sml1 following DNA damage, albeit to a lesser extent. This mutant still shows initial phosphorylation of Sml1 following DNA damage. Furthermore, *sml1-SA$_2$* is stabilized in the nucleus, indicating a translocation of Sml1 from the cytoplasm to the nucleus following DNA damage (Andreson et al., ms. in prep).

The translocation of Sml1 to the nucleus was consistent with data that showed that in mutants of the proteasome, *pre1-1* and *pre2-2*, Sml1 was stabilized before and after DNA damage in the nucleus (Figure 1-4) (Andreson et al., ms. in prep). The degradation of Sml1 by the proteasome indicated that Sml1 is potentially ubiquitylated as well. This notion was confirmed after a screen for mutants in which Sml1 is stabilized following DNA damage as described in Chapter 3. From this screen, the Rad6-Ubr2-Mub1 complex was identified as the ubiquitin ligase directly responsible for Sml1 ubiquitylation. In mutants of the complex, Sml1 was enriched in the nucleus and present in its phosphorylated state (see attached Appendix) (Andreson et al., 2010).

In summary, following DNA damage, Sml1 is phosphorylated, leading to its dissociation from Rnr1. Dissociated Sml1 is then translocated to the nucleus from the cytoplasm where it is phosphorylated a second time. Phosphorylated Sml1 is then ubiquitylated by Rad6-Ubr2-Mub1 before being degraded by the 26S proteasome (Figure 1-4). However, some questions still remain. Firstly, what other pathways and modifications are important for Sml1 function? Secondly, is there a function related to the relocalization of Sml1 to the nucleus and its subsequent phosphorylation?

Spindle Assembly Checkpoint: Components and Activators

To facilitate accurate repair, the DDR needs to arrest the cell-cycle to prevent damaged DNA from being passed on to the daughter cells. In order to efficiently arrest the cell-cycle at different points, the DDR coordinates with different groups of proteins. The G2/M arrest to prevent the metaphase to anaphase transition requires both the DDR and the spindle assembly checkpoint (SAC). The SAC is a conserved pathway that surveys the accurate orientation of the chromosomes in all eukaryotes to ensure the fidelity of DNA segregation.

The primary members of the SAC were identified by two screens performed in *S. cerevisiae* as mutants that bypass the ability of cells to arrest in mitosis in response to spindle poisons (Hoyt et al., 1991; Li and Murray, 1991). The genes identified encompassed the MAD (mitotic-arrest deficient) genes, *MAD1*, *MAD2*, and *MAD3* (human *BUBR1*) and the BUB (budding uninhibited by benzimidazole) genes, *BUB1* (Hoyt et al., 1991; Li and Murray, 1991). Additionally, in a search for a suppressor of a *bub1-1* mutant, *BUB3* was identified as another member of this group (Hoyt et al., 1991).

This group of genes, along with *MPS1* and *IPL1* (human Aurora B), comprises the 'core' SAC components (Tanaka et al., 2002; Weiss and Winey, 1996). Additionally, Shugoshin (Sgo1), initially identified as a protector of centromeric cohesin during meiosis I (Kitajima et al., 2004), functions in conjunction with the SAC, although the precise role of Sgo1 with the SAC is unknown. Defects in *sgo1*Δ mutants mimic *ipl1* mutants and can be suppressed by overexpression of *IPL1* (Indjeian et al., 2005; Storchova et al., 2011). However, Ipl1 localization and activity is not affected in *sgo1*Δ. Furthermore, following Mps1 inactivation, overexpression of *SGO1* allows cells to survive mitosis, suggesting it likely functions in the same pathway as Mps1 and parallel to Ipl1 (Storchova et al., 2011).

The ultimate function of the SAC is to prevent the premature separation of the sister chromatids until all chromosomes are aligned at the metaphase plate and correctly attached to the mitotic spindle. Following replication of the DNA, sister chromatids are held together by cohesin rings that are cleaved only at mitosis by a protease, called separase, during the metaphase to anaphase transition (Guacci et al., 1997; Uhlmann et al., 1999). Prior to anaphase, separase is restrained by the inhibitor securin. Entry into anaphase requires degradation of securin by the 26S proteasome. To target securin to the proteasome, it is ubiquitylated by the ubiquitin ligase, the anaphase promoting complex, or cyclosome (APC/C). The specificity of the APC/C is determined by its co-factor, which in the case of securin is Cdc20. The binding of Cdc20 to the APC/C is prevented by the SAC, thus inhibiting the metaphase to anaphase transition (Lew and Burke, 2003; Musacchio and Salmon, 2007; Pinsky and Biggins, 2005).

Proper alignment of the sister chromatids depends on a structure called the kinetochore, which is located on the chromatin. Proper binding between all the kinetochores and the microtubules from the spindle pole is required to turn off the SAC (Musacchio and Salmon, 2007). It remains controversial as to how the kinetochore-microtubule interaction is able to modify the SAC. The simplest hypothesis states that components of the SAC are recruited to unattached kinetochores, and thus the checkpoint is kept active. Upon binding to microtubules, the SAC can no longer bind the kinetochore, leading to an abrogation of the signal. This model is supported by evidence showing accumulation of SAC proteins at unattached kinetochores in prometaphase that dissipate later in mitosis (Lew and Burke, 2003; Musacchio and Salmon, 2007). Furthermore, the presence of even one unattached kinetochore leads to an activated SAC (Nicklas et al., 1995; Rieder et al., 1995). The argument against this model, however, is the fact that an active SAC is detectable even in cells in which kinetochore assembly has been abrogated (Fraschini et al., 2001; Poddar et al., 2005). Furthermore, as early as metaphase, different components of the SAC dissipate unequally with some components persisting until anaphase. This indicates a possible second mechanism of checkpoint de-activation (Musacchio and Salmon, 2007). It is thought that the second mechanism is dependent on tension, as work with mantid XXY spermatocytes that were arrested in meiosis I were rescued upon artificial application of tension (Li and Nicklas, 1995). The model implicating tension would also explain activation of the SAC in instances where both kinetochores bind to the same SPB. In this case, kinetochore occupancy would be filled, but sufficient tension would not exist between the sister chromatids. Therefore, in the tension model, the kinetochore structure and assembly is key.

Kinetochore components and construction

Kinetochores are multi-protein complexes that are loaded at sites called centromeres on the DNA. The centromeres can vary in length between ~125bp (point centromeres) in *S. cerevisiae* and ~10 Mb (regional centromeres) (Burrack and Berman, 2012). Despite this difference, the mechanism for loading of kinetochores at these sites is well conserved. The process begins with the replacement of the histone H3 at centromeres with a CenH3 variant (Cse4 in *S. cerevisiae*; CENP-A in humans) (Meluh et al., 1998). This deposition is dependent on other factors as well. In *S. cerevisiae*, the combination of Scm3 and the kinetochore protein, Ndc10, are required for proper recruitment of Cse4 to the centromeres (Camahort et al., 2007). In *S. pombe* as well as in higher eukaryotes, the Scm3 homolog, HJURP, in conjunction with either the Mis16-Mis18 group of proteins or the Mis18 family of proteins, respectively, deposits *CENP-A* at centromeres (Foltz et al., 2009; Fujita et al., 2007; Hayashi et al., 2004). Misregulation of any of these factors severely affects kinetochore establishment (Foltz et al., 2009; Fujita et al., 2007; Hayashi et al., 2004), leading to chromosome loss and aneuploidy (Camahort et al., 2007; Mishra et al., 2011). Temporal recruitment of the remainder of the kinetochore proteins is not as well understood.

In higher eukaryotes the *CENP-A* bound centromere is bound to microtubules via the KMN network of subcomplexes (Przewloka and Glover, 2009). In *S. cerevisiae*, however, the KMN network serves as a linker complex to the DAM/DASH complex that is essential for stabilization of the kinetochore-microtubule interaction (Akiyoshi et al., 2010). On the other side, the KMN network binds Cse4 through its interaction with the COMA complex (Ortiz et al., 1999). In addition to their function as a linker complex,

some components of the COMA complex have also been implicated in establishment of pericentromeric cohesin (Ng et al., 2009).

Cohesin establishment in *Saccharomyces cerevisiae*

The cohesin ring is comprised of four components – Mcd1, Scc3, Smc1, and Smc3 – that form a ring structure. The complex is loaded onto DNA during the G1/S transition by Scc2 and Scc4 to promote sister chromatid association after DNA replication (Ciosk et al., 2000). After loading, cohesin needs to be established on the chromosome, which is done via acetylation of the cohesin ring by Eco1, and, in keeping with this, *eco1* mutants show reduced cohesin on chromosomes (Rolef Ben-Shahar et al., 2008; Skibbens et al., 1999). However, this reduction in cohesin is abrogated upon overexpression of the DNA polymerase processivity factor and sliding clamp proliferating cell nuclear antigen (PCNA), indicating a replication dependent role for cohesin establishment independent of Eco1 (Skibbens et al., 1999). The traditional factor important in loading PCNA onto DNA is the heteropentameric RFC complex (Diffley and Labib, 2002). However, in some instances, one of the components of the RFC, Rfc1, is replaced by Ctf8, Ctf18, and Dcc1 (Naiki et al., 2001). This complex is still able to load PCNA onto DNA (Bermudez et al., 2003). Interestingly, loss of *CTF8*, *CTF18*, or *DCC1* leads to a reduction in cohesin establishment (Mayer et al., 2001). Furthermore, the Ctf18-RFC complex has been found at regions that also contain replication forks (Lengronne et al., 2006). These data provide a potential model whereby the presence of Ctf8, Ctf18, and Dcc1 allows alteration of the shape of either the replication fork or cohesin to allow the replication fork to pass through

the cohesin ring. In their absence, the replication fork would cause removal of cohesin from DNA (Lengronne et al., 2006).

Another protein found to be required for SAC function is Bim1. Deletions of any member of the SAC led to synthetic lethality with a *bim1*Δ (Lee and Spencer, 2004; Schwartz et al., 1997). Functionally, Bim1 (human EB1) is important in establishment of the mitotic spindle by binding and stabilizing interpolar microtubules (Gardner et al., 2008). However, there is some question as to the function of Bim1, as loss of *BIM1* leads to reduced cohesin as well (Mayer et al., 2004).

In the following studies, I focused on Sml1 with particular emphasis on its regulation and its roles in different cellular processes. The first focus was on the regulation of telomeres by dNTPs. While previous studies have hinted at a connection between the two, I have shown that, in *S. cerevisiae*, telomere length is correlated to the relative amount of dGTP in the cell *in vivo*. This is due to the exquisite sensitivity of telomerase processivity to the amount of dGTP relative to the other nucleotides in the cell. The repeated cycles of stalling and dissociation seen previously in *S. cerevisiae* are exacerbated when the relative amount of dGTP is reduced, but abolished when the relative levels are increased. Therefore, this work provides a potential mechanism for nucleotide addition processivity in *S. cerevisae* that results in the degenerate telomeres. Furthermore, the study showed that the repeat addition processivity seen in human telomerases is also sensitive to the levels of dGTP, despite the biochemical differences between *S. cerevisiae* and human telomerases. The common regulation provides an interesting evolutionary link and suggests new methods of regulation of telomerase.

Secondly, I sought to identify other factors important in regulation of Sml1. In the course of this study, I was able to identify a novel role for Sml1 as the human Mis18α ortholog. In this capacity, Sml1 is necessary for the timely assembly of kinetochores in the cell. Therefore, loss of *SML1* leads to a delay in kinetochore assembly and causes subsequent spindle defects. While these delays have no discernable effect on growth and chromosome loss, they are synergistic with defects in cohesion, spindle assembly, or a defective SAC. The sensitivity of these mutants to *sml1*Δ is exclusively due to the kinetochore function of Sml1. This work hints at a model whereby phosphorylation of Sml1 by the DDR is necessary for kinetochore formation. Therefore, in DDR mutants, there would be a defect in kinetochore assembly, which would activate the SAC. This could provide the potential link between the DDR and the SAC that has only been hinted at previously.

Figure 1-1

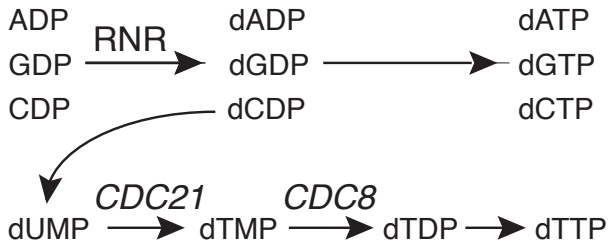

Figure 1-1: Mechanism of dNTP production in *Saccharomyces cerevisiae*. The ribonucleotide reductase (RNR) holoenzyme reduces ADP, GDP, and CDP to their respective deoxy forms which are further processed to give the corresponding dNTPs. dTTP is produced by further processing of dCDP by numerous enzymes including *CDC21* and *CDC8*.

Figure 1-2

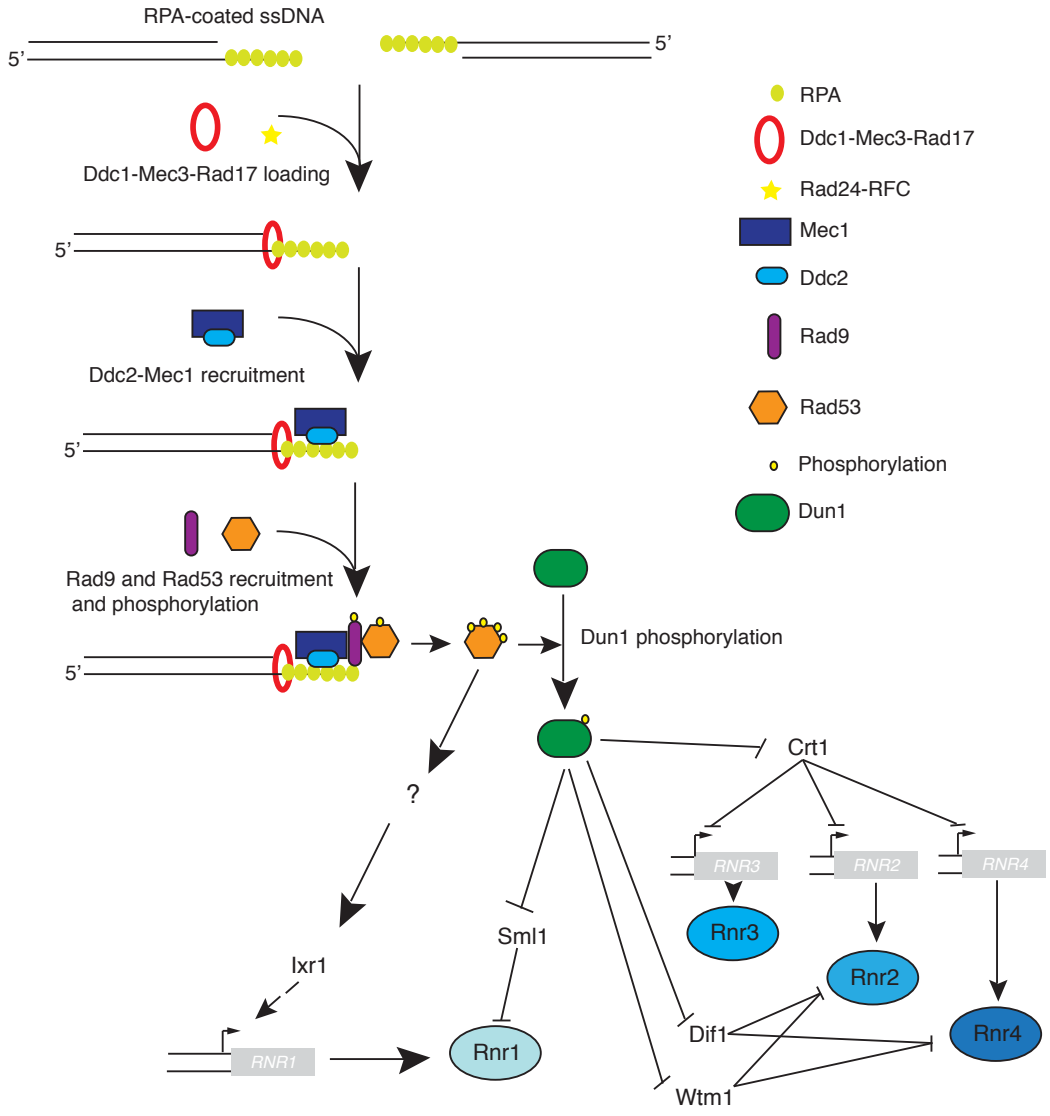
RPA-coated ssDNA
5'
5'
Ddc1-Mec3-Rad17 loading
5'
Ddc2-Mec1 recruitment
5'
Rad9 and Rad53 recruitment
and phosphorylation
5'
Dun1 phosphorylation
?
Crt1
RNR3
RNR2
RNR4
Rnr3
Rnr2
Rnr4
Sml1
Ixr1
RNR1
Rnr1
Dif1
Wtm1
RPA
Ddc1-Mec3-Rad17
Rad24-RFC
Mec1
Ddc2
Rad9
Rad53
Phosphorylation
Dun1

Figure 1-2: Regulation of dNTPs by the DDR. Following DNA damage, the ends of DNA are resected and the 3' overhang is coated with RPA. RPA-coated ssDNA serves to recruit Ddc1-Mec3-Rad17 and Ddc2-Mec1 to the site of damage and, in doing so, activates Mec1. Activated Mec1 phosphorylates Rad53 with the assistance of the adaptor, Rad9. Rad53 is autophosphorylated to amplify the signal and proceeds to phosphorylate Dun1. Additionally, Rad53, through an unknown mechanism, phosphorylates Ixr1, a transcription factor involved in upregulation of *RNR1* transcription. Upon activation, Dun1 phosphorylates Crt1, Dif1, Mtw1, and Sml1, which function as inhibitors of the RNR pathway. Crt1 is a transcriptional inhibitor of the other *RNR* genes and, upon its phosphorylation, *RNR2*, *RNR3*, and *RNR4* are transcribed at higher levels. Both Dif1 and Wtm1 jointly function to sequester Rnr2 and Rnr4 in the nucleus. Upon phosphorylation, the block is lifted and Rnr2/Rnr4 are translocated to the cytoplasm. However, Rnr1 in the cytoplasm is actively inhibited by Sml1. Removal of Sml1 by Dun1 phosphorylation is necessary to alleviate the block on Rnr1, allowing its binding to Rnr2/Rnr4 to form an active RNR holoenzyme.

Figure 1-3

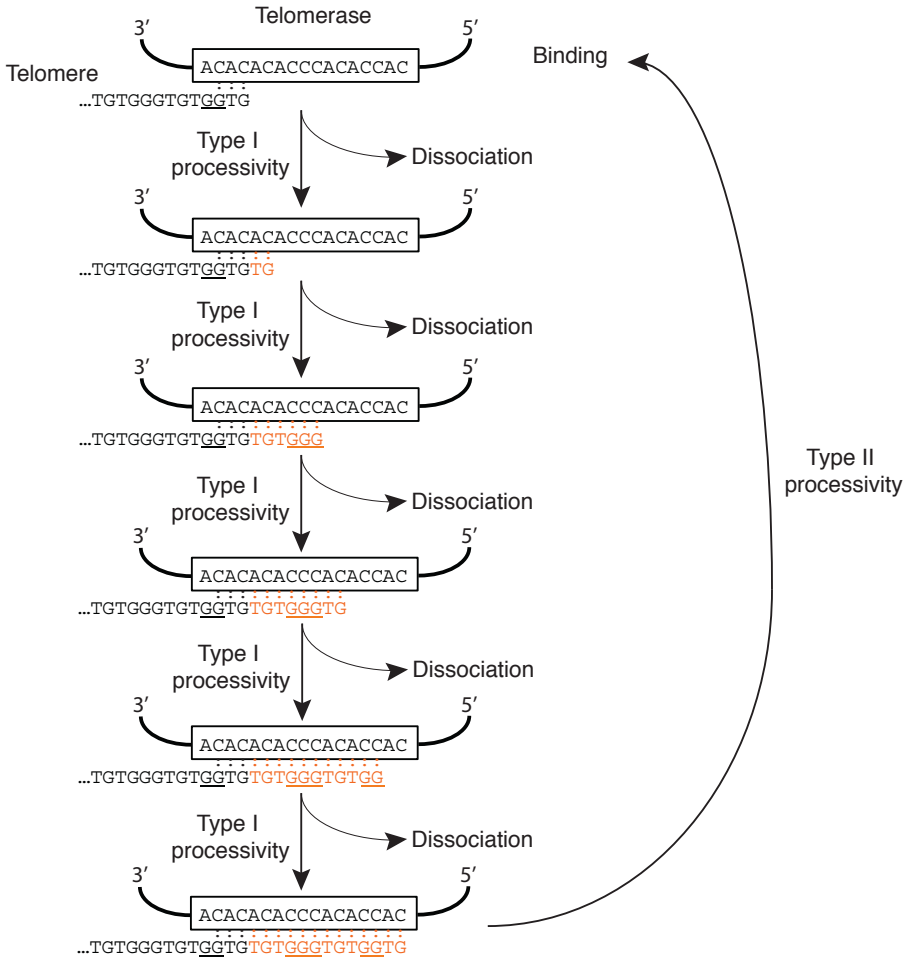

Figure 1-3: The telomerase reaction cycle. Upon binding to telomeres, telomerase begins to add nucleotides. However during this process, telomerase often dissociates from telomeres. The ability of telomerase to repeatedly add nucleotides is termed type I processivity. Type II processivity, on the other hand, is the ability of telomerase to reanneal to telomere ends upon reaching the end of the telomerase template and processively add multiple telomere repeats.

Figure 1-4

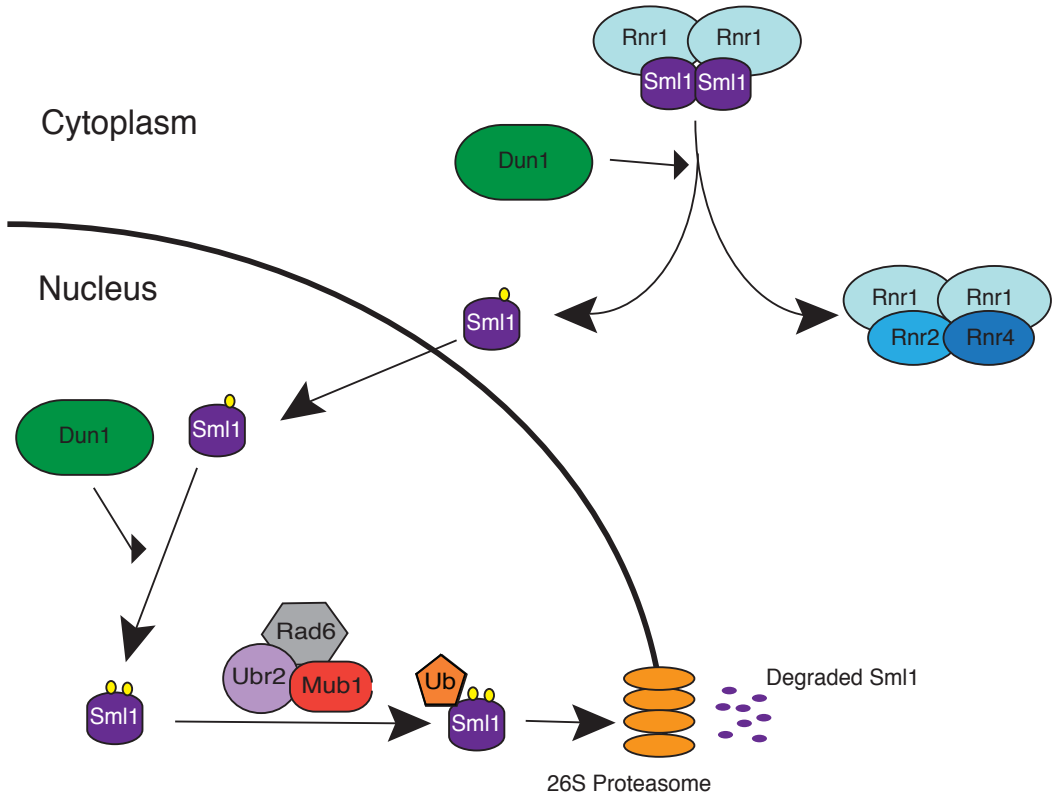

Figure 1-4: Sml1 regulation in the cell. Sml1 directly binds and inhibits Rnr1 in a 1:1 ratio. Following DNA damage and activation of Dun1, Sml1 is phosphorylated by Dun1. Phosphorylated Sml1 dissociates from Rnr1 and is translocated to the nucleus. Meanwhile, Rnr1, associates with Rnr2/Rnr4 to form the active holoenzyme RNR. In the nucleus, Sml1 is phosphorylated a second time by Dun1 before being degraded by the 26S proteasome.

CHAPTER 2:

TELOMERE LENGTH HOMEOSTASIS RESPONDS TO CHANGES IN dNTP POOLS

THIS WORK IS A MANUSCRIPT IN PREPARATION FOR SUBMISSION TO PLOS GENETICS

ABSTRACT

Telomerase counteracts telomere erosion using deoxyribonucleoside triphosphates (dNTPs) to extend telomeres. We examined whether altering the levels of the dNTP pools or changing the relative ratios of the four dNTPs in *Saccharomyces cerevisiae* would affect the length of the telomeres. Lowering dNTP levels leads to a modest shortening of telomeres, while increasing dNTP pools only slightly increases telomere length. Strikingly, altering the ratio of the four dNTPs dramatically affects telomere length homeostasis, both positively and negatively. Specifically, telomere length positively correlates with intracellular dGTP levels and we find that dGTP levels influence the nucleotide addition processivity of telomerase. Furthermore, we show that human telomerase activity is also greatly affected by changes in dGTP levels. Our findings reveal a novel evolutionarily-conserved link between telomere length homeostasis and dNTP regulation, and suggests that telomerase activity can be modulated by adjusting dGTP levels.

INTRODUCTION

All eukaryotes, as well as some prokaryotes with linear chromosomes, contain repetitive sequences called telomeres at the ends of their DNA (Hug and Lingner, 2006). Telomeric DNA is bound by proteins that protect chromosome ends from being recognized as genotoxic DNA double-strand breaks in need of repair (de Lange, 2009). However, telomeres shorten due to incomplete DNA replication and nucleolytic degradation. Left unchecked, this telomere erosion eventually results in very short, unprotected telomeres, resulting in cell cycle arrest and replicative senescence (Harley et al., 1990; Lundblad and Szostak, 1989; Yu et al., 1990).

Telomere shortening is counteracted by a specialized reverse transcriptase called telomerase (Greider and Blackburn, 1985), whose core consists of a protein catalytic subunit and an RNA moiety – hTERT and hTR, respectively, in humans (Feng et al., 1995; Nakamura et al., 1997) and Est2 and TLC1, respectively, in the budding yeast *Saccharomyces cerevisiae* (Lingner et al., 1997b; Singer and Gottschling, 1994). Telomerase extends telomeres by repeated reverse transcription of a short sequence to the 3′ ends of telomeres, using the RNA subunit as a template (Greider and Blackburn, 1989; Singer and Gottschling, 1994; Yu et al., 1990). Although the sequence of the telomeric repeats differs between species, a common feature is that they are all G-rich. In vertebrates, the repeat sequence is TTAGGG (Meyne et al., 1989), while in *S. cerevisiae*, the telomeric repeats have a consensus sequence of $(TG)_{0\text{-}6}TGGGTGTG(G)_{0\text{-}1}$ (Forstemann and Lingner, 2001).

dNTPs are the building blocks of DNA and their production needs to be tightly regulated as imbalances in dNTP pools can be mutagenic (Reichard, 1988). In *S.*

cerevisiae, the sole mode of dNTP production is through *de novo* dNTP synthesis and the primary enzyme in this process is ribonucleotide reductase (RNR). RNR catalyzes the reduction of ADP, GDP, CDP, and UDP to their respective deoxy forms, which are then converted to dATP, dGTP, dCTP, and dTTP (Reichard, 1988). Since RNR is the rate-limiting step in dNTP production, it is tightly regulated to maintain proper dNTP levels. In *S. cerevisiae*, overall pool sizes are controlled by: a) allosteric regulation of RNR activity by dATP (Reichard, 1988), b) transcriptional regulation of the *RNR* genes by Crt1, Ixr1, as well as the MBF complex (de Bruin et al., 2006; Huang et al., 1998; Tsaponina et al., 2011), c) direct inhibition of the large subunit of RNR, Rnr1, by Sml1 (Chabes et al., 1999; Zhao et al., 1998), and d) relocalization of the small subunits of RNR, Rnr2 and Rnr4, to the nucleus by Wtm1 and Dif1 (Lee and Elledge, 2006; Lee et al., 2008; Wu and Huang, 2008). The regulation of the proteins Wtm1, Dif1, Crt1, and Sml1 is dependent on Mec1, the ATR ortholog in yeast, in a manner dependent on Dun1, a CHK2 ortholog (Huang et al., 1998; Lee and Elledge, 2006; Lee et al., 2008; Zhao et al., 2001). In addition, an allosteric specificity site on RNR is important for maintaining the proper balance of the four individual dNTPs (Reichard, 1988).

Previous studies have implicated dNTP pools in telomere length homeostasis. Both *rnr1*Δ and *dun1*Δ mutants were found to have short telomeres in a genome-wide screen that measured the telomere lengths of strains in the yeast gene deletion library (Gatbonton et al., 2006). Given that both Rnr1 and Dun1 are positive regulators of dNTP levels, the shortened telomeres of the *rnr1*Δ and *dun1*Δ mutants may be a product of reduced dNTPs. Indeed, the dNTP pool sizes in a *dun1*Δ strain are reduced two-fold compared to wild type (Fasullo et al., 2010). Furthermore, *cdc8-1* strains, which express

defective thymidylate kinase, involved in production of dTTP, possess shortened telomeres (Toussaint et al., 2005). All of these observations suggest a possible link between telomere length homeostasis and regulation of dNTP pools.

In this study, we investigated this link by systematically varying dNTP pool levels and observed that reducing the overall pool size does indeed result in shortened telomeres. Interestingly, increasing dNTP levels has a very mild effect on telomere length homeostasis. Furthermore, we show that Mec1 and Dun1 function in the same pathway to regulate dNTP pools and telomere length homeostasis. However, Mec1 also functions with Tel1, the yeast ATM ortholog, to regulate telomerase in a Dun1-independent manner. Furthermore, by using *rnr1* mutants that perturb the balance of the four dNTPs, we find dramatic effects on telomere length homeostasis, both positive and negative. In particular, dGTP levels positively correlate with telomere length and telomerase nucleotide addition processivity. Strikingly, using a cell-free system, we find that human telomerase activity is also dramatically affected by dGTP concentration. Altogether, our results reveal a novel link between telomere length homeostasis and dNTP pools, and show that alterations in intracellular dGTP levels can modulate telomerase activity.

RESULTS

Decreased dNTP pools lead to shortened telomeres

To determine whether altered dNTP pools affect telomere length homeostasis, we isolated meiotic products from the sporulation of a *dun1*Δ/+ *sml1*Δ/+ diploid and examined these haploid progeny for both telomere length and dNTP pool size. Consistent with previous observations (Gatbonton et al., 2006), the *dun1*Δ mutant shows slightly

shorter telomeres compared to wild type strains (about 50 bp shorter, Figure 2-1A and 2-2). This phenotype is rescued by additional deletion of *SML1* (Figure 2-1A and 2-2). Since *dun1*Δ strains have a two-fold reduction in dNTP pools and *dun1*Δ *sml1*Δ double mutants show a 2.5-fold increase in dNTP pools similar to a *sml1*Δ mutant (Fasullo et al., 2010) (Figure 2-1B), the shortened telomeres in a *dun1*Δ mutant are likely caused by reduced dNTP pools. Interestingly, despite the increased dNTP pools in the *sml1*Δ and *dun1*Δ *sml1*Δ strains, there is only a very mild increase in telomere length in either strain. Since deletion of *CRT1* has previously been shown to increase dNTP pools two-fold (Tang et al., 2009), we constructed *sml1*Δ *crt1*Δ strains hoping to further increase dNTP levels. Indeed, *sml1*Δ *crt1*Δ strains have total dNTP pools approximately four-fold above wild type levels (Figure 2-1C), but the increase in telomere length is less than 20 bp (Figure 2-2D), indicating that an increase in dNTP pools above wild type levels does not dramatically affect telomere length homeostasis.

Elucidating the role of Mec1 at telomeres

The phosphoinositide-3-kinase-related kinases Tel1 and Mec1, yeast orthologs of human ATM (ataxia telangiectasia mutated) and ATR (ATM and Rad3-related), respectively, are needed for proper regulation of telomerase (Arnerić and Lingner, 2007; Ritchie et al., 1999). Yeast cells lacking Tel1 have very short telomeres (Greenwell et al., 1995), while a *mec1-21* mutant has slightly short telomeres (Ritchie et al., 1999). Previous work has shown that *mec1-21*, *dun1*Δ, and *dun1*Δ *mec1-21* mutants all have similar dNTP pool sizes (Fasullo et al., 2010), indicating that Mec1 also functions in a pathway with Dun1 to regulate dNTP pools. Therefore we determined whether Mec1 and Dun1 also function in

the same pathway to regulate telomere length homeostasis. We measured telomere length in a *dun1*Δ *mec1-21* double mutant compared to the *dun1*Δ and *mec1-21* single mutants and all three strains show the same telomere length (Figure 2-3). Thus, Mec1 and Dun1 function in the same pathway to regulate both dNTP pools and telomere length. In contrast, we find that Tel1 and Dun1 function in separate pathways to regulate telomere length since the effect of combining *DUN1* and *TEL1* deletions is additive: *dun1*Δ *tel1*Δ double mutants have shorter telomeres than either *dun1*Δ or *tel1*Δ single mutants (Figure 2-3).

We next examined these three genes for their role in senescence. It was previously shown that *mec1-21 tel1*Δ strains senesce due to a lack of telomerase-mediated telomere extension, a phenotype similar to that of telomerase-negative strains (Arnerić and Lingner, 2007; Ritchie et al., 1999). Since *MEC1* and *DUN1* act in the same pathway for nucleotide pools and telomere length, we tested whether *dun1*Δ *tel1*Δ double mutants also senesce like *mec1-21 tel1*Δ strains. Interestingly, we find that *dun1*Δ *tel1*Δ cells do not senesce despite repeated subculturings. These observations indicate that *MEC1* and *TEL1* function to prevent senescence in a pathway that is not dependent on Dun1.

Altering the ratio of the four dNTPs affects telomere length homeostasis

Having established that limiting dNTP pools leads to shorter telomeres, we explored whether perturbing the balance of the four dNTPs would also affect telomere length homeostasis. We have previously shown that the ratio of the four dNTPs can be severely imbalanced by making mutations in loop 2 of Rnr1 (Kumar et al., 2010). We focused on four *rnr1* mutants, *rnr1-Q288E*, *rnr1-Q288A*, *rnr1-R293A*, and *rnr1-Y285A*, with

imbalanced dNTP pools (Figure 2-4A). We find that the *rnr1-Q288E* and *rnr1-Q288A* mutants both show elongated telomeres compared to wild type while the *rnr1-R293A* and *rnr1-Y285A* mutants both have dramatically shortened telomeres, almost 200 bp shorter than wild type telomeres, which is much greater than the ~50 bp decrease seen in the *dun1*Δ mutant (Figures 2-4B and 2-1A). These results indicate that disrupting the ratio of the four dNTPs can greatly affect telomere length homeostasis both positively and negatively. The increase in telomere lengths in the *rnr1-Q288E* and *rnr1-Q288A* mutants correlates with increases in total dNTP levels. However, the *rnr1-Y285A* mutant has very short telomeres despite having significantly increased total dNTP levels. Thus, the telomere length changes cannot be easily explained by changes in total dNTP levels (Figure 2-5A). Neither can growth rate provide an explanation since both the *rnr1-Q288A* and *rnr1-R293A* mutants grow very poorly (Kumar et al., 2010) but exhibit opposite effects on telomere length.

Next, we compared the change in telomere length to the amount of each of the four dNTPs as a percentage of the total dNTP pool size. We found no correlation in length homeostasis in comparison to the dCTP, dTTP, and dATP pools in these strains (Figure 2-5A). On the other hand, we found an interesting association between telomere length and dGTP pools: both the *rnr1-R293A* and the *rnr1-Y285A* mutants, which have short telomeres, show reduced dGTP while the two mutants with long telomeres, *rnr1-Q288E* and *rnr1-Q288A*, have increased dGTP as a percentage of the total dNTP levels (Figure 2-4C). These results indicate that telomere length is correlated with the percentage of intracellular dGTP more so than the absolute size of the dNTP pool. Consistent with this idea, the mutants analyzed in Figure 2-1 do not have altered

percentages of dGTP (Figure 2-5B), resulting in much milder effects on telomere length homeostasis.

To determine whether telomere length changes in these *rnr1* mutants are dependent on telomerase, we made double mutants of the *rnr1* point mutants with *tlc1*Δ by isolating haploid meiotic progeny after the sporulation of *rnr1*/+ *tlc1*Δ/+ diploids. We were unable to measure the telomere length of *rnr1-R293A tlc1*Δ double mutants as isolates of this strain senesced before we were able to extract DNA. The other double mutants, *tlc1*Δ *rnr1-Q288E*, *tlc1*Δ *rnr1-Q288A*, and *tlc1*Δ *rnr1-Y285A,* all exhibit telomere lengths that are similar to *tlc1*Δ single mutants (Figure 2-4D), indicating that the telomere length changes associated with the *rnr1-Q288E*, *rnr1-Q288A*, and *rnr1-Y285A* mutants are all telomerase-dependent.

Altering dGTP affects telomerase nucleotide addition processivity

Since the telomere length changes are telomerase-dependent in the three *rnr1* mutants that we could test, we examined the effect of imbalanced dNTP pools on the efficiency with which telomerase adds dNTPs to the 3′ terminus of telomeres (i.e. the nucleotide addition processivity of telomerase). Although the *S. cerevisiae* telomerase RNA subunit, TLC1, is predicted to specify the synthesis of the sequence 5′-TGTGTGGGTGTGGTG-3′ if reverse transcription of each repeat is completely processive, yeast telomerase adds imperfect, degenerate repeats with a consensus sequence of 5′-$(TG)_{0-6}$TGGGTGTG$(G)_{0-1}$-3′ (Forstemann and Lingner, 2001). Thus, telomerase nucleotide addition processivity can be assessed by analyzing the frequency of sequence elements within this consensus. Since almost all telomeric repeats contain the -TGGGTGT- sequence motif, we can

analyze reverse transcription of the 5′ portion of the TLC1 template region after the synthesis of this core motif, as well as reverse transcription of the 3′ portion of the template region leading up to the core motif. To study the telomeric sequences, we amplified, cloned, and sequenced telomere VI-R from wild type and the four different *rnr1* strains. The distal region of the telomeres has sequences that are divergent because telomerase adds imperfect, degenerate repeats (Forstemann et al., 2000). To ensure that the sequences analyzed were due to telomerase-mediated extension events, only sequences that diverged from bulk telomere sequences were examined.

To assay reverse transcription of the 5′ portion of the TLC1 template region, we analyzed how often the core -TGGGTGT- sequence is followed by a GG dinucleotide, as predicted from the template region of TLC1, to produce either -TGGGTGTGGT- or -TGGG$(TG)_n$TGGGT- repeats (Figure 2-6A). In a wild type strain, the core -TGGGTGT- sequence is followed in 52% of all cases by a GG dinucleotide (Figure 2-6A), similar to what has been previously reported (Forstemann and Lingner, 2001). We find that the fraction of repeats that contain the GG dinucleotide in the *rnr1-Q288E* and *rnr1-Q288A* mutants is increased to 59% and 61%, respectively, indicating that telomerase processivity for the 5′ region is enhanced in these two mutants (Figure 2-6B). This observation may provide an explanation for the elongated telomeres seen in the *rnr1-Q288E* and *rnr1-Q288A* strains. However, no statistically significant difference was observed for the other two *rnr1* mutants.

To assess the processivity of the reverse transcription of the 3′ portion of TLC1 template region, we first considered all repeats containing the GG dinucleotide (i.e. -TGGGTGTGGT- repeats). Since the 3′ portion of the template consists of a stretch of CA

dinucleotides, multiple alignments are possible for a telomere ending in -TGGT or -TGGTG (Figure 2-7A). This variable alignment gives rise to the variable number of TG dinucleotides between a GG dinucleotide and the following TGGG motif (Figure 2-7A and 2-7B). In wild type cells, we find that there are typically one or two TG dinucleotides between a TGG and the subsequent TGGG motif (Figure 2-7B), consistent with previous observations (Forstemann and Lingner, 2001). In the *rnr1-Q288E* and the *rnr1-Q288A* mutants, both of which have increases in the percentage of dGTP and elongated telomeres, there is a shift towards having fewer TG dinucleotides ($P = 1 \times 10^{-6}$ for *rnr1-Q288E* and $P = 4 \times 10^{-10}$ for *rnr1-Q288A*, as determined by chi-squared tests; Figure 2-7B). In contrast, the *rnr1-R293A* and the *rnr1-Y285A* mutants, which both have decreased percentages of dGTP and shortened telomeres, show an increase in the number TG dinucleotides between a TGG and the following TGGG motif ($P = 6 \times 10^{-16}$ for *rnr1-R293A* and $P = 2 \times 10^{-9}$ for *rnr1-Y285A*, as determined by chi-squared tests; Figure 2-7B). If nucleotide addition processivity is low, telomerase would dissociate before reverse transcription proceeds to the next TGGG motif. A cycle of stalling, where telomerase dissociates prematurely, realigns and reattempts reverse transcription, would increase the number of TG dinucleotides between a TGG and the next TGGG motif. Thus, telomerase in the *rnr1-R293A* and *rnr1-Y285A* mutants exhibits reduced nucleotide addition processivity likely due to the low relative levels of dGTP in these mutants.

Similarly, we can consider all repeats that do not have a GG dinucleotide (i.e. -$TGGG(TG)_nTGGGT$- repeats) and measure the number of TG dinucleotides between a TGGG and the following TGGG. In wild type cells, one TG dinucleotide usually separates a TGGG and the next TGGG (Figure 2-7C). Similar to the scenario above, if

telomerase nucleotide addition processivity is low, the number of TG dinucleotides between the TGGG motifs would be increased. The *rnr1-R293A* and *rnr1-Y285A* mutants, both of which have a reduced percentage of dGTP and shortened telomeres, show a striking increase in the number of TG dinucleotides ($P = 1 \times 10^{-5}$ for *rnr1-R293A* and $P = 2 \times 10^{-23}$ for *rnr1-Y285A*, as determined by chi-squared tests; Figure 2-7C), indicating that telomerase processivity is reduced in these strains.

It is possible that these sequence changes are not telomerase-dependent and are instead a consequence of mutations inserted by DNA polymerases. To rule out this possibility, we eliminated telomerase activity in the *rnr1* mutants by deleting *TLC1*. Sequence divergence was mostly eliminated in the *rnr1 tlc1*Δ double mutants (Figure 2-8A), to levels similar to what has been previously observed in telomerase-negative strains (Teixeira et al., 2004). Furthermore, almost all telomeres analyzed in this study, regardless of the strain, have an identical internal region of 60 bp (Figure 2-8B), meaning that the sequence changes in the *rnr1 TLC1* mutants recorded in Figure 2-7 were confined to the distal end of the telomeres, where telomerase acts. If replication-induced mutations are responsible for the sequence changes in the *rnr1 TLC1* mutants, these changes would still be observed in the *rnr1 tlc1*Δ mutants, and the changes would also be observed within the internal 60 bp region. Thus, the telomere sequence changes in all four *rnr1* mutants are telomerase-dependent.

In this section, we show that all four *rnr1* mutants have altered telomerase processivity, even the *rnr1-R293A* mutant, for which we were unable to test telomerase epistasis. We find that telomerase nucleotide addition processivity is influenced by intracellular dGTP levels, with reverse transcription of the 3′ portion of the TLC1

template region being more dramatically affected than the 5′ portion. Altogether, we show that the percentage of dGTP positively correlates both with telomerase processivity and with telomere length.

Characterization of the *rnr1*Δ deletion

Given our results with the *rnr1* point mutants, we decided to examine the effect of an *rnr1*Δ deletion. Interestingly, while *RNR1* is essential in the YNN402 (Elledge and Davis, 1990) and W303 backgrounds (I. Sunjevarić and R. Rothstein, unpublished data), an *rnr1*Δ strain is present in the nonessential gene deletion collection (Giaever et al., 2002), which is in the BY4741 strain, a derivative of the S288C background. This *rnr1*Δ strain has been reported to have really short telomeres, more than 200 bp shorter than wild type strains (Gatbonton et al., 2006), but considering the discrepancy in the reported viability of *rnr1*Δ mutants, we decided to validate the reported phenotypes ourselves. We first confirmed that the *rnr1*Δ mutant from the deletion collection has really short telomeres (data not shown). In this strain, the *RNR1* gene has been replaced with the kanMX4 cassette, which provides resistance to the drug geneticin (also known as G418). We backcrossed the *rnr1*Δ strain twice to a BY4741 wild type strain and found that the short telomere phenotype always cosegregated with resistance to G418 and slow growth (Figure 2-9A and 2-9B). We then verified the location of the kanMX4 cassette by PCR amplification of the junctions between the cassette and locations upstream and downstream of *RNR1* (data not shown).

Flow cytometric analysis revealed defects in cell cycle progression in the *rnr1*Δ mutant, with many cells delayed in S phase (Figure 2-9C). We also find that there is

upregulation of Rnr2, Rnr4, and most significantly, Rnr3 (Figure 2-9D). Rnr3 is a minor isoform of the large subunit of RNR that is only expressed following DNA damage or replication blocks in response to an increased need for dNTPs (Elledge and Davis, 1990). Furthermore, Sml1 is degraded in *rnr1*Δ strains (Figure 2-9D), which normally occurs during S phase or in response to DNA damage (Zhao et al., 2001). Although the changes in RNR and Sml1 levels are likely responsible for keeping the cells viable, it is currently unclear why a deletion of *RNR1* is viable in the BY4741 background, but lethal in the YNN402 and W303 backgrounds.

We next examined the levels of the different dNTPs in the *rnr1*Δ mutant. While the levels of dATP appear similar between wild type cells and *rnr1*Δ mutants, the levels of the other three dNTPs are substantially reduced (Figure 2-9E). In particular, the percentage of dGTP is reduced from 16% in wild type cells to 6.6% in the *rnr1*Δ strain (Figure 2-9E). This reduction in dGTP, combined with the overall reduction in dNTPs, provides an explanation for the significantly shortened telomeres seen in *rnr1*Δ mutants (Figure 2-9A).

Human telomerase activity is dramatically affected by changes in dGTP concentration

Since our results suggest that telomerase and telomere length are extremely sensitive to dGTP levels, we decided to test whether our findings in yeast are evolutionarily conserved. We used the Telospot assay (Cristofari et al., 2007) to measure human telomerase activity while altering dNTP concentrations. In this assay, the telomerase RNA subunit, hTR, and the protein catalytic subunit, hTERT, are both strongly

overexpressed after transient transfection, yielding a situation referred to as "super-telomerase." Crude super-telomerase extract is incubated with a telomeric $(TTAGGG)_3$ primer with varying concentrations of dNTPs. A small fraction of the reaction is directly spotted onto a nylon membrane, which is then probed with a randomly radiolabeled telomeric probe. Since mammalian and *S. cerevisiae* dNTP pools are similar in concentration and in terms of the ratio of the four dNTPs (Nick McElhinny et al., 2010a; Sabouri et al., 2008; Traut, 1994), we used the yeast dNTP concentrations determined from the wild type strain used in Figure 2-4A as the starting point for our assays (Figure 2-10A). We maintained three of the dNTPs at these "physiological concentrations" while varying the fourth. Since human telomerase does not incorporate dCTP into telomeres, it is not surprising that varying dCTP has negligible effect on telomerase activity (Figure 2-10A and 2-10B). Titration of either dATP or dTTP does not dramatically affect telomerase activity either. However, consistent with our results from the yeast experiments, alteration of dGTP has a striking effect on telomerase activity (Figure 2-10A and 2-10B). Human telomerase activity is markedly reduced when dGTP concentrations are lowered, while activity is greatly increased even with modest increases in dGTP concentration.

An increase in telomerase activity in the Telospot assay is likely due to processive addition of telomere repeats to the primers to yield long extended products, but it could also result from many primers extended only shortly. To differentiate between these two scenarios, we repeated the reactions where dGTP concentration was varied using a 5′-biotinylated $(TTAGGG)_3$ primer and resolved the products on a polyacrylamide gel after purification with streptavidin-coated beads. The DNA was transferred onto a nylon

membrane and probed as in a standard Telospot assay (Figure 2-10C). Consistent with our telomerase activity measurements, telomerase repeat addition processivity, as measured by the increase in size of the fragments, positively correlates with dGTP concentration. These results indicate that the effect of dGTP levels on telomerase activity is an evolutionarily conserved feature.

DISCUSSION

In this study, we examined the effect of changing dNTP levels, including unbalancing the four dNTPs, on telomere length homeostasis in *S. cerevisiae*. When the ratio of the four dNTPs is maintained, we find that telomere length positively, but modestly, correlates with total dNTP levels. However, we demonstrate that altering the ratio of the dNTPs has a much more pronounced effect on telomere length homeostasis. Specifically, we show that both telomerase nucleotide addition processivity and telomere length positively correlate with dGTP levels. Furthermore, we find that the effect of dGTP on telomerase activity is conserved in humans.

Reduction of dNTPs leads to shorter telomeres but increase of dNTPs does not significantly affect telomere length

Although previous studies hinted at a connection between dNTP pools and telomere length homeostasis, our work is the first to document their precise relationship. We find that changing the total levels of dNTPs, without altering the ratio of the dNTPs, leads to a modest change in telomere length. Deletion of *DUN1* leads to a two-fold reduction in dNTPs and a ~50 bp reduction in telomere length (Figure 2-1A and 2-2). However, a

four-fold increase in dNTP levels leads to an increase in telomere length of less than 20 bp (Figure 2-2D). Thus, an excess of dNTPs results in a rather minimal increase in telomere length. We were unable to probe the telomere length effects of a reduction of dNTP levels greater than two-fold, without altering the ratio of the four dNTPs, because a mutant with such low levels has not been reported. Presumably, such a mutant would be inviable due to insufficient levels of dNTP required for DNA synthesis.

Mec1 mediates telomere length homeostasis by regulating dNTP levels

Previous work has shown that *mec1-21* mutants have shortened telomeres that can be rescued by deletion of *SML1* (Ritchie et al., 1999). Given that *mec1-21*, *dun1*Δ, and *dun1*Δ *mec1-21* mutants all have similar dNTP levels (Fasullo et al., 2010), we asked whether the shortened telomeres in the *mec1-21* mutant are due to reduced activation of Dun1. By epistasis analysis, we show this to be the case, with a *dun1*Δ *mec1-21* double mutant having the same telomere length as each of the single mutants (Figure 2-3). However, Mec1 has functions at the telomere that are Dun1-independent. While *mec1-21* *tel1*Δ double mutants senesce, similar to a telomerase-negative strain (Ritchie et al., 1999), *dun1*Δ *tel1*Δ mutants fail to senesce, despite repeated subculturings. Thus, while Mec1 affects telomere length homeostasis through Dun1-mediated regulation of dNTP pools, Mec1 also has Dun1-independent functions at the telomere.

Intracellular dGTP levels affect telomere length homeostasis by altering telomerase nucleotide addition processivity

The most surprising finding from our work is the strong dependence of telomere length homeostasis and telomerase activity on the levels of dGTP in the cell. Specifically, we find that the length of yeast telomeres positively correlates with intracellular dGTP levels (Figure 2-4). Furthermore, we show that yeast telomerase nucleotide addition processivity (Figure 2-7) and in vitro human telomerase activity (Figure 2-10) are both positively correlated with dGTP levels.

Consistent with our observations, yeast telomerase mutants that alter nucleotide addition processivity, as measured in vitro, positively correlate with the in vivo length of the telomeres (Peng et al., 2001), and this processivity is enhanced by increasing dGTP concentrations (Bosoy and Lue, 2004). However, these in vitro telomerase assays only examined the processivity of nucleotide addition using the 5′ portion of the TLC1 template region, whereas we were able to examine in vivo both the 3′ and 5′ portions and have found that reverse transcription of the 3′ portion is more dramatically affected by changes in dGTP levels.

Telomerase enzymes can also be characterized by their ability to add multiple repeats before dissociating (i.e. their repeat addition processivity). Yeast telomerase is generally non-processive at adding repeats, both in vitro (Cohn and Blackburn, 1995) and in vivo (Chang et al., 2007). However, yeast telomerase has the ability to processively elongate critically short telomeres in vivo (Chang et al., 2007), and limited repeat addition processivity can be observed in vitro by increasing dGTP concentration (Bosoy and Lue, 2004). In agreement with these findings in budding yeast, we also show that in

vitro human telomerase repeat addition processivity also positively correlates with dGTP levels (Figure 2-10C). In vitro studies of endogenous *Euplotes aediculatus* telomerase and recombinant *Tetrahymena thermophila* telomerase have also revealed a correlation between dGTP concentration and telomerase activity (Hammond and Cech, 1997, 1998; Hardy et al., 2001). However, these studies did not use in vivo dNTP concentrations as was done our in vitro human telomerase assays. Nevertheless, the ciliate studies revealed that binding of dGTP to telomerase stimulates repeat addition processivity. Interestingly, while we find that the percentage of total dNTPs that is dGTP is important in vivo in yeast (Figure 2-7), we find that it is the absolute concentration of dGTP, independent of the levels of the other three dNTPs, which is important for in vitro human telomerase activity (Figure 2-10). It is noteworthy that the biochemical characteristics of yeast, ciliate, and human telomerases are quite different. For example, they show differences in processivity, associate with different complements of proteins, and their RNA templates vastly differ (Mason et al., 2011). Thus, it is quite remarkable that the importance of dGTP levels on telomerase activity is highly conserved, even if the precise mechanism may differ in different species.

Our results indicate that intracellular dGTP levels are rate-limiting for both yeast and human telomerase activity. dNTP levels are most likely optimized for the DNA synthesis machinery. Low levels of dNTPs cause DNA replication fork stalling (Desany et al., 1998) while high levels of dNTPs result in an increase in mutation rate (Chabes et al., 2003a; Reichard, 1988). It has also been shown that even mild dNTP pool imbalances are mutagenic (Kumar et al., 2010). However, our work suggests that telomere length homeostasis may also impose selective pressure on optimal intracellular dGTP levels.

Indeed, of the four dNTPs, dGTP levels are kept the lowest both in yeast (Chabes et al., 2003a) and mammalian cells (Traut, 1994) perhaps reflecting an evolutionarily conserved mechanism to regulate telomerase activity and telomere length homeostasis.

Finally, our findings may provide new strategies to regulate telomerase activity therapeutically. For example, telomerase is repressed in most human somatic cells but is expressed in ~85% of cancers (Shay and Bacchetti, 1997) and telomerase has been viewed as an ideal target to inhibit the growth of a wide range of tumors. Identifying agents that reduce intracellular dGTP levels may be effective in limiting the proliferation of cancer cells. Furthermore, several human diseases are associated with shortened telomeres. Individuals born with reduced telomerase activity have short telomeres, leading to telomere dysfunction in highly proliferative cells (Armanios, 2009). Indeed, many of these individuals are haploinsufficient for telomerase and have shortened lifespans, suggesting that full telomerase activity is important in preventing these diseases. Perhaps elevating the levels of dGTP to increase telomerase activity will be effective in treating these individuals. Thus, it will be of significant interest to find ways to modulate intracellular dGTP levels as a mechanism to regulate telomerase activity.

EXPERIMENTAL PROCEDURES

Yeast media and strains

Standard yeast media and growth conditions were used (Sherman, 1991). Yeast strains used in this study are listed in Table 2-1.

Telomere PCR and sequencing

Yeast genomic DNA was isolated using a Yeast DNA Extraction Kit (Thermo Scientific). Y′ telomeres and telomere VI-R were amplified by PCR as previous described (Chang et al., 2007; Pardo et al., 2006). Telomere VI-R PCR products were cloned using a PCR Cloning Kit (Qiagen). Sequencing was performed by GENEWIZ (New Jersey, USA) and BaseClear (the Netherlands) and the resulting sequence data were analyzed using Sequencher software (Gene Codes).

Determination of dNTP pools

dNTP levels were measured as previously described (Chabes et al., 2003a).

Flow cytometry

Flow cytometry was performed as previously described (Sabouri et al., 2008).

Protein blotting

Protein extracts were prepared as previously described (Peter et al., 1993). For Rnr2, Rnr3, and Sml1 detection, affinity purified rabbit polyclonal anti-Rnr2 (AS09 575), anti-Rnr3 (AS09 574), and anti-Sml1 (AS10 847) antibodies (Agrisera AB, Sweden) were used at 1:500,000, 1:1000 and 1:5000 dilutions, respectively. For detection of both Rnr4 and α-tubulin, YL1/2 rat monoclonal antibody (Sigma) was used at a 1:2500 dilution (Tsaponina et al., 2011).

Telospot

Telospot assays were performed as previously described (Cristofari et al., 2007), except that the membrane was not denatured with NaOH. For Figure 2-10C, Telospot reactions were performed with 35 nM 5′-biotinylated $(TTAGGG)_3$ primer, which were then purified using 10 µl of streptavidin-coated M-280 Dynabeads (Invitrogen) according to the manufacturer's protocol. Samples were heated to 98°C for 5 min in 98% formamide-10 mM EDTA, resolved on a 12% polyacrylamide-urea gel, and transferred onto a positively charged Nylon membrane (GE Healthcare) using a semi-dry electrophoretic transfer cell (Transblot SD, BIO-RAD). After UV-crosslinking, the membrane was probed as in a standard Telospot assay.

ACKNOWLEDGEMENTS

We would like to thank Peter Thorpe for constructive comments on the manuscript; Stephen Elledge for providing strains; Dinesh Kumar for help in constructing yeast strains; Ivana Sunjevarić for allowing us to cite her unpublished data; and Gaël Cristofari for advice on the Telospot assays. S.S. was supported by a stipend from the Wenner-Gren Foundations. M.C. was supported by a Terry Fox Foundation Fellowship Award. This work was supported by funds from the Swiss National Science Foundation and a European Research Council advanced investigator grant (to J.L.); the Swedish Foundation for Strategic Research, the Swedish Research Council, and the Swedish Cancer Society (to A.C.); and the US National Institutes of Health (GM50237 and GM67055 to R.R.).

Note added in dissertation:

This work was performed under the supervision of Michael Chang and in collaboration with the labs of Andrei Chabes and Joachim Lingner. The members of the Chabes lab performed the dNTP measurements in the different strains and provided the *rnr1* mutants. The Lingner lab performed the telospot assay. However, special thanks must go to Michael Chang who assisted in experimental design and analysis.

Figure 2-1

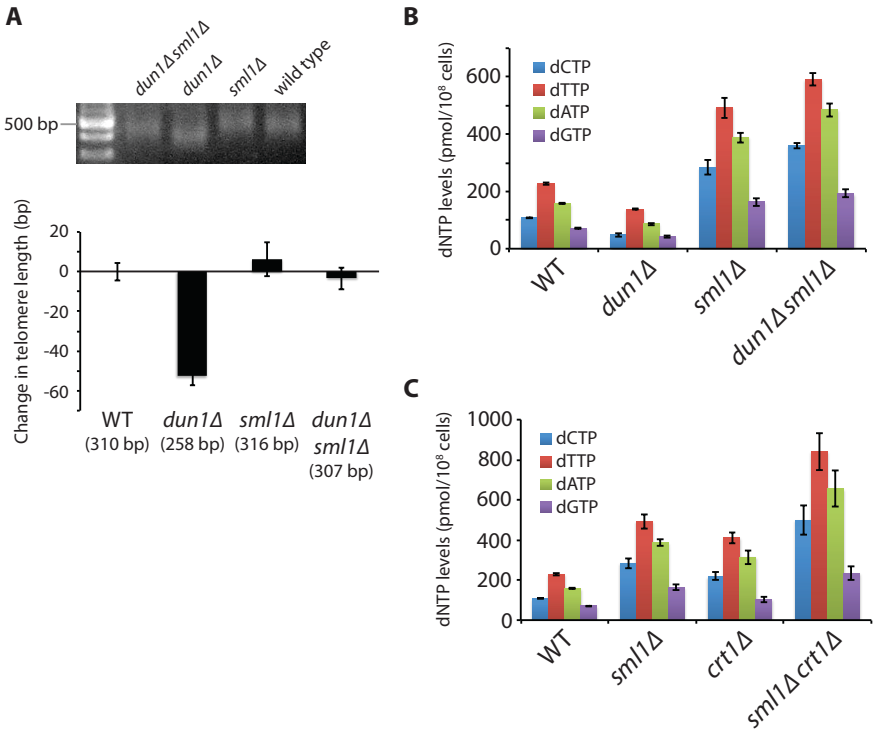

Figure 2-1: Decreasing dNTP levels results in shorter telomeres. (**A**) Strains of the indicated genotypes, generated from the sporulation of a *dun1*Δ/+ *sml1*Δ/+ diploid, were assayed for telomere length by Y′ telomere PCR after being passaged for at least 100 generations. The change in telomere length, compared to wild type telomere length, was quantified and plotted. Mean ± standard error for four independent isolates of each strain are shown. Similar results were obtained by assaying telomere length by telomere I-L PCR and by denaturing in-gel hybridization (Figure 2-2). (**B**) Strains in **A** were assayed for dNTP levels. Four independent isogenic strains for each genotype were analyzed. Data are represented as mean ± standard error. (**C**) Strains of the indicated genotypes were assayed for dNTP levels, as in **B**.

Figure 2-2

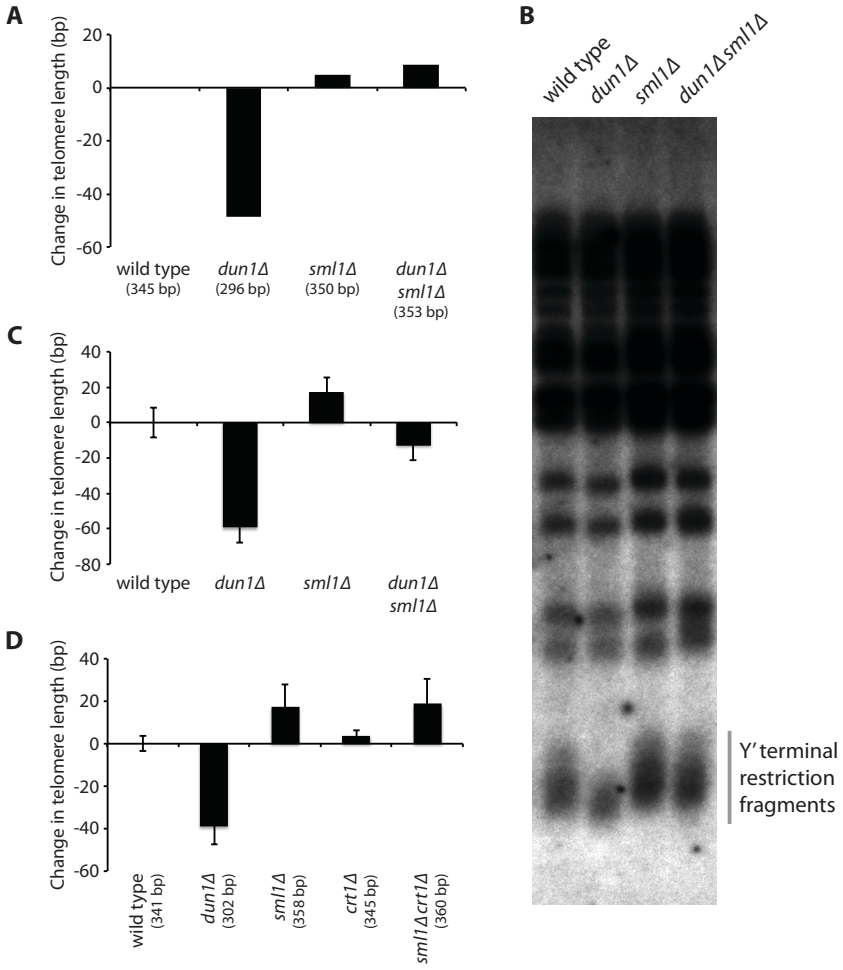
A
Change in telomere length (bp)
20
0
-20
-40
-60
wild type
(345 bp)
dun1Δ
(296 bp)
sml1Δ
(350 bp)
dun1Δ
sml1Δ
(353 bp)
B
wild type
dun1Δ
sml1Δ
dun1Δsml1Δ
Y′ terminal
restriction
fragments
C
Change in telomere length (bp)
40
20
0
-20
-40
-60
-80
wild type
dun1Δ
sml1Δ
dun1Δ
sml1Δ
D
Change in telomere length (bp)
40
20
0
-20
-40
-60
wild type
(341 bp)
dun1Δ
(302 bp)
sml1Δ
(358 bp)
crt1Δ
(345 bp)
sml1Δ crt1Δ
(360 bp)

Figure 2-2: Telomeres are shortened in cells lacking Dun1. (**A**) Strains of the indicated genotypes were assayed for telomere length by telomere I-L PCR after being passaged for at least 100 generations. The change in telomere length, compared to wild type telomere length, was quantified and plotted. (**B**) Strains in **A** were assayed for telomere length by denaturing in-gel hybridization (see Materials and Methods). The vertical bar indicates the position of the terminal restriction fragments of Y' telomeres, which represent more than half of yeast telomeres. Larger bands represent non-Y'-containing telomeres. (**C**) The change in telomere length, compared to wild type telomere length, of each strain indicated in **B** was quantified and plotted. Mean ± standard error for four independent isolates of each genotype are shown. (**D**) The change in telomere length, compared to wild type telomere length, of strains of the indicated genotypes, as assayed by Y' telomere PCR, was quantified and plotted. Mean ± standard error for at least three independent isolates for each genotype are shown.

Figure 2-3

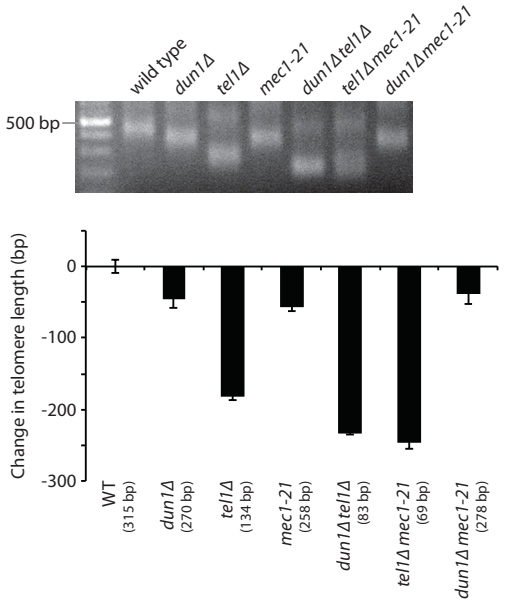

Figure 2-3: Mec1 and Dun1 function in the same pathway to regulate dNTP pools and telomere length homeostasis. Strains of the indicated genotypes, generated from the sporulation of a *dun1*Δ/+ *tel1*Δ/+ *mec1-21*/+ diploid, were assayed for telomere length by Y′ telomere PCR after being passaged for ~50 generations. The change in telomere length, compared to wild type telomere length, was quantified and plotted. Mean ± standard error for three independent isolates are shown. Note that the triple mutant is not viable (data not shown).

Figure 2-4

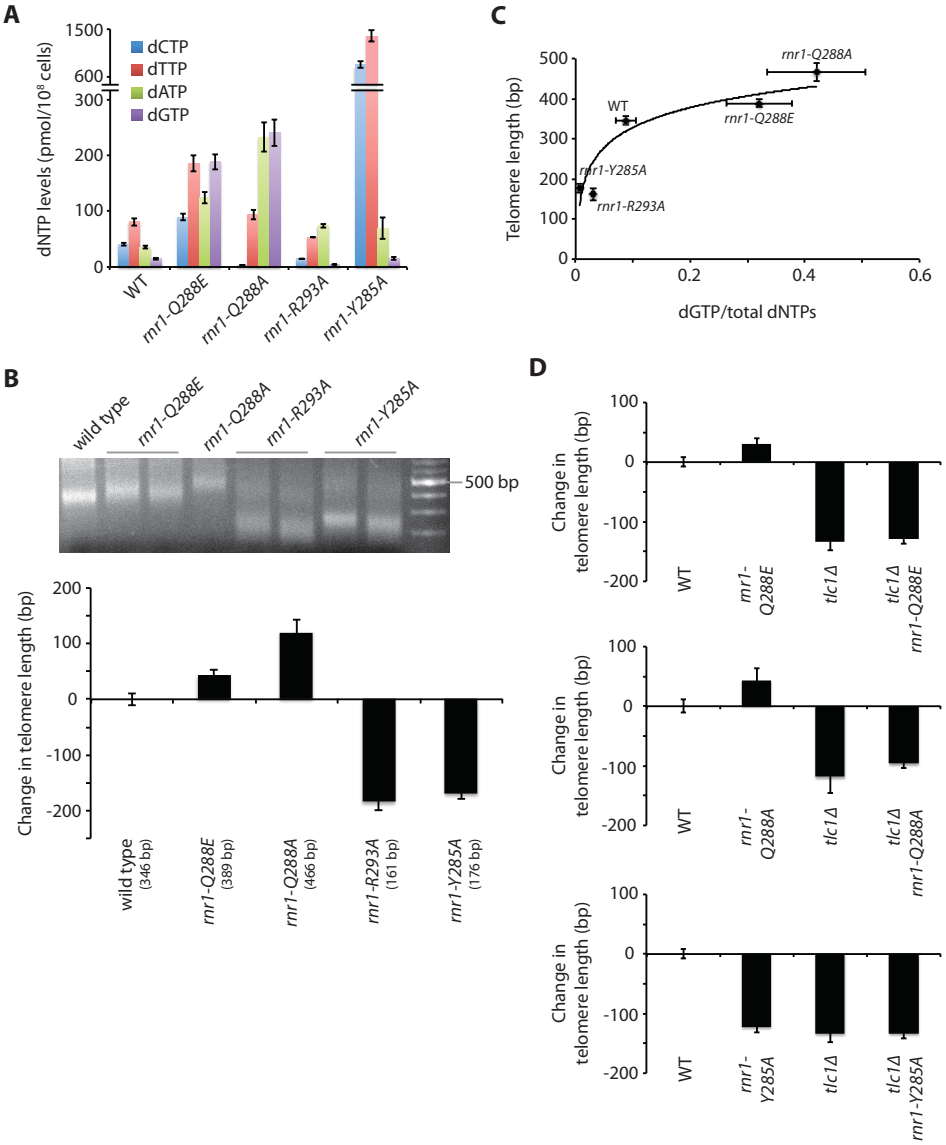
A
dNTP levels (pmol/10^8 cells)
dCTP
dTTP
dATP
dGTP
WT
rnr1-Q288E
rnr1-Q288A
rnr1-R293A
rnr1-Y285A
C
Telomere length (bp)
dGTP/total dNTPs
WT
rnr1-Q288A
rnr1-Q288E
rnr1-Y285A
rnr1-R293A
B
wild type
rnr1-Q288E
rnr1-Q288A
rnr1-R293A
rnr1-Y285A
500 bp
Change in telomere length (bp)
wild type (346 bp)
rnr1-Q288E (389 bp)
rnr1-Q288A (466 bp)
rnr1-R293A (161 bp)
rnr1-Y285A (176 bp)
D
Change in telomere length (bp)
WT
rnr1-Q288E
tlc1Δ
tlc1Δ rnr1-Q288E
rnr1-Q288A
tlc1Δ rnr1-Q288A
rnr1-Y285A
tlc1Δ rnr1-Y285A

Figure 2-4: Telomere length positively correlates with percentage of intracellular dGTP. (**A**) dNTP concentrations in a wild type strain and the *rnr1* mutants were measured. Mean ± standard error is shown for each strain. Data for the wild type, *rnr1-Q288A*, *rnr1-R293A*, and *rnr1-Y285A* strains were previous reported (Kumar et al., 2010). (**B**) Strains of the indicated genotypes were assayed for telomere length by telomere VI-R PCR after being passaged for at least 100 generations. The change in telomere length, compared to wild type telomere length, was quantified and plotted. Mean ± standard error for at least three independent isolates are shown. (**C**) Strains of the indicated genotype were plotted for telomere length versus dGTP as a fraction of total dNTP levels. Each point indicates the mean for each of these values and error bars indicate the standard error. (**D**) Strains of the indicated genotypes, generated from the sporulation of *rnr1*/+ *tlc1*Δ/+ diploids, were assayed for telomere length by Y′ telomere PCR after being passaged for ~30 generations. The change in telomere length, compared to wild type telomere length, was quantified and plotted. Mean ± standard error for three independent isolates are shown.

Figure 2-5

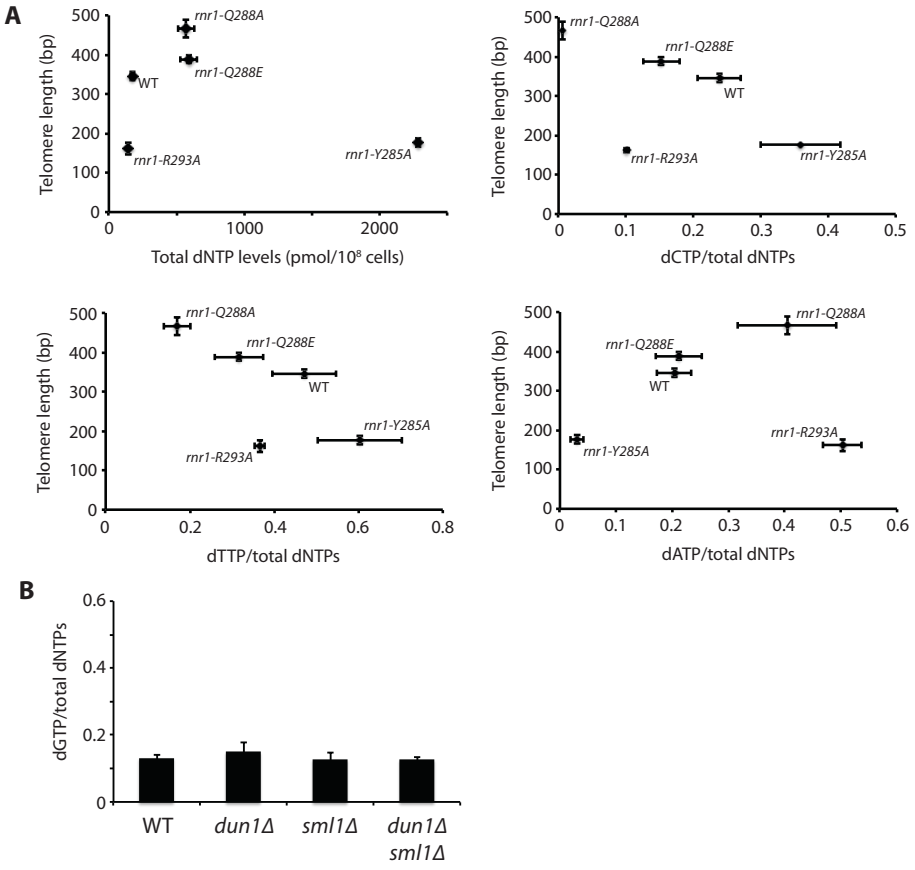

Figure 2-5: Altering relative amounts of dCTP, dTTP, or dATP shows no correlation with telomere length homeostasis. (**A**) Telomere length changes observed in the *rnr1* mutants do not correlate with total dNTP levels (top left), or the percentages of dCTP (top right), dTTP (bottom left), or dATP (bottom right). (**B**) Percentage of dGTP is unchanged in the strains analyzed in Figure 2-1

Figure 2-6

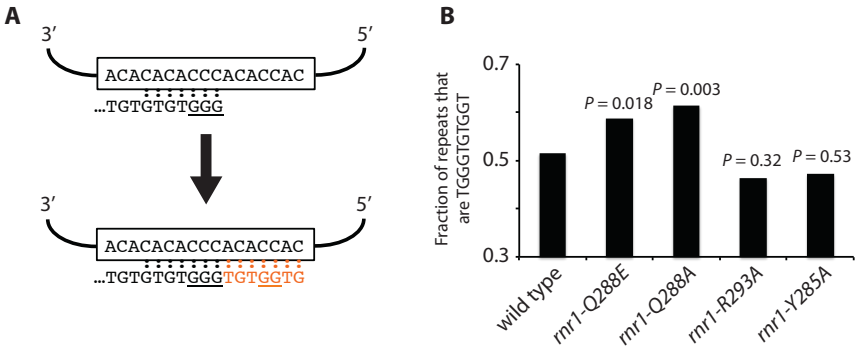

Figure 2-6: The processivity of reverse transcription of the 5' portion of the TLC1 template region is increased in the *rnr1-Q288E* and *rnr1-Q288A* mutants. (**A**) Schematic illustrating the reverse transcription of the 5' portion of the TLC1 template region, which is shown in the boxed area. Almost all telomeric repeats contain a GGG trinucleotide, but only about 50% of these repeats also contain the GG dinucleotide specified by the 5' portion of the template region. (**B**) The fraction of GG-containing repeats (i.e. TGGGTGTGGT) is plotted for a wild type strain and the four *rnr1* mutants. The rnr1-Q288E and rnr1-Q288A mutants, which have elongated telomeres, exhibitan increase in the presence of GG-containing repeats, indicating that telomerase nucleotide addition processivity for the 5' portion of the TLC1 template region is increased. *P* values were determined using a chi-squared test to look whether a given mutant was significantly different from wild type.

Figure 2-7

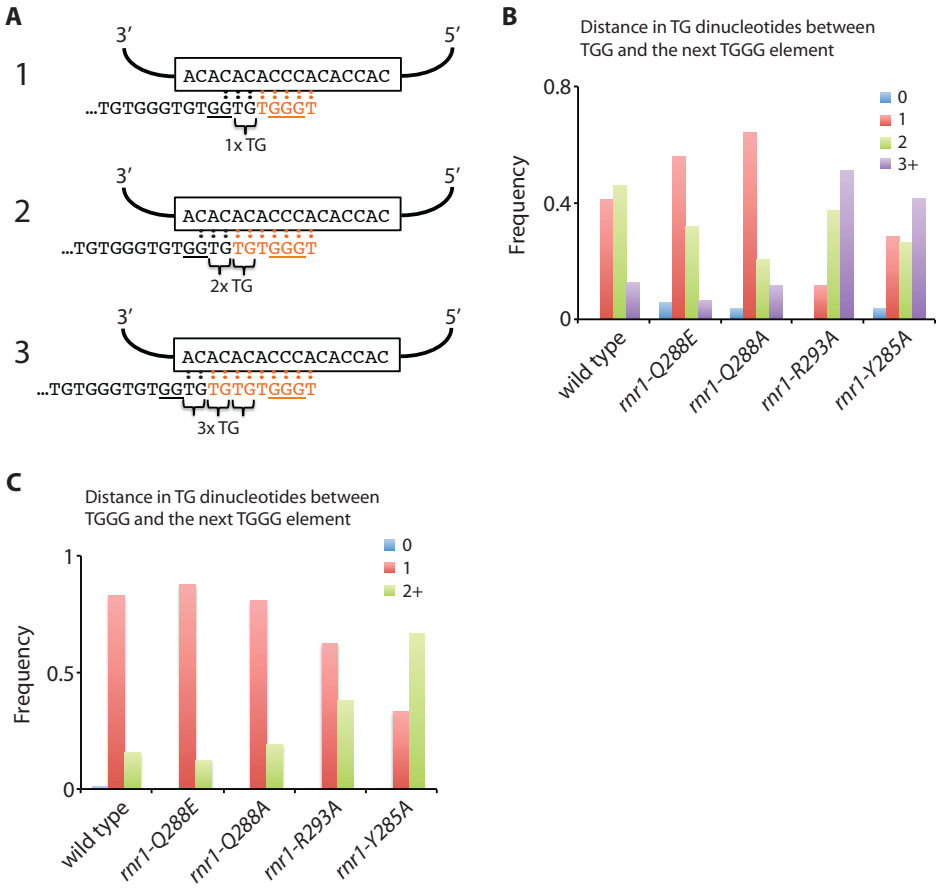

Figure 2-7: Telomerase nucleotide addition processivity is affected by dGTP levels. (**A**) Schematic illustrating three possible alignments for a telomere ending in -TGGTG with the template region of TLC1. Following reverse transcription and extension of the telomere (with added nucleotides shown in orange), the number of TG dinucleotides between the TGG motif and the following TGGG motif will vary. (**B**, **C**) For strains of the indicated genotypes, telomere VI-R was amplified by PCR, cloned and sequenced. (**B**) The frequency of having 0, 1, 2, or 3 and higher TG dinucleotides between a TGG and the following TGGG was plotted for each strain. (**C**) The frequency of having 0, 1, or 2 and higher TG dinucleotides between a TGGG and the following TGGG was plotted for each strain.

Figure 2-8

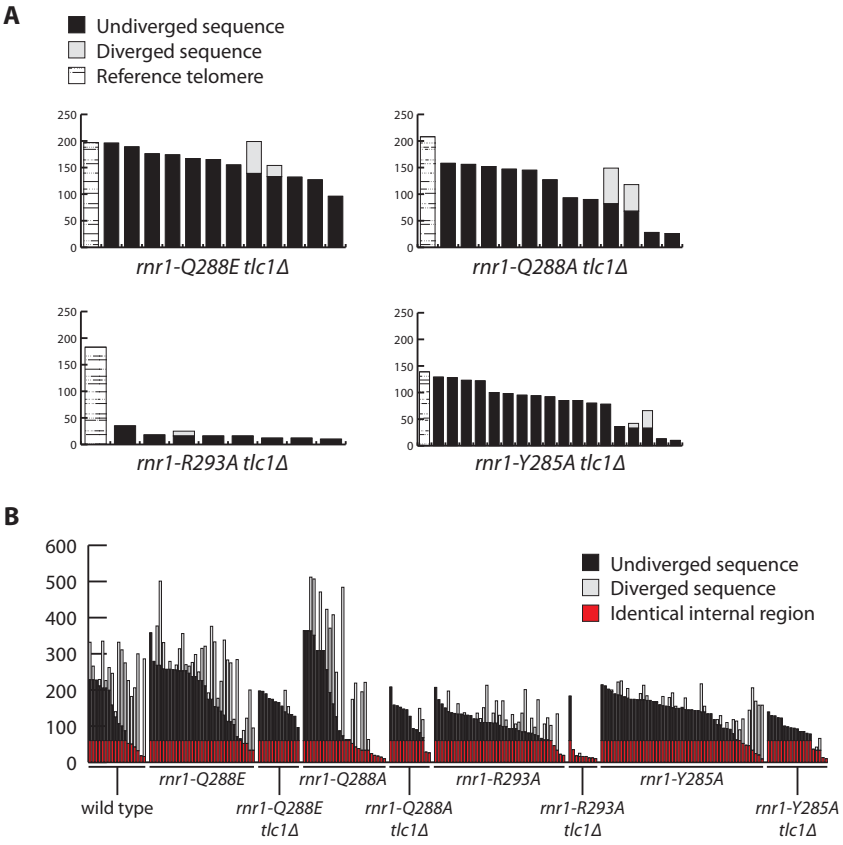

Figure 2-8: The telomere sequence changes in the *rnr1* mutants recorded in Figure 2-7 are telomerase dependent. (**A**) Analysis of sequenced VI-R telomeres after ~30 generations of clonal expansion. Each bar represents an individual VI-R telomere and bars are sorted by the length of the undiverged sequence. The black portion of each bar represents the undiverged region of the telomere. The light gray portion represents the diverged region of the telomere. For each strain, the longest telomere without divergent sequence (hashed bar) is used as a reference telomere to which all other telomeres are compared to determine whether divergence has occurred. (**B**) All telomeres from all strains analyzed in this study share an identical internal region (as indicated by the red portion of each bar).

Figure 2-9

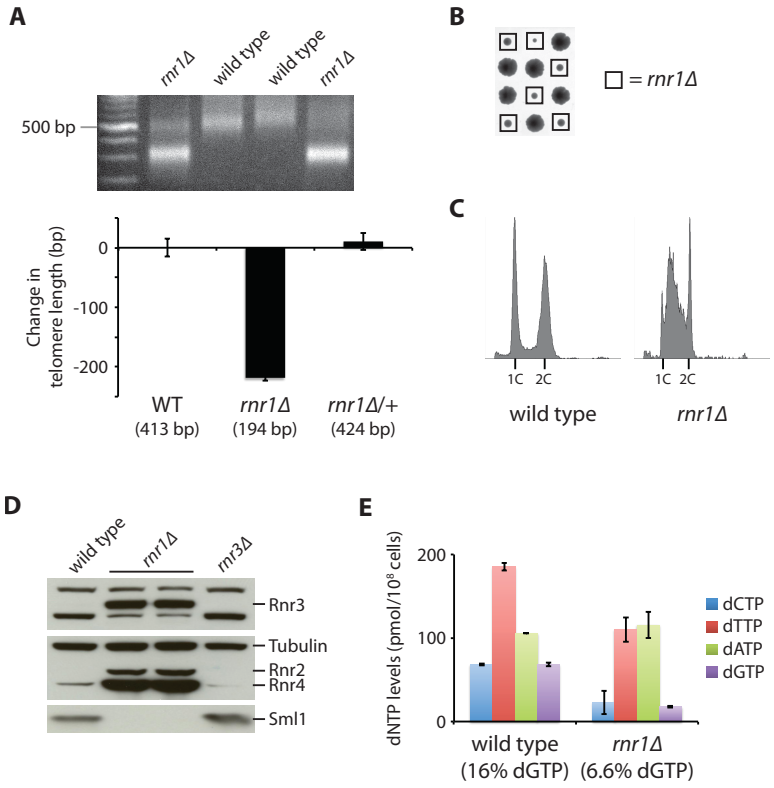

Figure 2-9: *rnr1*Δ mutants have shortened telomeres due to reduced dGTP levels. (**A**) An *rnr1*Δ mutant from the yeast gene deletion collection was backcrossed to wild type strain (BY4741) twice. The resulting wild type and *rnr1*Δ progeny strains, along with a heterozygous *rnr1*Δ/+ diploid, were assayed for telomere length by Y′ telomere PCR after being passaged for at least 100 generations. The change in telomere length, compared to wild type telomere length, was quantified and plotted. Mean ± standard error for at least four independent isolates (two for the *rnr1*Δ/+ diploid) are plotted. (**B**) Tetrad analysis reveals that an *rnr1*Δ strain exhibits slow growth. Each column of four colonies is a single tetrad derived from the sporulation of an *rnr1*Δ/+ diploid followed by the separation of the four haploid spores by micromanipulation. (**C**) Flow cytometry histograms for the indicated strains derived from **B**. (**D**) Wild type, *rnr1*Δ, and *rnr3*Δ strains were assayed for Rnr3, Rnr2, Rnr4, and Sml1 protein levels by protein blot analysis. Tubulin levels were also assayed as a loading control. (**E**) dNTP pools in the wild type and *rnr1*Δ strains were measured. Data are represented as mean ± standard error. dGTP levels, as a percentage of total dNTPs, are indicated for each strain.

Figure 2-10

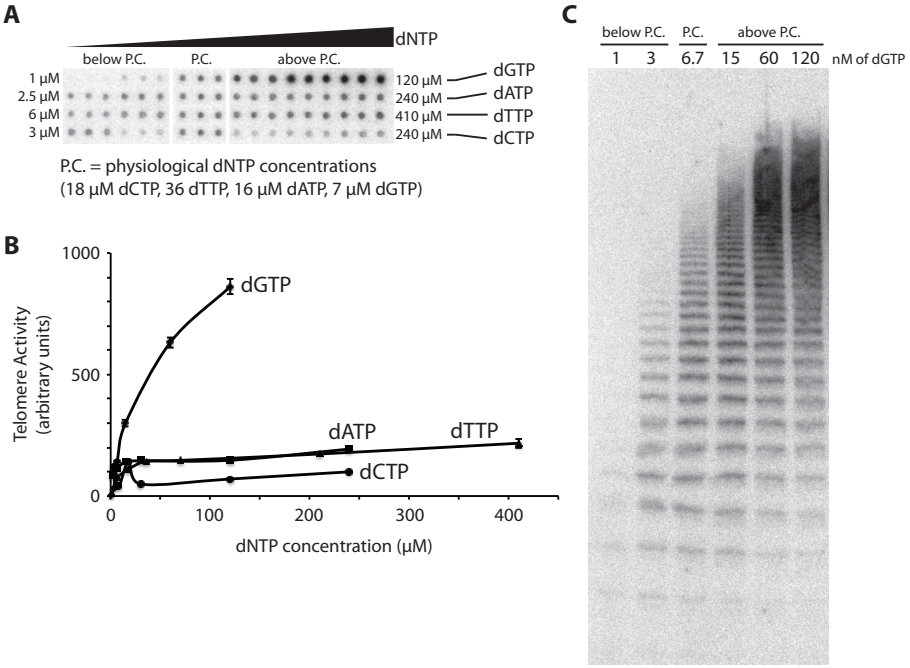
A
dNTP
below P.C.
P.C.
above P.C.
1 µM
2.5 µM
6 µM
3 µM
120 µM
240 µM
410 µM
240 µM
dGTP
dATP
dTTP
dCTP
P.C. = physiological dNTP concentrations
(18 µM dCTP, 36 dTTP, 16 µM dATP, 7 µM dGTP)
B
Telomere Activity
(arbitrary units)
1000
500
0
dGTP
dATP
dTTP
dCTP
0
100
200
300
400
dNTP concentration (µM)
C
below P.C.
P.C.
above P.C.
1
3
6.7
15
60
120
nM of dGTP

Figure 2-10: Human telomerase activity positively correlates with dGTP levels. (**A**) Telospot assay was performed by incubating crude "super-telomerase" extracts with a telomeric $(TTAGGG)_3$ primer and varying concentrations of dNTPs. "Physiological dNTP concentrations" used are derived from concentrations in yeast, although concentrations in mammalian cells are in the same range, as explained in the text. A small fraction of the reaction was directly spotted onto a nylon membrane, which is then probed with a randomly radiolabeled telomeric probe. Each reaction was spotted in triplicate. Each row of spots varies one of the four dNTPs, as indicated, from the lowest concentration shown on the left side to the highest concentration shown on the right. The reaction performed using physiological concentrations of all four dNTPs were spotted in triplicate, and then copy and pasted into each row for clarity. (**B**) Activity in each spot from **A** was quantified, and the mean for each reaction was plotted as a function of the concentration of the indicated dNTP. Error bars indicate the standard error. (**C**) The Telospot reactions with varying dGTP concentrations were repeated using a 5′-biotinylated $(TTAGGG)_3$ primer, purified with streptavidin-coated beads, resolved on a polyacrylamide gel, and transferred onto a nylon membrane. The membrane was then probed as in **A**. The concentration of dGTP used for each reaction is indicated above each lane.

Table 2-1: Yeast strains used in this study. All strains are derivatives of W1588-4C, except for BY4742 and W9882. W9882 is a derivative of BY4742.

Strain	Genotype	Reference
W1588-4C	*MAT***a** *ade2-1 can1-100 his3-11,15 leu2-3,112 trp1-1 ura3-1 RAD5*	(Zhao et al., 1998)
W9557	*MAT***a**/α *dun1Δ::TRP1*/+ *sml1Δ::HIS3*/+	This study
W9875	*MAT***a**/α *dun1Δ::TRP1*/+ *sml1Δ::HIS3*/+ *crt1Δ::LEU2*/+	This study
W9877	*MAT***a**/α *dun1Δ::TRP1*/+ *tel1Δ::URA3*/+ *mec1-21*/+	This study
DK2A	*MAT*α *rnr1::[rnr1-R293A-URA3-pGAL-RNR1]*	(Kumar et al., 2010)
DK2D	*MAT***a** *rnr1::[rnr1-R293A-URA3-pGAL-RNR1]*	(Kumar et al., 2010)
DK8A	*MAT***a** *rnr1::[rnr1-Y285A-URA3-pGAL-RNR1]*	(Kumar et al., 2010)
DK8E	*MAT*α *rnr1::[rnr1-Y285A-URA3-pGAL-RNR1]*	(Kumar et al., 2010)
DK10E	*MAT***a** *rnr1::[rnr1-Q288A-URA3-pGAL-RNR1]*	(Kumar et al., 2010)
JAK11-5B	*MAT*α *rnr1::[rnr1-Q288E-URA3-pGAL-RNR1]*	This study
JAK11-5C	*MAT***a** *rnr1::[rnr1-Q288E-URA3-pGAL-RNR1]*	This study
W9878	*MAT***a**/α *rnr1::[rnr1-Q288E-URA3-pGAL-RNR1]*/+ *tlc1Δ::HIS3*/+	This study
W9879	*MAT***a**/α *rnr1::[rnr1-Q288A-URA3-pGAL-RNR1]*/+ *tlc1Δ::HIS3*/+	This study
W9880	*MAT***a**/α *rnr1::[rnr1-R293A-URA3-pGAL-RNR1]*/+ *tlc1Δ::HIS3*/+	This study
W9881	*MAT***a**/α *rnr1::[rnr1-Y285A-URA3-pGAL RNR1]*/+ *tlc1Δ::HIS3*/+	This study
BY4742	*MAT*α *his3Δ1 leu2Δ0 lys2Δ0 ura3Δ0*	(Brachmann et al., 1998)
W9882	*MAT***a**/α *rnr1Δ::kanMX*/+	This study

CHAPTER 3:

NOVEL FUNCTION OF SML1, THE HUMAN MIS18α ORTHOLOG, LINKS THE DNA DAMAGE AND SPINDLE ASSEMBLY CHECKPOINTS

ABSTRACT

Sml1, the inhibitor of the large subunit of ribonucleotide reductase (RNR), Rnr1, is a downstream target of the DNA damage checkpoint that is rapidly degraded following damage. We performed a high-throughput screen to identify novel *Saccharomyces cerevisiae* genes that function in the regulation of Sml1. We found a strong enrichment in genes involved in mitosis, including factors important for kinetochore function, sister chromatid cohesion and the spindle assembly checkpoint. Strikingly, loss of *SML1* in conjunction with deletions of these mitosis-related genes leads to synthetic growth defects that are independent of altered dNTP levels, thus indicating a novel function for Sml1. We discovered that loss of *SML1* results in increased chromosome loss as a consequence of spindle defects. These defects can further be traced to a delay in kinetochore assembly due to a reduction in Scm3 localization. This result, along with protein sequence comparison, allowed us to identify Sml1 as the ortholog of human Mis18α, a factor important in kinetochore establishment. Furthermore, both *Schizosaccharomyces pombe* Mis18 and human Mis18α complement the kinetochore defect seen in a *sml1*Δ strain as well as the growth defect seen in the double mutants containing *sml1*Δ and the mitosis mutants. Here, we propose a new model whereby Sml1 connects the DNA damage checkpoint and the spindle assembly checkpoint by virtue of its novel function.

INTRODUCTION

Cell propagation in all eukaryotes depends on accurate chromosome segregation. To assure accuracy, eukaryotic cells utilize two evolutionarily conserved checkpoints to delay cell cycle progression in cells with genomic problems: the spindle assembly checkpoint (SAC) and the DNA damage checkpoint or response (DDR) (Finn et al., 2011; Musacchio and Salmon, 2007). While the SAC ensures that all chromosomes are correctly bioriented at the metaphase plate for an accurate mitosis, the DDR monitors the status of the DNA to verify that it is free of lesions.

The primary functions of the DDR is to ensure that, following DNA damage, the cell has adequate nucleotides to repair its DNA (Chabes et al., 2003a). In *S. cerevisiae*, *de novo* dNTP production by the enzyme ribonucleotide reductase (RNR) is the sole method of nucleotide production, leading to multifaceted regulation of this enzyme (Huang et al., 1998; Lee and Elledge, 2006; Lee et al., 2008; Reichard, 1988; Wu and Huang, 2008; Zhao et al., 1998). Modulation of RNR occurs through transcriptional repression of the *RNR* genes by Crt1 (Huang et al., 1998), relocalization of the small subunits of RNR, Rnr2 and Rnr4, to the nucleus by Wtm1 and Dif1 (Lee and Elledge, 2006; Lee et al., 2008; Wu and Huang, 2008), and crucially, by direct inhibition of the large subunit of RNR, Rnr1, by Sml1 (Chabes et al., 1999; Zhao et al., 1998). Following DNA damage, Dun1 phosphorylates Crt1 (Huang et al., 1998), Sml1 (Zhao and Rothstein, 2002) Wtm1, and Dif1 (Lee and Elledge, 2006; Lee et al., 2008; Wu and Huang, 2008), leading to an increase in dNTP pools. Phosphorylated Sml1 no longer associates with Rnr1 and is subsequently ubiquitylated by the Rad6-Ubr2-Mub1 ubiquitin ligase complex, facilitating its degradation by the proteasome (Figure 3-1A) (Andreson et al., 2010). The degradation

of Sml1 occurs rapidly and is often detectable before significant Rad53 phosphorylation is seen (Barlow et al., 2008; Torres-Rosell et al., 2007). As such, monitoring Sml1 degradation serves as a very sensitive indicator of DNA damage.

The evolutionarily conserved DDR acts at three different stages to arrest the cell cycle and enable repair of the DNA following a break, including at G2/M, where it acts in conjunction with the SAC (Paulovich et al., 1997). In *S. cerevisiae*, as well as in higher eukaryotes, the apical kinases, Mec1 (yeast ortholog of human ATR) and Tel1 (yeast ortholog of human ATM), play a critical role in the DDR pathway (Finn et al., 2011; Navadgi-Patil and Burgers, 2009). Repair of a DNA double-strand break begins with processing of the broken ends by numerous resection factors (Mimitou and Symington, 2011). The resulting single-stranded DNA (ssDNA) is coated by the multi-protein complex, RPA, which is subsequently bound by the 9-1-1 clamp complex—Ddc1, Mec3, and Rad17 in *S. cerevisiae*—with the assistance of the RFC-like clamp loader Rad24-RFC (Navadgi-Patil and Burgers, 2009). The combination of both the RPA-coated ssDNA and the 9-1-1 complex recruits Mec1 along with its partner Ddc2 (Barlow et al., 2008). Mec1 transduces the signal further through phosphorylation of the downstream signaling kinase Rad53 (yeast ortholog of human CHK2), which in turn phosphorylates Dun1 (Figure 1A) (Zhou and Elledge, 1993). At the G2/M checkpoint, the Mec1-Rad53-Dun1 pathway contributes 50% to the arrest. However, Mec1 has also been shown to regulate Pds1, which makes up the other 50% of the arrest (Gardner et al., 1999).

Pds1 is the yeast securin protein, which inhibits the separation of sister chromatids by binding separase. Pds1 stability is dependent on the alignment of the chromosomes as detected by the SAC. However, the SAC is triggered by numerous

events, including lack of microtubule-kinetochore attachments (Musacchio and Salmon, 2007; Pinsky and Biggins, 2005), kinetochore establishment defects (Camahort et al., 2007; Stoler et al., 2007), and defects in the DDR (Garber and Rine, 2002; Kim and Burke, 2008). The SAC is comprised of Mad1, Mad2, Mad3 (BubR1 in humans), Bub1, and Bub3 (Musacchio and Salmon, 2007). Several other proteins assist the SAC to ensure the fidelity of chromosome attachments, including tension sensor Sgo1 (Indjeian et al., 2005; Pinsky and Biggins, 2005). The SAC is turned off when all chromosomes are correctly bioriented and aligned on the metaphase plate (Musacchio and Salmon, 2007) with appropriate tension between the sister chromatids (Pinsky and Biggins, 2005). This allows Pds1 to be degraded and the chromosomes to appropriately segregate.

In this study, we performed a high-throughput microscopy screen, monitoring Sml1 degradation following DNA damage and discovered cross-talk between the DDR with genes involved at the kinetochore, including both the SAC as well as the tension sensor, Sgo1. Further analysis revealed that the stabilization of Sml1 in mutants of the SAC, the alternative-RFC, and Sgo1 was important for growth of the cells. Interestingly, we found that the interaction was not due to increased dNTP levels, thus indicating an additional function for Sml1 that is independent of its effect on the regulation of nucleotide pool levels. A homology search against other kinetochore establishment proteins implicated Sml1 as the yeast ortholog of the human Mis18α and the *S. pombe* Mis18 proteins, which are necessary for recruiting centromere proteins. Either hMis18α or spMis18 complements the kinetochore defects seen in *sml1*Δ strains.Thus, a second function for Sml1 was identified as a role in kinetochore establishment.

RESULTS

Systematic identification of genes involved in Sml1 degradation following DNA damage

Sml1 is a very sensitive indicator of DNA damage, with degradation of Sml1 coinciding with checkpoint activation (Barlow et al., 2008; Torres-Rosell et al., 2007). We took advantage of this sensitivity to screen for genes that are involved in the degradation of Sml1 following damage. We constructed a plasmid containing YFP-Sml1 under control of its native promoter and introduced it into the non-essential yeast deletion library (Winzeler et al., 1999) using selective ploidy ablation (Reid et al., 2011). The resulting strains were grown up in 96 well plates at 23˚C and treated with 100 Gy of γ-rays. Cells from each plate were placed on two 48-agar pedestal arrays (Werner et al., 2009) and scored by eye under the microscope for presence of YFP-Sml1 between 45 and 105 minutes after damage (Figure 3-1B). Mutants that showed significant YFP-Sml1 stabilization were re-tested to confirm the phenotype.

For most strains, the YFP-Sml1 signal was completely abolished following DNA damage (Figure 3-1C). However, in 39 mutants, YFP-Sml1 was still visible even as late as 105 minutes following irradiation (Figure 3-1C; Table 3-1). Some of these genes, such as *MEC3*, *DDC1*, *RAD24*, *RAD9*, and *DUN1*, function in the DDR (Harrison and Haber, 2006; Navadgi-Patil and Burgers, 2009) (Figure 3-1A), and have all been previously implicated in Sml1 stability (Zhao et al., 2001; Zhao and Rothstein, 2002). Furthermore, the screen also identified the *RAD6*, *UBR2*, and *MUB1* group of genes that function together to ubiquitylate Sml1 (Andreson et al., 2010). Identification of these previously implicated genes highlights the sensitivity of the screen.

Surprisingly, the largest group of mutants identified by the screen was the kinetochore/spindle group of genes, which includes the SAC – *MAD1*, *MAD2*, *MAD3*, *BUB1*, and *BUB3* – as well as the tension sensor, *SGO1* (Table 3-1). Furthermore, many components involved in sister chromatid cohesion were also identified. Taken together, these data indicate that genes that function in mitosis may also play a role in YFP-Sml1 stability. Previous work from the Rine and Burke labs showed that, following DNA damage, the DDR and the SAC redundantly function to arrest the cells to allow for repair (Garber and Rine, 2002; Kim and Burke, 2008). Our data indicate that the SAC and the components of the kinetochore may play a more direct role in regulating one of the downstream targets of the DDR following DNA damage.

Determining synthetic interactions with *sml1*Δ

To understand what roles these different genes play in Sml1 regulation, we next tested whether stabilization of Sml1 was necessary for viability in the different mutants. All 39 mutants identified by the screen (Table 3-1) were crossed to a *sml1*Δ strain, and the growth of all four haploid progeny was monitored (see Materials and Methods). Since some of the genes analyzed can affect meiosis (Petronczki et al., 2004), we performed tetrad analysis to allow the identification and removal of spore clones that were the products of aberrant meiosis, thus leading to a more accurate measurement of growth for the two parental and two recombinant genotypes. Furthermore, viable and inviable spore clones were separated and analyzed independently to control for instances where single mutants showed increased spore lethality, which aberrantly underestimates the expected colony size of the double mutant (see Materials and Methods for details). We used the

growth analysis to identify significant interactions, which were then filtered based on spore lethality.

The only mutants that grew significantly better following deletion of *SML1* are those involved in the DDR: *dun1*Δ*, mec3*Δ, *ddc1*Δ, and *rad24*Δ (Figure 3-1A and 3-2, white bars) (Zhao et al., 2001; Zhao and Rothstein, 2002). We find that in their absence, Rad53 activation is abrogated (Figure 3-3A), likely leading to reduced Sml1 phosphorylation following DNA damage. Since unmodified Sml1 binds strongly to Rnr1 and thereby limits production of dNTPs, leading to slower growth (Andreson et al., 2010), we suspect that deleting *SML1* alleviates the block, allowing the mutants to grow better. No other double mutant combination exhibits a significant increase in colony size compared to the single mutants. Furthermore, none of these other mutants affect Rad53 activation following DNA damage (data not shown), indicating that they do not directly function in the DDR and likely interact with Sml1 independently of the Mec1-Rad53-Dun1 pathway.

Interestingly, nine double mutant combinations showed significant growth defects compared to each single mutant (Figure 3-2; black bars). Two double mutants, *lsm6*Δ *sml1*Δ and *rrg1*Δ *sml1*Δ, also show a percentage change from expected that is comparable to the significant double mutant combinations. However, these mutants were excluded since their colony size variability is large, thus rendering the percentage change insignificant (Figure 3-2). In addition, *mcm21*Δ and *ssz1*Δ were not studied further since neither, in combination with *sml1*Δ*,* exhibit reduced spore viability (Figure 3-2 and 3-3B). Therefore, we pursued the seven mutants - *mad2*Δ, *mad1*Δ, *bim1*Δ, *dcc1*Δ, *ctf18*Δ, *bub3*Δ, *sgo1*Δ - that showed both a significant growth defect as well as decreased spore

viability (Figure 3-2 and 3-3B). Interestingly, these seven genes all play a role during chromosome segregation, indicating a possible novel link between *SML1* and mitosis (Mayer et al., 2001; Musacchio and Salmon, 2007).

The synthetic genetic defects are not dNTP-related

Although the only known role for Sml1 is in the inhibition of Rnr1 (Zhao et al., 1998), given the strong synthetic interactions between *sml1*Δ and mutants involved in mitosis, we hypothesized that Sml1 may have an additional function unrelated to nucleotide pools. To test this hypothesis, we used two different methods to alter dNTP levels in a Sml1-independent manner. First, we used a *crt1*Δ mutant to increase dNTP pools independently of Sml1 regulation. Crt1 is a transcriptional regulator that suppresses transcription of *RNR1*, *RNR2*, and *RNR4* (Huang et al., 1998). In its absence, the levels of all three proteins are increased, leading to an elevation of the dNTPs to levels higher than those seen in a *sml1*Δ (Tang et al., 2009). If the synthetic effects seen in the seven mutants with *sml1*Δ were due solely to changes in dNTP levels, then the same mutants should show similar effects in a *crt1*Δ strain. None of the double mutants showed any synthetic growth defects, and, furthermore, *crt1*Δ suppresses the growth defect seen in *sgo1*Δ and *bub3*Δ strains (Figure 3-4A). Therefore, the mutants are not sensitive solely to an elevation in dNTP levels.

Next, to test whether lowering the dNTP pool levels suppresses the growth defect seen in the double mutants, we treated cells with hydroxyurea (HU), an RNR inhibitor (Slater M L 1973). Since *sgo1*Δ *sml1*Δ and *bub3*Δ *sml1*Δ are inviable, we dissected heterozygous diploids *sml1*Δ/+ *sgo1*Δ/+ and *sml1*Δ/+ *bub3*Δ/+ onto plates containing

10mM HU to see if any colonies would form – no viable double mutant spore clones germinated (data not shown). Of the remaining five strains, *ctf18*Δ *sml1*Δ and *dcc1*Δ *sml1*Δ are the only double mutants that are rescued by growth on HU (Figure 3-4B and 3-5). Therefore, *ctf18*Δ and *dcc1*Δ are sensitive to the combined loss of both the dNTP function as well as the dNTP-independent function of Sml1. The lack of suppression by HU combined with the lack of synthetic growth defects with *crt1*Δ led us to conclude that five mutants – *sgo1*Δ, *bub3*Δ, *bim1*Δ, *mad1*Δ, and *mad2*Δ - rely solely on an alternate function of Sml1 that is unrelated to its role in regulating dNTP pools.

Loss of *SML1* leads to spindle defects

To help identify this alternative function of *SML1*, we did an *in silico* search for mutants that show common synthetic growth defects or synthetic lethality with the five deletions that are sensitive only to the loss of the alternative *SML1* function: *sgo1*Δ, *bub3*Δ, *bim1*Δ, *mad1*Δ, and *mad2*Δ. Interestingly, *tub3*Δ and *cik1*Δ both show synthetic growth defects with all five query genes (Stark et al., 2011). *TUB3* is one of two alpha tubulin genes in *S. cerevisiae* (Schatz et al., 1986) while *CIK1* encodes a non-motor protein that associates with kinesin-related protein *KAR3* to alter the movement of the motor (Chu et al., 2005; Page and Snyder, 1992). Crucially, loss of *CIK1* has been linked to defects in establishment of mitotic spindle orientation (Cottingham et al., 1999). Furthermore, following DNA replication stress due to HU treatment, *cik1*Δ mutants are defective in establishing a kinetochore-microtubule interaction (Liu et al., 2011). Therefore, since *cik1* and *tub3* mutants both affect spindle orientation, we reasoned that loss of *SML1* may result in similar defects.

To test for spindle defects, wild-type (WT), *bim1*Δ, *mad1*Δ, and *mad2*Δ mutants, with and without *SML1*, were transformed with a plasmid containing CFP-tagged Spc29 to label spindle pole bodies (SPBs). We were unable to test *sgo1*Δ *sml1*Δ or *bub3*Δ *sml1*Δ since these mutants are inviable (Figure 3-3B). Cells were visualized by fluorescent microscopy, and the location of both spindle pole bodies was noted in cells with a bud to mother ratio of 0.6 or greater (indicating G2/M cells). Interestingly, in *sml1*Δ cells, a larger proportion of large budded cells contain both SPBs in one cell body as opposed to WT cells, which mostly had one SPB focus in each cell (Figure 3-6). Furthermore, loss of *SML1* also elicits a similar phenotype when combined with the other mutants with the exception of a *bim1*Δ *sml1*Δ*,* which shows an increase in cells containing multiple SPBs (Figure 3-6).

Another hallmark of spindle defects is an increase in chromosome loss. We measured this defect in our mutants by assaying for the loss of chromosome III in the same previous eight genotypes. Chromosome III contains the mating locus, and loss of this chromosome from *MAT*α cells allows these to behave as an "**a**-like faker" and mate with other *MAT*α cells (Strathern et al., 1981). Thus, by counting the number of colonies that mate with *MAT*α cells compared to those that mate with *MAT***a** cells, a chromosome loss rate was computed and normalized to WT. The *bim1*Δ *sml1*Δ double shows a 5-fold increase in chromosome loss compared to *bim1*Δ single mutant, while in the absence of *SML1*, chromosome loss is elevated 13- and 44-fold for *mad1*Δ and *mad2*Δ, respectively (Table 3-2). Taken together with SPB mislocalization, these data indicate that loss of *SML1* leads to spindle defects that exacerbate the defects that are already present in the spindle mutants.

SML1 plays a role in kinetochore establishment

Given that a large number of mutants involved at the kinetochore were identified in the primary screen for Sml1 stability, we hypothesized that the spindle defects seen in a *sml1*Δ may be linked to the kinetochore. Indeed, previous work from the Gerton lab has shown that defects in kinetochore assembly lead to spindle defects similar to those seen here (Camahort et al., 2007). To test whether there is a kinetochore defect in the absence of *SML1*, we introduced a plasmid containing CFP-tagged Mtw1 into WT and *sml1*Δ cells. At least two hundred cells of each genotype were scored for both bud to mother ratio as well as presence of one or two kinetochore foci. In WT cells, almost immediately upon appearance of a bud, cells show two distinct Mtw1 foci, which persist through the rest of the cell cycle (Figure 3-7A). Startlingly, in *sml1*Δ cells, the appearance of two kinetochore foci is significantly delayed until a bud to mother ratio between 0.6 to 0.8 is achieved (Figure 3-7A). This delay is not seen in a *crt1*Δ strain (Figure 3-7A), showing that the effect is not due to increased dNTP levels. Therefore, we conclude that the kinetochore defect is unique to the non-dNTP function of Sml1.

The delay in appearance of two kinetochore foci can be explained by two hypotheses: (i) loss of *SML1* affects the molecular motors that would normally function in separating the two kinetochores or (ii) Sml1 plays a role in establishment of the kinetochore. To distinguish between these two possibilities, we studied Scm3 (yeast ortholog of human HJURP), which plays an early role in kinetochore establishment by aiding in the recruitment of Cse4 (yeast ortholog of human CENP-A) to centromeres (Camahort et al., 2007; Foltz et al., 2009; Stoler et al., 2007). In approximately 60% of G1 WT cells, Scm3 is localized to the kinetochore (Figure 3-7B). We reasoned that if

Sml1 plays a role with the molecular motors that separate the kinetochores, it would have no effect on Scm3, which acts upstream of kinetochore separation. We visualized GFP-Scm3 in *sml1*Δ and WT unbudded cells and saw a 50% reduction in foci in the *sml1*Δ cells (Figure 3-7B). This defect was not due to reduced levels of GFP-Scm3 (data not shown), indicating that the defect in these *sml1*Δ cells only affects recruitment of the Scm3 protein to the kinetochore and suggesting that its effect is upstream of kinetochore separation.

Sml1 is the ortholog of hMis18α

In higher eukaryotes as well as in *S. pombe*, recruitment of Scm3 (HJURP) to centromeres requires additional factors. The primary group of proteins that perform this function are in the Mis18 family. *S. pombe* contains only one Mis18 (spMis18) protein while humans contain three – Mis18α, Mis18β, and M18BP1 (Fujita et al., 2007; Hayashi et al., 2004). *S. cerevisiae* does not contain a protein from the Mis18 family, however, based on the results outlined above, we reasoned that Sml1 may be playing a similar role. We compared the protein sequences of Sml1 and the Mis18 family; while Sml1 showed no homology with most members of this family, there is a significant region of homology between hMis18α and Sml1 (Figure 3-8A). This region is upstream of the consensus sequence seen in all Mis18 orthologs (Fujita et al., 2007). Interestingly, it contains several amino acids that have previously been implicated in Sml1 regulation (Andreson et al., 2010).

To determine whether Mis18α is the ortholog of Sml1, we transformed a *sml1*Δ mutant strain containing a CFP-tagged Mtw1 construct with plasmids containing either

hMis18α, hMis18β, spMis18 or an empty vector to test if any of them could complement loss of Sml1 function. For each transformed strain, over 200 cells were measured for bud to mother ratio and were quantified for the number of kinetochore foci. The *sml1*Δ strain containing an empty vector shows a significant delay in the appearance of two Mtw1 foci (Figure 3-8). Strikingly, expression of either hMis18α or spMis18 suppresses this defect, since two kinetochore foci appear in these strains with wild-type kinetics (compare Figure 3-8B to Figure 3-7A). Expression of hMis18β shows an intermediate phenotype between hMis18α and the empty vector control (Figure 3-8B).

To further establish the functional redundancy between Sml1 and Mis18, we asked whether the Mis18 genes could complement the growth defect observed in several of the *sml1*Δ double mutants shown in Figure 3-2. Heterozygous diploids containing *sml1*Δ and *sgo1*Δ, *bub3*Δ, *bim1*Δ, *mad1*Δ, or *mad2*Δ were transformed with a plasmid containing either hMis18α, hMis18β, or spMis18, and the transformants were sporulated and dissected. The presence of the plasmids did not affect the growth of the wild type or any of the single mutant segregants in the haploid progeny (data not shown). On the other hand, the double mutants grew better in all dissections containing either hMis18α or spMis18 when compared to the control (Figure 3-8C). In the case of *sgo1*Δ and *bub3*Δ, although many double mutants were inviable, at least two double mutant spore clones were viable after expression of either hMis18α, hMis18β, or spMis18 (data not shown). However, hMis18β, was only able to rescue the growth defect in some instances (Figure 3-8C). This result is consistent with Sml1 being the ortholog of hMis18α and spMis18.

DISCUSSION

In this study, we discovered new Sml1 genetic interactions that regulate its activity. Interestingly, the largest class of genes identified has functions at the kinetochore, including components of the SAC. Synthetic genetic analysis indicated that the presence of Sml1 is necessary for growth in many of these mutants. However, most of these mutants are not sensitive to changes in dNTP levels, pointing to a secondary function for Sml1. Further analysis revealed that the loss of *SML1* leads to defects in the spindle that stem from defects in kinetochore assembly. By functional analysis and sequence comparison, we identified Sml1 as the yeast ortholog of hMis18α. Furthermore, *sml1*Δ defects were complemented by hMis18α, thus identifying a dual role for Sml1 in the cell and providing a potential link between the DDR and the SAC.

Numerous cell processes beyond those involved in DNA repair play a role in Sml1 stability

Previous studies have utilized Sml1 as a marker of an activated DNA damage checkpoint – specifically the Mec1-Rad53-Dun1 pathway – and it has been thought to be exclusively regulated in this manner in both undamaged and treated cells. Here we show that there are numerous other processes in the cell that can affect Sml1 levels following DNA damage independently of Rad53 (Table 3-1 and data not shown). Most significantly, a large group of genes involved at mitosis were identified, including those that function in kinetochore structure, sister chromatid cohesion, the SAC, and the tension sensor, *SGO1*. While the identification of this group was surprising, we were convinced of their validity

due to the presence of known regulators of Sml1 stability following DNA damage – *DUN1, MEC3, DDC1, RAD24, RAD9, RAD6, UBR2,* and *MUB1* (Andreson et al., 2010; Zhao et al., 2001; Zhao and Rothstein, 2002).

Sml1 is linked to mitosis independently of its dNTP-related function

While *sml1*Δ has not been reported to have many synthetic interactions in large-scale genomic studies, we queried whether there were indeed some interactions that were not identified due to the high-throughput nature of the genome-wide screens. Additionally, some of the mutants we identified have previously been implicated in chromosome loss during mitosis and meiosis (Barnhart et al., 2011a; Indjeian et al., 2005; Petronczki et al., 2004; Spencer et al., 1990). The tetrad dissection based technique that we used allowed us to specifically analyze tetrads that were not the products of aberrant meioses. Using this method, we could identify if the stability of Sml1 that was seen in the mutants identified by the fluorescence screen was necessary for survival of the mutant. Interestingly, only mutants that are members of the DDR grew better in the absence of *SML1* (Figure 3-2). On the other hand, the mutants involved in mitosis showed a synthetic growth defect (Figure 3-2 and 3-3B). Interestingly, most of these synthetic effects are not due to the elevated dNTP levels caused by loss of *SML1* (Figure 3-4A), strongly indicating a novel function for Sml1.

Sml1 is the ortholog of hMis18α and affects kinetochore assembly by recruitment of Scm3

The most striking finding of our work was the identification of Sml1 as the functional ortholog of human Mis18α. Specifically, we found that a *sml1*Δ strain has a kinetochore assembly defect that is likely due to its reduced ability to recruit Scm3 to the kinetochore (Figures 3-7A and 3-7B). These defects, as well as the synthetic interactions seen with the mitosis mutants, are rescued by complementation with either human Mis18α or *S. pombe* Mis18, indicating that Sml1 indeed is the ortholog (Figure 3-8B and 3-8C).

In mammalian cells, the localization of CENP-A to centromeres is dependent on the Mis18 group of proteins (Fujita et al., 2007), which are important for recruitment of the CENP-A loader, HJURP, to the centromeres (Barnhart et al., 2011b; Foltz et al., 2009). Furthermore, the recruitment of the Mis18 group of proteins is a co-dependent process that requires interaction between Mis18α, Mis18β, and M18BP1 (Fujita et al., 2007). While Mis18α and Mis18β are homologous, they are only 26% similar, suggesting that they have different functions (Fujita et al., 2007). This difference may explain the intermediate phenotype seen when Mis18β is introduced into a *sml1*Δ strain (Figure 3-8B). Interestingly, Mis18α is 30% similar to *S. pombe* Mis18, which is the only copy present in fission yeast (Fujita et al., 2007). However, *S. pombe* Mis18 also suppresses the *sml1*Δ kinetochore defect (Figure 3-8B), indicating that its similarity with Mis18α potentially encompasses the region that complements Sml1 function.

Taken together, our findings show that Sml1 has an alternate function at the kinetochore, in addition to regulation of Rnr1. This dual function suggests a model in which, following DNA damage, Sml1 dissociates from Rnr1 and moves to the nucleus,

where it assists in recruitment of Scm3 to allow proper assembly of the kinetochore (see Figure 4-2). Interestingly, recent work from the Kearsey lab has shown that the *S. pombe* homolog of Sml1, Spd1, also associates with PCNA independent of its dNTP function, and this association is important for its degradation (Salguero et al., 2012). If Sml1 were similarly regulated, then perhaps its degradation is dependent on its role in kinetochore assembly. Indeed, unpublished work from our lab has shown that Dun1 dependent phosphorylation of Sml1 triggers its translocation from the cytoplasm to the nucleus, where it is degraded (Andreson et al., manuscript in preparation). Furthermore, the region of Sml1 phosphorylated by Dun1 following DNA damage shows the greatest degree of homology with Mis18α (Figure 3-8A) (Andreson et al., 2010). This model elegantly links the DNA damage and spindle assembly checkpoints since Sml1, a downstream target of the Mec1-Rad53-Dun1 pathway after DNA damage, only moves into the nucleus upon phosphorylation by Dun1. Thus, failure of the checkpoint pathway would abrogate Sml1 phosphorylation thereby preventing proper assembly of the kinetochore, which in turn would trigger the SAC (see Figure 4-2).

EXPERIMENTAL PROCEDURES

Yeast media and strains

Standard yeast media and growth conditions were used (Sherman, 1991).

pWJ 1775 was constructed by cutting pRS415 (Sikorski and Hieter, 1989) with NaeI (New England Biolabs, Ipswich, MA) and co-transforming with a PCR product containing YFP-Sml1 as well as 500bp upstream and downstream. The fragment also

contained sequences homologous to the cut site, allowing for *in vivo* recombination. The plasmid was verified by sequencing and by fluorescence signal before and after damage.

For pWJ 1998, pWJ 1250 (Alvaro et al., 2007) was digested with with HpaI (New England Biolabs, Ipswich, MA) and co-transformation with a PCR product containing SPC29-CFP along with 500 bp upstream and downstream as well as C and D adaptamers (Reid et al., 2002). pWJ 1807 was constructed by gap repair to introduce Mtw1-CFP along with 500 bp upstream and downstream into a pWJ1512 plasmid containing Rdh54-YFP under a *CUP* promoter.

pGBD-hMis18α, pGBD-hMis18β, pGBD-spMis18, and pGBT9 were generous gifts from Takeshi Hayashi. The plasmids were marker swapped to URA using pTU10 (Cross, 1997). Primers available upon request.

Plasmids are listed in Table 3-3. Yeast strains used in this study are listed in Table 3-4.

Genome-wide screen for Sml1 stability

pWJ1775 was introduced into the non-essential yeast deletion library (Winzeler et al., 1999) by synthetic ploidy ablation (Reid et al., 2011). Transformants were grown in 96-well plates in liquid medium for two days, diluted at 1/5 and grown overnight. Plates were treated with 100 Gy γ-rays using a Gammacell 220 Cobalt-60 Irradiator (Gammacell). After 45 minutes, cells were concentrated by centrifugation and pippeted onto two 48-pad agar pedestals (Werner et al., 2009) and visualized using a Leica HCX

PL APO 100x objective 1.46 NA mounted on a Leica CTR5500 microscope. Cells were scored by eye for presence of or absence of fluorescence. Mutants in which Sml1 fluorescence was observed were imaged using a cooled Orca-ER CCD camera and processed with Volocity Acquisition software (Improvision, Lexington, MA). The screen was performed twice, and mutants identified in both screens were re-arrayed onto a new 384 YPD plate and re-assayed.

Synthetic growth analysis

MAT **a** *sml1::KanMx* strain (Open Biosystems, Lafayette, CO) was used and the KanMx cassette was replaced by a NatMx. Resulting strain was verified by PCR and back-cross for proper integration. MAT**a** *sml1::NatMx* was crossed to MATα versions of the deletions identified in the stability screen. Diploids were sporulated, dissected, and scored the deletions as well as other markers. Tetrads in which any of the markers did not segregate 2:2 were discarded from further analysis. All tetrads from the same plate were analyzed together for colony size using the Yeast Dissection Reader (Open Source, Rothstein Lab). The sizes of both single mutants (f_s and f_m, respectively) and the double mutant (f_{ms}) were normalized to the average growth of the WT for each plate after two days of growth. Plates were discarded from further analysis if either WT or *sml1*Δ showed a >15% spore lethality or growth of a *sml1*Δ was not between 1.05 and 1.2. Multiple plates were used for each mutant, thereby providing between 15 and 30 usable tetrads per cross for analysis.

Expected growth was determined as a product of the growth of the two single mutants, $f_s.f_m$. Percent change from expected was calculated by subtracting expected

growth from actual growth and normalizing to the expected growth using the formula: Percent change from expected = $((f_{ms} - f_s.f_m)/(f_s.f_m)) \times 100$. To compute significance, we used standard error (SE) of all the mutants. The SE of the two single mutants is used to determine a SE of the expected double mutant. Using this error along with the expected growth we calculated a z score for the growth of the double mutant from which significance was calculated. Only mutants with a p-value<0.01 were highlighted.

The same analysis was used for Figure 3-8C.

A similar analysis was used for the *crt1*Δ dissections with the exception that *crt1*Δ mutants grew at a size similar to wild type and were not used as a quality control. Furthermore, to analyze the mutants from these crosses, we compared the fold change in actual growth of the double mutants to the expected growth.

Protein blots

Protein blots were performed essentially as described in (Pike et al., 2001).

Spot assays

Cells were grown up and serially diluted at 1/5 dilutions. Dilutions were then spotted onto SC and SC + 10mM HU.

Live Cell Imaging and Fluorescence Microscopy

Cells were prepared for fluorescence microscopy as described previously (Lisby et al., 2001). Images were captured as previously described (Bernstein et al., 2011) with the exception that all images were taken with 21 stacks instead of 11. Exposure times for the

different strains were as follows: difference interference contrast (15ms), Spc29-CFP (600ms), CFP-Mtw1 (500 ms), and Scm3-GFP (2800ms). Measurement of mother and bud lengths as well as identification of foci is performed with Volocity Acquisition software (Improvision, Lexington, MA).

a-like faker assay

Cells of different genotypes were grown up overnight in YPD and diluted to an OD of 0.1 in YPD. Cultures were grown 4-6 hours. 2ml of culture were spun down and spread on plates previously covered by a MATα tester strain. At the same time, the culture was diluted at 10^{-5} and spread on plates covered by MAT**a** tester. The plates were replica plated to SD media after 18-24 hours and colonies counted 2 days after. Chromosome loss rate was computed for each genotype by dividing number of colonies growing on the MATα tester mating by the number of colony forming units in the culture as determined from the number of colonies growing on the MAT**a** tester. For each experiment, chromosome loss rate was normalized to WT.

Search for Sml1 homolog

Sml1 homolog was determined by comparing protein sequence of Sml1 to human Mis18α, Mis18β, M18BP1, and *S. pombe* Mis18 using MacVector (MacVector Inc., Cary, NC).

ACKNOWLEDGEMENTS

We would like to thank Michael Chang for constructive comments on the manuscript; Peter Thorpe, Rebecca Burgess, and Orna Cohen-Fix for helpful suggestions during this study; Takeshi Hayashi for the Mis18 plasmids; and Jörg Heierhorst for Rad53 antibody. This work was supported by the US National Institutes of Health (GM50237 and GM67055 to R.R.).

Figure 3-1

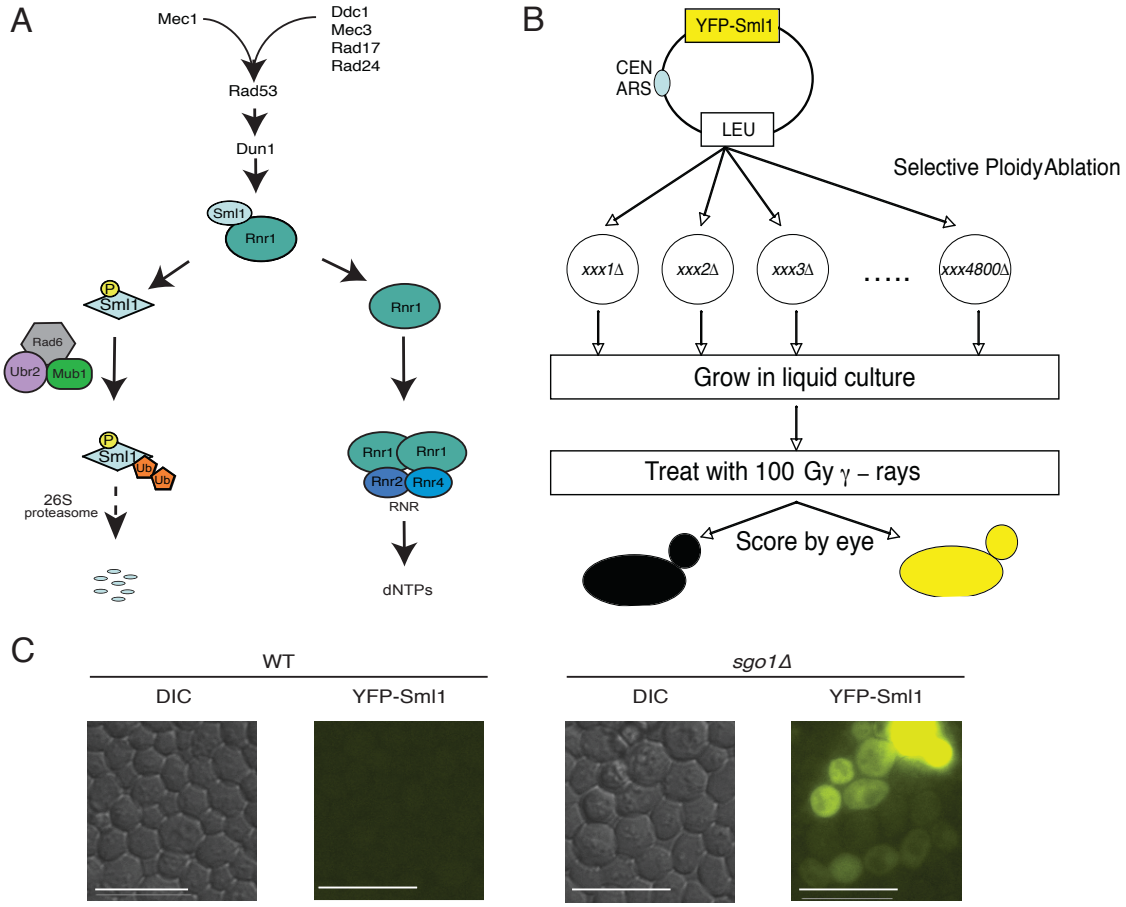

Figure 3-1: Identifying novel factors involved in Sml1 regulation. (A) Model for Sml1 regulation in yeast (adapted from Andreson et al., 2010). Following DNA damage, Rad53 is phosphorylated in a Mec1 dependent manner. Activated Rad53 phosphorylates Dun1which in turn phosphorylates Sml1. Modified Sml1 dissociates from Rnr1 and is then ubiquitylated by the Rad6-Ubr2-Mub1 complex and degraded by the 26S proteasome. (B) Method for identification of genes involved in Sml1 degradation utilizing the methods shown previously (Reid et al., 2011; Werner et al., 2009). Briefly, YFP-Sml1 was introduced into the nonessential yeast deletion library using selective ploidy ablation. Strains containing the plasmid were grown and visualized on agar pedestals between 45 and 105 minutes after 100 Gy γ-irradiation and scored for presence or absence of fluorescence. (C) Examples of genes identified. DIC and YFP visualized after damage in a wild-type and in a *sgo1*Δ strain. The scale bar is 13μm.

Figure 3-2

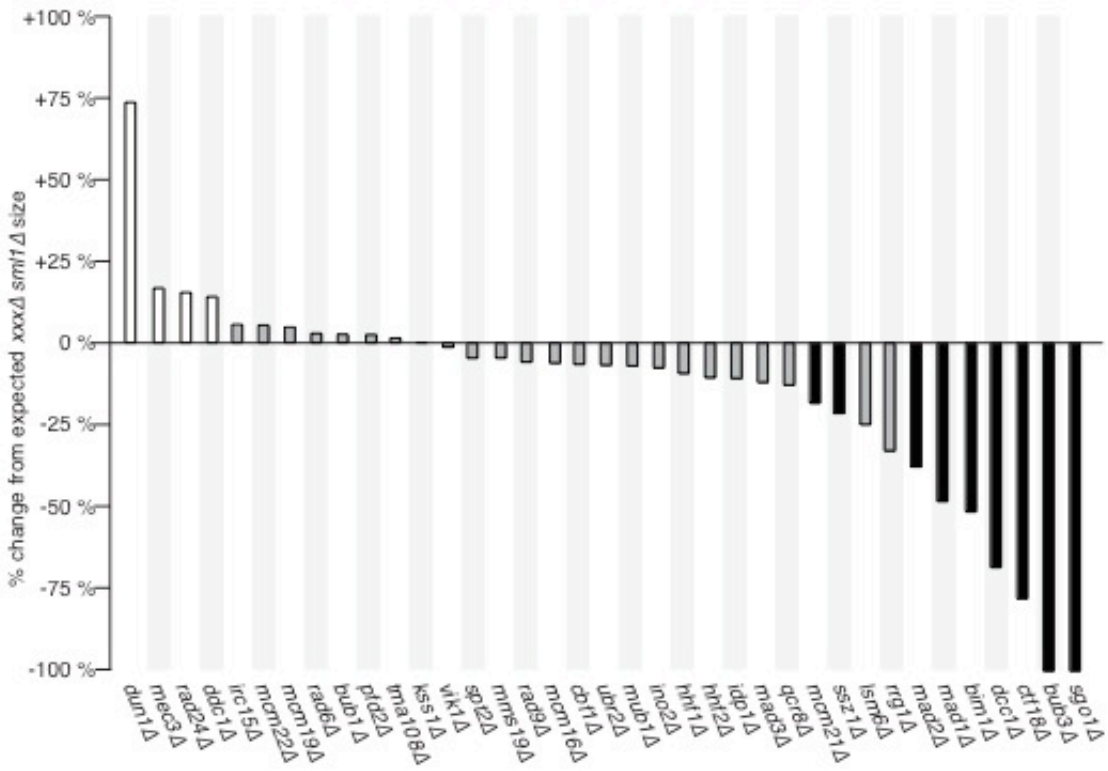

Figure 3-2: Synthetic interactions with *sml1*Δ**.** Mutants identified in Figure 3-1 (Table 3-1) were crossed to a *sml1*Δ (U3223). Resulting spores were measured and an expected double mutant size was computed (see Experimental Procedures). Deviation of actual size from the expected size was computed and plotted as described in Experimental Procedures. Double mutants that grew significantly better than expected (p-value < 0.01) are shown with white bars. Conversely, mutants that grew significantly worse than expected are represented by black bars (p-value < 0.01).

Figure 3-3

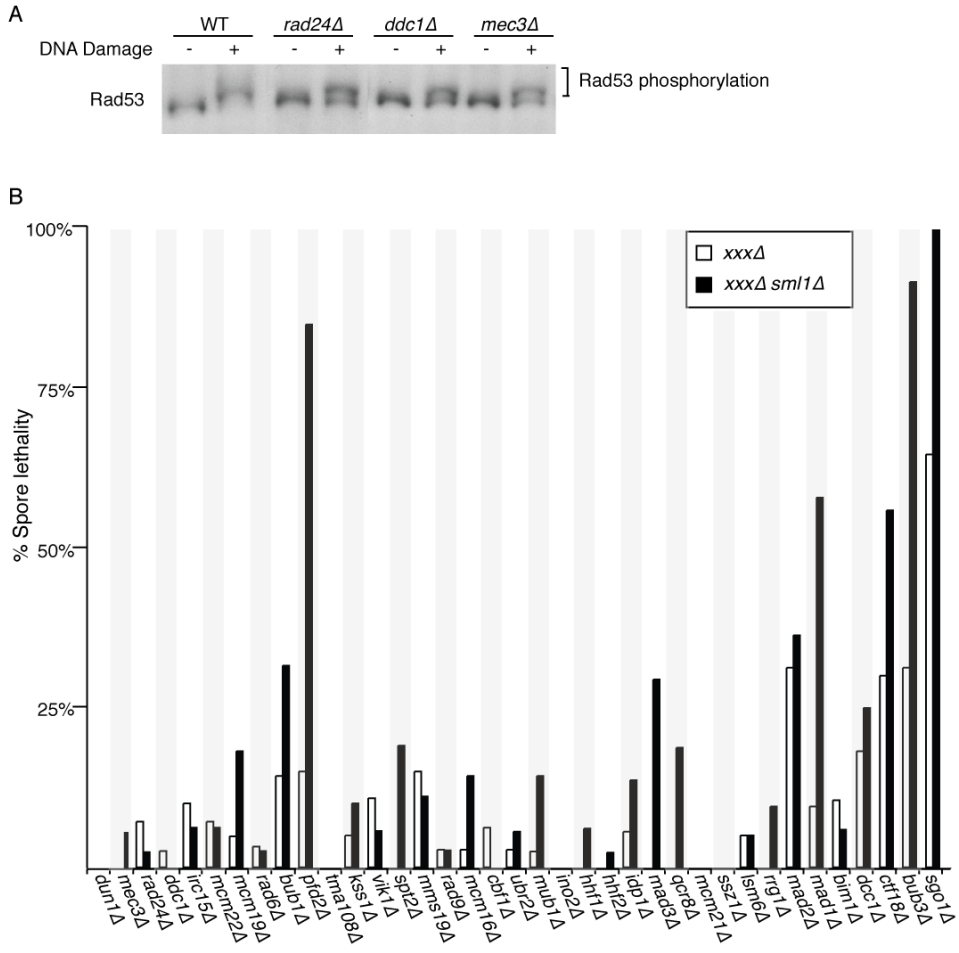

Figure 3-3: Differential effects of mutants synthetic with *sml1*Δ. (A) *RAD24*, *DDC1*, and *MEC3* are involved in Rad53 activation. *his3*Δ, *rad24*Δ, *ddc1*Δ, and *mec3*Δ strains from the yeast non-essential gene deletion collection (Winzeler et al., 1999) were grown to log phase and treated with 100 Gy γ-irradiation. Proteins were extracted before and after damage and blotted for Rad53. The slower migrating band represents phosphorylated Rad53. (B) Spore lethality of the single and double mutants. Dissections in Figure 3-2 were also analyzed for lethality of the spores. Lethality of the single mutants is represented by white bars while lethality of the double mutants with *sml1*Δ is represented by black bars.

Figure 3-4

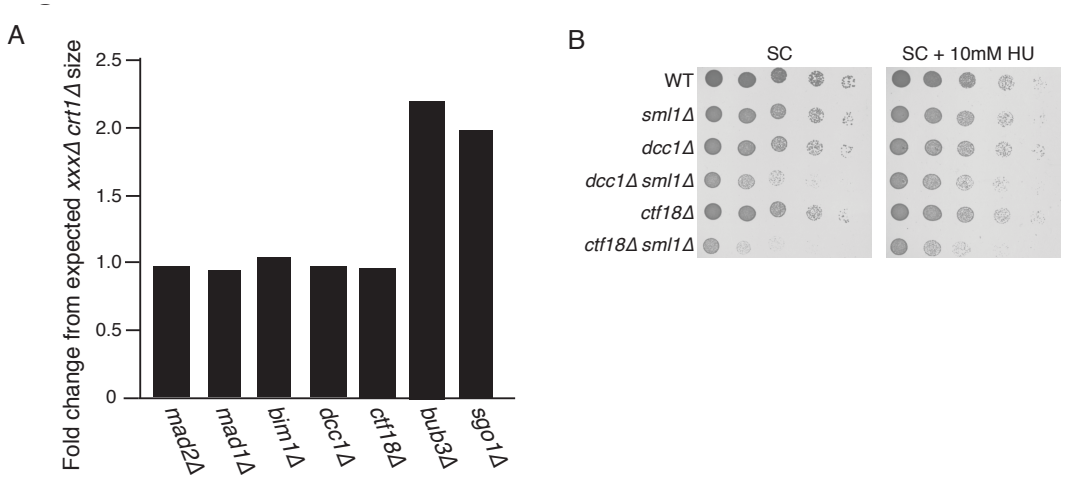

Figure 3-4: Synthetic growth defects with the loss of *SML1* is due to the loss of a dNTP-independent function (A) *crt1*Δ does not have any synthetic growth defects with the genes synthetic with *sml1*Δ. The seven most significant single mutants as identified by Figure 3-2 were crossed to a *crt1*Δ (U32234). Fold change of actual double mutant size compared to expected double mutant size is plotted. Only the values for *bub3*Δ and *sgo1*Δ were found to be significant (p-value < 0.01). (B) The synthetic growth defects of *ctf18*Δ *sml1*Δ and *dcc1*Δ *sml1*Δ are rescued by reducing dNTP levels. W10000-61B (WT), W10000-16B (*sml1*Δ), W10004-4B (*dcc1*Δ), W10004-8A (*dcc1*Δ *sml1*Δ), W10005-1B (*ctf18*Δ), and W10005-4D (*ctf18*Δ *sml1*Δ) were serially diluted five-fold and spotted on to either SC or SC media containing 10mM hydroxyurea (HU). Plates were scanned after 2 days of growth.

Figure 3-5

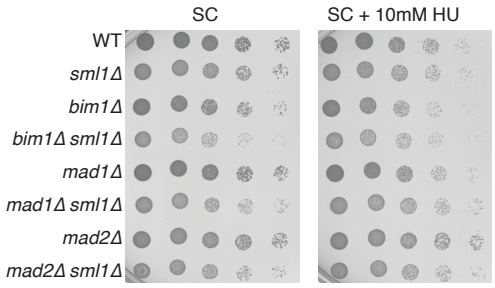

Figure 3-5: The synthetic growth defects of *bim1*Δ *sml1*Δ, *mad1*Δ *sml1*Δ and *mad2*Δ *sml1*Δ are unaffected by a reduction in dNTP levels. W10000-61B (WT), W10000-16B (*sml1*Δ), W10001-13B (*bim1*Δ), W10001-31C (*bim1*Δ *sml1*Δ), W10002-15A (*mad1*Δ), W10002-22B (*mad1*Δ *sml1*Δ), W10003-11C (*mad2*Δ), and W10003-11A (*mad2*Δ *sml1*Δ) were serially diluted five-fold and spotted onto either SC or SC media containing 10mM hydroxyurea (HU). Plates were scanned after 2 days of growth.

Figure 3-6

WT	74.1	25.9	0.0
sml1Δ	38.1	61.9	0.0
bim1Δ	57.1	42.9	0.0
bim1Δ sml1Δ	14.3	42.9	42.9
mad1Δ	100.0	0.0	0.0
mad1Δ sml1Δ	44.4	55.6	0.0
mad2Δ	85.7	14.3	0.0
mad2Δ sml1Δ	72.0	28.0	0.0

Figure 3-6: Abnormal spindle pole body distribution seen with the deletion of *SML1*. W10000-61B (WT), W10000-16B (*sml1*Δ), W10001-13B (*bim1*Δ), W10001-31C (*bim1*Δ *sml1*Δ), W10002-15A (*mad1*Δ), W10002-22B (*mad1*Δ *sml1*Δ), W10003-11C (*mad2*Δ), and W10003-11A (*mad2*Δ *sml1*Δ) were transformed with pWJ1998 (Spc29-CFP), grown to log phase and imaged by fluorescence microscopy. Large budded cells (bud/mother ratio > 0.6) for all genotypes were classified based on the location of the two Spc29-CFP foci: one focus in each cell, both foci in the same cell, and cells with multiple foci.

Figure 3-7

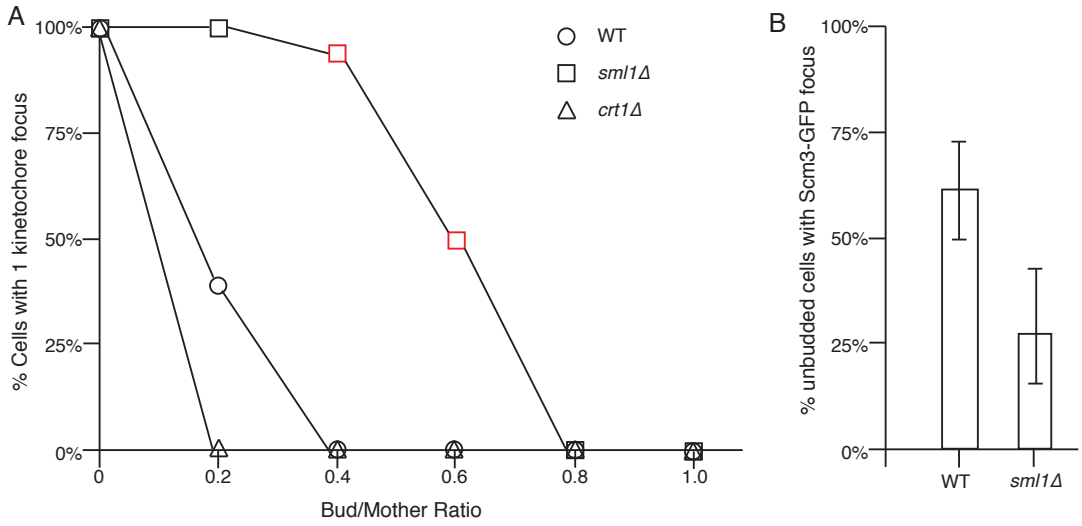

Figure 3-7: Sml1 plays a role in kinetochore assembly. (A) Loss of *SML1* results in a delayed appearance of two kinetochore foci. BY4741 (WT), U3223 (*sml1*Δ), and U3224 (*crt1*Δ) strains containing pWJ1807 (Mtw1-CFP) were grown to log phase and fluorescence and DIC images were captured. At least 200 cells were measured for their bud/mother ratios and the number of foci for each genotype. All unbudded cells were represented with a bud/mother ratio of 0. Cells with bud/mother ratios greater than 0 but less than or equal to 0.2 were designated as 0.2. Similar grouping was done for the higher bud/mother ratios as well. Points were plotted based on percentage of cells in the different bud/mother ratio groups containing one focus as opposed to two foci. Significance was calculated based on a bimodal distribution compared to wild-type percentages at the same bud/mother ratio. Data points in red show p-values < 0.01 compared to wild-type. (B) Unbudded cells with Scm3-GFP foci are reduced in a *sml1*Δ. R1654 (Scm3-GFP) and W10006-2D (SCM3-GFP *sml1*Δ) were grown up to log phase and visualized by fluorescence microscopy. One hundred unbudded cells of each genotype were scored for presence or absence of a focus. Percentage of cells is plotted along with 95% confidence intervals.

Figure 3-8

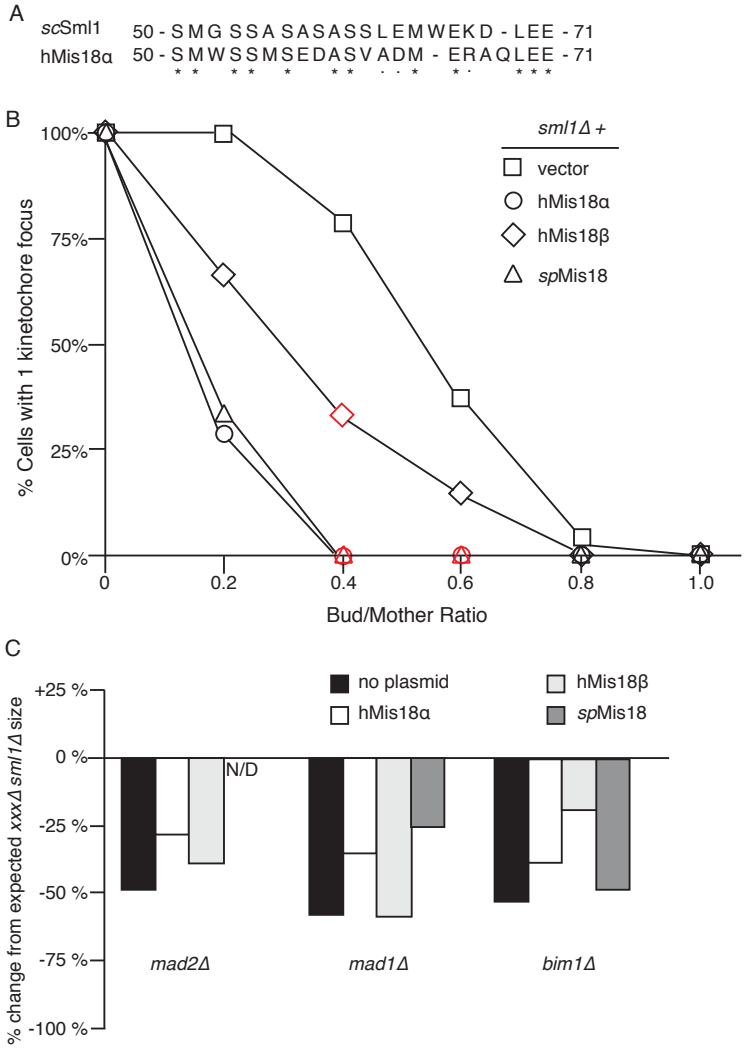
A
scSml1 50 - S M G S S A S A S A S S L E M W E K D - L E E - 71
hMis18α 50 - S M W S S M S E D A S V A D M - E R A Q L E E - 71
B
100%
75%
50%
25%
0%
% Cells with 1 kinetochore focus
0
0.2
0.4
0.6
0.8
1.0
Bud/Mother Ratio
sml1Δ +
vector
hMis18α
hMis18β
spMis18
C
+25 %
0 %
-25 %
-50 %
-75 %
-100 %
% change from expected xxxΔ sml1Δ size
no plasmid
hMis18α
hMis18β
spMis18
N/D
mad2Δ
mad1Δ
bim1Δ

Figure 3-8: Sml1 is the hMis18α ortholog. (A) Identification of a Sml1 ortholog. The conserved region of Sml1 and hMis18α is shown. Asterisks indicate exact amino acid matches while dots indicate similar amino acids. (B) Complementation of the *sml1*Δ kinetochore delay phenotype by Mis18. U3223 (*sml1*Δ) containing pWJ1807 (Mtw1-CFP) as seen in Figure 3-7 were transformed with either pWJ2046 (empty vector), pWJ2030 (human Mis18α), pWJ2031 (human Mis18β), or pWJ 2032 (*S. pombe* Mis18). Logarithmically growing cells were imaged by fluorescence microscopy and analyzed the same way as in Figure 3-7. Significance was calculated based on a bimodal distribution compared to pWJ2046 (empty vector) containing cells at the same bud/mother ratio. Data points in red show p-values < 0.01 compared to pWJ2046 (empty vector). (C) Mis18α complements the synthetic growth defects seen with a *sml1*Δ. W10001 (*bim1*Δ/+ *sml1*Δ/+), W10002 (*mad1*Δ/+*sml1*Δ/+), and W10003 (*mad2*Δ/+ *sml1*Δ/+) were transformed with pWJ2030 (human Mis18α), pWJ2031 (human Mis18β), or pWJ2032 (*S. pombe* Mis18). The untransformed strains as well as the resulting transformants were dissected and analyzed as in Figure 3-2.

Table 3-1. Genes involved in Sml1 stability as identified by the visual screen

Gene Ontology	Gene(s)
DNA Repair	*MMS19, RAD24, DDC1, MEC3, DUN1, RAD9*
Kinetochore/Spindle	*IRC15, BIM1, MAD1, MAD2, MAD3, BUB1, BUB3, SGO1, MCM16, MCM19, MCM21, MCM22, CBF1*
Chromatid Cohesion	*CTF18, DCC1, VIK1*
Ubiquitin	*RAD6, UBR2, MUB1*
Transcription/RNA	*SPT2, INO2, PAT1, LSM6*
Histones	*HHF2, HHF1, HTA1*
Mitochondria	*QCR8, IDP1*
Ribosomes	*TMA108, SSZ1*
Vacuole	*RRG1*
Kinase	*KSS1*
Chaperone	*PFD2*

Table 3-2. Chromosome loss rate. Chromosome loss rate was measured by the **a**-like faker assay (see Experimental Procedures) and normalized to wild type. Fold change as compared to the single mutant is expressed in parentheses.

	- (Chromosome loss rate normalized to WT ± SD)	*sml1*Δ (Chromosome loss rate normalized to WT ± SD)
WT	1.00 ± 0.00	0.72 ± 0.15 (0.72)
*bim1*Δ	49.32 ± 42.10	246.58 ± 126.92 (5.00)
*mad1*Δ	1.56 ± 0.74	20.53 ± 4.47 (13.18)
*mad2*Δ	0.64 ± 0.21	28.35 ± 15.06 (44.28)

Table 3-3. Plasmids used in this study

Plasmid	Relevant Markers	Reference
pWJ 1775	*Amp^r CEN LEU2 YFP-SML1*	This study
pWJ 1998	*Amp^r CEN URA3 SPC29-CFP*	This study
pWJ 1807	*Amp^r CEN LEU2 MTW1-CFP P_{CUP}-RDH54-YFP*	This study
pWJ 2030	*Amp^r 2μ URA3 P_{ADH1}-GBD-hMIS18α*	This study
pWJ 2031	*Amp^r 2μ URA3 P_{ADH1}-GBD-hMIS18β*	This study
pWJ 2032	*Amp^r 2μ URA3 P_{ADH1}-GBD-spMIS18*	This study
pWJ 2046	*Amp^r 2μ URA3 P_{ADH1}-GBD*	This study

Table 3-4. Yeast strains used in this study. All strains are derivatives of either BY4741 or BY4742. All *MAT***a** strains have the same genotype as BY4741 and all *MATα* have the same genotype as BY4742

Strain	Genotype	Reference
BY4741	*MAT***a** *his3Δ1 leu2Δ0 met15Δ0 ura3Δ0*	(Winzeler et al., 1999)
BY4742	*MATα his3Δ1 leu2Δ0 lys2Δ0 ura3Δ0*	(Winzeler et al., 1999)
U3223	*MAT***a** *sml1Δ::NATMx*	This study
U3224	*MAT***a** *crt1Δ::NATMx*	This study
W10000-61B	*MATα*	This study
W10000-16B	*MATα sml1Δ::NATMx*	This study
W10001-13B	*MATα bim1Δ::KANMx*	This study
W10001-31C	*MATα bim1Δ::KANMx sml1Δ::NATMx*	This study
W10002-15A	*MATα mad1Δ::KANMx*	This study
W10002-22B	*MATα mad1Δ::KANMx sml1Δ::NATMx*	This study
W10003-11C	*MATα mad2Δ::KANMx*	This study
W10003-11A	*MATα mad2Δ::KANMx sml1Δ::NATMx*	This study
W10004-4B	*MATα dcc1Δ::KANMx*	This study
W10004-8A	*MATα dcc1Δ::KANMx sml1Δ::NATMx*	This study
W10005-1B	*MATα ctf18Δ::KANMx*	This study
W10005-4D	*MATα ctf18Δ::KANMx sml1Δ::NATMx*	This study
R1654	*MAT***a** *SCM3-GFP-HIS3Mx*	(Huh et al., 2003)
W10006-2A	*MAT***a** *sml1Δ::NATMx SCM3-GFP-HIS3Mx*	This study

CHAPTER 4:

DISCUSSION

INTRODUCTION

The aim of this study was two-fold: (i) Explore additional processes affected by Sml1 in its canonical function and (ii) use the sensitivity of Sml1 to DNA damage to determine novel genes involved in regulation of Sml1.

For the first aim, telomere length regulation was studied since previous studies hinted at an *in vivo* correlation between dNTP levels and telomere lengths. However, in both cases the altered dNTP levels were assumed and not measured (Ritchie et al., 1999; Toussaint et al., 2005). We performed a detailed analysis directly comparing telomere lengths to dNTP levels. Our initial experiments using *sml1*Δ and *dun1*Δ confirmed a positive correlation between telomere lengths and dNTP pools. Subsequent experiments using specific *rnr*1 mutants revealed the dependence of telomerase on relative amounts of dGTP. The dependence on relative dGTP is due to the sensitivity of telomerase to altered dNTP pools, which repeatedly stalls and dissociates from telomeres under conditions in which relative dGTP is limiting.

To fulfill the second aim, a cell biological approach was used to screen the yeast gene deletion library following DNA damage. The levels of YFP-Sml1 were qualitatively determined by eye allowing for rapid screening. Through this approach, we were able to identify the ubiquitin ligase important for Sml1 degradation – Rad6-Ubr2-Mub1 (Chapter 3 and Appendix). Furthermore, we identified numerous genes involved in Sml1 degradation that function at the kinetochore and in the SAC, thereby suggesting other functions for Sml1. Further work established Sml1 as the human Mis18α ortholog, providing a potential feed-forward pathway connecting the DDR and the SAC via the regulation of Sml1.

dNTPs and telomeres: Telomerase processivity correlates with dGTP

The maintenance of telomere length is required in all organisms to prevent extreme telomere shortening, which can lead to senescence (Harley et al., 1990; Lundblad and Szostak, 1989; Yu et al., 1990), and is achieved by the reverse transcriptase, telomerase (Greider and Blackburn, 1985; Yu et al., 1990). Telomerases from different organisms have the same basic components, with an RNA template and a protein subunit that contains the catalytic domain for the enzyme (Feng et al., 1995; Lingner et al., 1997b; Nakamura et al., 1997; Singer and Gottschling, 1994). There are, however, differences between these related telomerases as well as different proteins that associate with them (Greider, 1996; Hug and Lingner, 2006). It is likely that some of these differences contribute to the processivity of the enzyme, since *S. cerevisiae* telomerase is not processive while telomerase from *Tetrahymena*, *Euplotes*, and humans display higher processivities (Chang et al., 2007; Greider, 1991; Hammond and Cech, 1998; Morin, 1989). Despite these differences, all telomerases are dependent upon the concentration of dGTP *in vitro* (Bosoy and Lue, 2004; Hammond and Cech, 1998; Hardy et al., 2001). Furthermore, there have been indications in *S. cerevisiae* that telomere length correlates with overall dNTP pool sizes *in vivo* (Gatbonton et al., 2006; Ritchie et al., 1999; Toussaint et al., 2005).

In this study, we measured dNTP levels as well as telomere lengths *in vivo* in *S. cerevisisae* to determine whether or not they correlate. Interestingly, although we did find a correlation between dNTP pool sizes and telomere lengths, this was only found at reduced dNTP levels (Figure 2-1). However, once a threshold dNTP level has been achieved, there is a negligible effect on telomere lengths (Figure 2-1). On the other hand,

telomerase is exquisitely sensitive to imbalances in dNTP ratios (Figure 2-4). In particular, there is a strong effect of dGTP on telomerase activity, consistent with previous *in vitro* studies. However, this study shows that it is not the absolute concentration of dGTP that is important, but the ratio of dGTP relative to the other dNTPs that is crucial for telomerase nucleotide addition processivity *in vivo* in *S. cerevisiae*. Strains with increased relative dGTP levels show increased nucleotide addition processivity leading to longer telomeres (Figure 2-6). The changes in telomere length with altered relative dGTP are also consistent with previous work that show that the Rap1 counting mechanism binds G rich regions of the telomere (Larson et al., 1994; Ray and Runge, 1999). Indeed, the mutants with higher relative dGTP showed longer telomeres but the increase in telomere length was much less than the decrease seen with mutants with lower relative dGTP (Figure 2-4). It is likely that with longer telomeres that are a result of increased nucleotide processivity and increased relative dGTP, the number of Rap1 binding sites would increase leading to a reduction in overall telomere length increase. However, the most crucial finding of this study is that the finding provides a mechanism for telomerase processivity seen in *S. cereveisiae in vivo*. It appears that limiting dGTP relative to the other dNTP leads to stalling of telomerase and its dissociation from telomeres.

While the altered dNTP ratios also have an effect on DNA polymerase (Kumar et al., 2011), the change in telomere length is specific to telomerase (Figures 2-6 and 2-7). These findings highlight a key difference between DNA polymerase and telomerase. While DNA polymerase can processively add incorrect nucleotides when relative dGTP is reduced (Kumar et al., 2011), telomerase is unable to do so and dissociates from

telomeres. Thus during periods of dGTP depletion, the cell would continue to replicate DNA while simultaneously reducing telomere extension, thereby allowing the cell to efficiently use the limited dNTP resources.

Furthermore, consistent with *in vitro* work, strains with increased relative dGTP levels also show limited repeat addition processivity (Bosoy and Lue, 2004). Additionally, our study showed that human telomerase repeat addition processivity is also dependent on dGTP (Figure 2-10). The difference, however is that in human telomerase, it is the absolute concentration of dGTP, as opposed to the relative concentration, that is important. Given that human telomerase and *S. cerevisiae* telomerase function differently, the conservation of dGTP dependence upon activity is striking. However, this conservation of regulation of human and yeast telomerase also leads to the question as to why *S. cerevisiae* telomerase is not proficient at repeat addition processivity.

Two hypotheses could explain this difference. First, related telomerases are biochemically different with regard to processivity, despite the conservation in most of the reverse transcriptase domains (Lue et al., 2003). Second, the difference in processivity is due to the longer telomerase template in *S. cerevisiae* compared to other organisms. In humans, *Tetrahymena*, and *Euplotes*, telomerase is highly processive, adding one full telomeric repeat at a time. In all these organisms, a full repeat ranges between 6 and 8 bp (Greider, 1996). In *S. cerevisiae*, however, if telomerase were completely processive, the telomere repeat would be between 12 and 14 bp. It is possible that this increased length leads to telomerase being unable to add one repeat at a time. Thus, when relative dGTP is increased, organisms with shorter telomeric repeats show repeat addition processivity, while *S. cerevisiae* shows nucleotide addition processivity.

To confirm this, we could test if reducing the length of the telomerase RNA template in *S. cerevisiae*, or replacing it with telomerase RNA from other organisms, results in increased telomerase repeat addition processivity. If this were the case, it would indicate that the mechanism of telomerase regulation is conserved across all organisms and is closely tied to the levels of dGTP in the cells.

Identifying genes involved in Sml1 stability

In addition to affecting telomere length homeostasis, the regulation of dNTP levels is critical following DNA damage (Chabes et al., 2003a). During DDR, Sml1 is rapidly degraded, relieving the inhibition of the large subunit of RNR, Rnr1 (Zhao et al., 2001). The degradation of Sml1 is necessary to allow the small subunits of RNR to interact with Rnr1 to form a functional holoenzyme (Zhang et al., 2007). Therefore, phosphorylation and degradation of Sml1 is often seen even before Rad53 activation (Barlow et al., 2008; Torres-Rosell et al., 2007). In this study, we utilized this sensitivity to screen for other genes involved in Sml1 regulation following DNA damage.

We took a cell biological approach to identify regulators of Sml1. A plasmid containing YFP-Sml1 was introduced into the entire haploid non-essential yeast deletion collection using selective ploidy ablation (Reid et al., 2011). The strains containing the plasmids were transferred to liquid cultures and grown for two days without agitation in 96-well plates. The cultures were then diluted and grown for 8 hours (to reduce the number of dead cells in the culture) before being irradiated with 100 Gy of γ-rays. After 45 minutes, cells were transferred to agar pedestals (Werner et al., 2009) and visualized for the presence of YFP-Sml1. Cells were counted by eye, and this qualitative screen

allowed us to rapidly screen the deletion library. The ease and rapidity of this method justified its use over a technique involving measuring Sml1 levels by protein blots. A drawback of this method, however, is that growth of cells in 96-well cultures with no agitation is reduced. Thus, some slow growing mutants were at a disadvantage and were not analyzed during the screen.

Furthermore, it can be argued that by narrowing the parameters of our search to just identifying mutants following DNA damage, we would only identify a small subset of proteins that play a role in Sml1 regulation. However, given that levels of Sml1 fluctuate throughout the cell cycle (Zhao et al., 1998), an accurate quantitative screen for Sml1 concentration would require a method to synchronize all mutants at the same stage of the cell cycle.

DNA damage and ubiquitin mutants highlight the specificity of the screen

One of the concerns following a genome-wide screen is the level of false positives and mutants that affect the assay rather than the regulation of Sml1 levels. For example, *pat1*Δ, *lsm6*Δ, and *ssz1*Δ were identified in this screen. The first two mutants function in RNA metabolism and have frequently shown up in other genome wide screens performed in the lab. It is possible that these mutants globally upregulate the amount of mRNA, resulting in increased protein levels. A similar pleiotropic protein increase would also account for the identification of *SSZ1*, given its role in translation at the ribosome.

In this screen, the identification of members of the DDR pathway and most crucially, *dun1*Δ, confirmed that we were able to identify expected target genes. Indeed, these mutants were the only genes previously implicated in Sml1 regulation (Zhao et al.,

2001; Zhao and Rothstein, 2002). Mec3, Ddc1, and Rad24 constitute the 9-1-1 clamp and associated clamp loader that serve to activate Mec1 (Majka et al., 2006b). However, one of the components of the 9-1-1 clamp, Rad17, was not found to be important in Sml1 regulation following DNA damage. Further retests of *rad17*Δ validated that YFP-Sml1 is degraded after DNA damage in this mutant. This is in contrast to previous work that showed abrogated Sml1 degradation in a *rad17*Δ mutant following DNA damage by protein blot (Zhao et al., 2001). It could be argued, however, that in the previous study, of all the deletions tested, Sml1 was degraded at a higher level in *rad17*Δ mutants following DNA damage compared to other mutants of the 9-1-1 complex. This likely indicates that the amount of Sml1 required to constitute a "hit" for our screen was high.

From the screen, we also identified all the components of a ubiquitin ligase complex - Rad6, Ubr2 and Mub1 (see Appendix). Given that the non-essential yeast deletion library contains 36 E3s and 6 E2s, it was remarkable that we identified just one E3, Ubr2, and its corresponding E2, Rad6. Furthermore, the screen also identified an associated helper protein, Mub1, which is required for the ubiquitin ligase to functionally bind its substrate. Follow-up experiments showed that the Rad6-Ubr2-Mub1 complex is required for degradation of phosphorylated Sml1 through direct interaction with Sml1 (Andreson et al., 2010). Taken together, the identification of this complex as well as the members of the DDR highlighted not only the sensitivity of the screen, but the specificity as well.

Screen hits indicate regulation of Sml1 outside of the Rad53-Dun1 pathway

Given the specificity of the screen, we were surprised that the largest group of proteins identified encompassed the SAC, kinetochore genes, as well as genes involved in sister chromatid cohesion (Table 3-1). While the SAC has previously been implicated in activation of Rad53 following treatment with nocodazole (Clemenson and Marsolier-Kergoat, 2006), deletion of the components of the SAC did not abrogate Rad53 activation following γ-irradiation (data not shown). Similarly, the rest of this group of mutants also failed to reduce Rad53 activation after damage. Furthermore, *ctf18*Δ, *dcc1*Δ, *irc15*Δ, and *bim1*Δ mutants all show some Rad53 phosphorylation in the absence of damage (data not shown).

To identify at what stage of the Sml1 regulation pathway the mutants identified in the screen were acting, we performed synthetic genetic analysis between each of them and *sml1*Δ. Our expectation was that the phenotype of mutants that normally fail to abrogate the Sml1-Rnr1 interaction during the cell cycle or after damage would be relieved if *SML1* were absent. And indeed, this was the case with mutants of the DDR, which grew better when combined with a *sml1*Δ mutant. However, this was not the case with any other mutants. This result suggested that in all the other mutants, the Sml1-Rnr1 interaction was properly regulated. Taken together, these data suggest that the stabilization of Sml1, in a number of the mutants identified, is through a pathway that is independent of the Rad53-Dun1 arm of the DDR.

Previous work, as well as this study, has shown that Sml1 is regulated not just by Dun1 phosphorylation, but also by Rad6-Ubr2-Mub1 ubiquitylation. It is possible that some of these mutants play a role at this stage of Sml1 regulation. This outcome is hinted

at by two findings: the novel function for Sml1 at the kinetochore shown in Chapter 3 (Figure 3-7), and co-purification of Rad6-Ubr2-Mub1 with the kinetochore in pull-downs that isolate intact kinetochores (Sue Biggins, personal communication). Furthermore, previous work has shown that another kinetochore component, Cse4, is also regulated by ubiquitylation via the E3 ubiquitin ligase, Psh1 (Hewawasam et al., 2010; Ranjitkar et al., 2010). While this model is plausible, it also raises additional questions as to how Rad6-Ubr2-Mub1 is localized to kinetochores as well as how it is regulated. Examining the mutants identified in stabilization of Sml1, we can hypothesize that a functional kinetochore, SAC, and cohesion may play a cooperative role in regulation of Rad6-Ubr2-Mub1, as the loss of any of them results in Sml1 stabilization. If this hypothesis were correct, the data would imply that proper formation of kinetochores and establishment of cohesin results in recruitment of Rad6-Ubr2-Mub1 to ubiquitylate and degrade components that are no longer part of the functional kinetochore. This degradation would prevent the ectopic formation of kinetochores that result in aberrant chromosome segregation. Interestingly, systematic identification of the mammalian proteome implicated hMis18α as being ubiquitylated as well thus indicating the importance of preventing aberrant formation of kinetochores (Kim et al., 2011).

The importance of Sml1 stabilization in mitosis mutants

An important finding from these studies was the identification of Sml1 as the human Mis18α ortholog (Figure 3-8). Indeed, loss of *SML1* resulted in delayed accumulation of Scm3 to distinct foci in the cell (Figure 3-7), similar to mutants of hMis18α (Barnhart et al., 2011b; Fujita et al., 2007). Since Scm3 is essential for

kinetochore assembly, the reduction in Scm3 may account for the subsequent delays in kinetochore assembly and spindle dynamics (Figures 3-6 and 3-7). These new findings may now explain some of the results found previously in the study. The kinetochore defects caused by loss of *SML1* would likely lead to a delay in kinetochore microtubule attachment and hence provide a requirement for a functional SAC to arrest the cell cycle, thereby allowing proper orientation of the spindles to prevent chromosome loss. In support of this idea, loss of the SAC genes *MAD1*, *MAD2*, *BUB3*, or *SGO1* show synthetic growth defects when combined with *sml1*Δ (Figure 3-2). Furthermore, *mad1*Δ *sml1*Δ and *mad2*Δ *sml1*Δ have elevated chromosome loss rates compared to the respective single mutants. Additionally, the loss of the kinetochore function of Sml1 would also explain the synthetic defect seen in a *bim1*Δ *sml1*Δ strain. Bim1 plays a role in stabilization of the inter-polar microtubules that are important for establishment of the spindle (Gardner et al., 2008), and it can be hypothesized that the loss of both *BIM1* and *SML1* would lead to a synergistic defect in kinetochore and spindle formation.

*ctf18*Δ and *dcc1*Δ, on the other hand, are sensitive to the loss of both the kinetochore function as well as the dNTP function of Sml1 (Figure 3-4). It is possible that the rapid progression of the replication fork that occurs in a *sml1*Δ strain (Poli et al., 2012) exacerbates the loss of cohesin seen in either a *ctf18*Δ or a *dcc1*Δ strain (Bermudez et al., 2003; Lengronne et al., 2006). This reduction in cohesin combined with a kinetochore establishment defect would lead to loss in tension between sister chromatids during mitosis, resulting in a G2/M arrest. Indeed, the double mutants (*sml1*Δ *ctf18*Δ or *sml1*Δ *dcc1*Δ) appear to arrest in G2/M by FACS analysis (data not shown). Given this

result, we hypothesize that increasing the amount of cohesin in the double mutant alleviates the growth defect seen.

Taken together, these data identify a novel role for Sml1 in kinetochore assembly. Loss of this function results in reduced recruitment of the kinetochore establishment factor, Scm3, leading to a delay in kinetochore assembly and subsequent kinetochore microtubule attachment. To compensate for the defect, the SAC is activated to arrest the cell cycle at G2/M. However, loss of some components of the SAC, reduction in cohesin, or affecting spindle assembly results in synthetic growth defects due to chromosome loss.

Future directions

The dual function of Sml1 combined with the fact that it is regulated by the DDR provides an intriguing link to the SAC. Previous work from the Burke and the Rine labs has shown that the DDR and SAC function redundantly to arrest cells at G2/M following DNA damage caused during replication (Garber and Rine, 2002; Kim and Burke, 2008). Furthermore, the Rad53-Dun1 pathway and Pds1 combine equally to arrest cells prior to anaphase following triggering of the DDR using a *cdc13-1* mutant (Gardner et al., 1999). One could hypothesize that this cross-talk could be as a result of a feed-forward mechanism triggered by regulation of Sml1.

Following DNA damage, Sml1 is phosphorylated, leading to its dissociation from Rnr1 (Zhao et al., 2001). This modification leads to the relocalization of Sml1 to the nucleus, where it is phosphorylated by Dun1 a second time before being degraded in a ubiquitin dependent manner. The relocalization is seen in a small percentage of unbudded

cells but mostly in cells that have a small bud (Andreson et al., manuscript in preparation). This coincides with the start of S-phase in *Saccharomyces cerevisiae*, which results in dissociation of kinetochores from the centromeres followed by re-establishment of kinetochores later in S-phase (Kitamura et al., 2007). Therefore, it can be inferred that the phosphorylation by the DDR and subsequent relocalization of Sml1 is important for establishment of new kinetochores in the cell. Furthermore, given that loss of *SML1* triggers a need for a functional SAC, we can create a model whereby the lack of a functional DDR triggers SAC activation due to Sml1 mislocalization (Figure 4-2).

To test this hypothesis, we would need to identify separation of function Sml1 mutants. Previous work from the Rothstein lab has identified numerous mutants that affect the interaction between Sml1 and Rnr1 that could be starting points for this analysis (Andreson et al., 2010; Zhao et al., 2000); Andreson et al., ms. in prep; data not shown). There were two groups of mutants that were focused on for further characterization. One group included mutations of the putative SUMO modification site of Sml1 as well as mutations of the other three lysines on Sml1 (Figure 4-1A). This group was chosen, as SUMO modifications have been previously implicated in uncovering secondary roles for proteins (Papouli et al., 2005). Loss of SUMO modification by these mutants or by deletion of SUMO E3 ligases, *SIZ1* and *SIZ2*, resulted in a reduction in Sml1 levels in the cell (Figure 4-1B and C). Preliminary analysis of these mutants indicated that loss of only the putative SUMO site caused a kinetochore assembly delay, while mutation of the other lysines did not (data not shown).

The second group included mutants that show modification in the region of homology between Sml1 and human Mis18α (Figure 3-8) and which contain two clusters

of serines that are modified by Dun1 following DNA damage (Andreson et al., 2010; Uchiki et al., 2004)Andreson et al., ms. in prep). Phosphorylation of the first serine cluster leads to dissociation of Sml1 from Rnr1 and subsequent relocalization. Blocking phosphorylation of this cluster (*sml1-SA1)* prevents relocalization, while mimicking it (*sml1-SD1*) leads to greater accumulation in the nucleus, even in the absence of damage. The second serine cluster is phosphorylated in the nucleus, promoting Sml1 degradation. In this case, blocking phosphorylation (*sml1-SA2*) resulted in nuclear accumulation of Sml1 following bud appearance or DNA damage, while mimicking phosphorylation (*sml1-SD2*) resulted in more rapid degradation of Sml1 (Andreson et al., manuscript in preparation). Preliminary analysis with these mutants indicated that either inhibition of Sml1 relocalization (*sml1-SA1*) or more rapid nuclear degradation of Sml1 (*sml1-SD2*) resulted in kinetochore establishment defects. Conversely, *sml1-SD1* and *sml1-SA2* mutants showed no such defects, and could thus be the separation of function mutants that would be required.

Of these groups of *sml1* mutants, the ones that are wild-type for kinetochore assembly would need to be followed further to determine if they are also wild type for kinetochore assembly in a *rad9*Δ *rad24*Δ mutant following DNA damage. This is important because, in this mutant, the DDR is abrogated and the cells show a G2/M arrest in a SAC dependent manner following damage (Kim and Burke, 2008). If however, these mutants are able to form kinetochores with kinetics similar to wild-type, it would be interesting to note if the cells now no longer show the characteristic G2/M arrest following damage.

Conclusion

Taken together, this work expanded our understanding of the role of Sml1 in telomere length homeostasis via dNTP pool regulation and also uncovered a novel role for Sml1 in kinetochore assembly. While the elucidation of the dependence of telomerase on dGTP was an important result, the most significant findings from this study centered on the secondary role of Sml1. These findings add to previous work that describes the modification and movement of Sml1 by providing an end point to the relocalization. Indeed, from this work we can state the following model: DNA damage induces Dun1-dependent Sml1 phosphorylation, which in turn causes Sml1 relocalization to the nucleus. In the nucleus, Sml1 plays a role in recruitment of Scm3 leading to proper kinetochore assembly. Once the kinetochores are properly assembled, Sml1 is phosphorylated a second time by Dun1, which leads to its ubiquitylation and subsequent degradation (Figure 4-2). Given that numerous studies utilize a *sml1*Δ to allow for survival of *mec1* and *rad53* mutants, this new finding is important in the interpretation of the data obtained.

Figure 4-1:

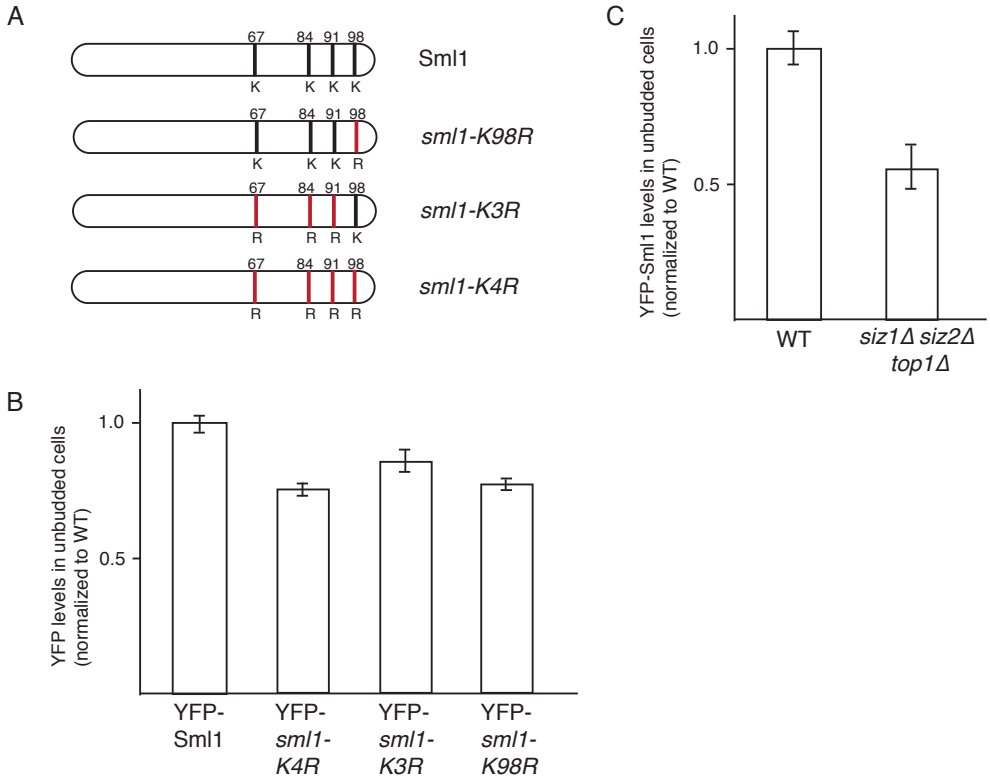

Figure 4-1: Loss of sumoylation reduces levels of Sml1 in the cell. (A) Location of lysines in Sml1. The lysine at position 98 is a putitive SUMO site and thus was mutated to arginine to give *sml1-K98R*. In the event that the sumoylation could occur non-specifically, all four lysines were mutated to arginines – *sml1-K4R*. To confirm SUMO specificity, the three non-SUMO lysines were mutated to arginines - *sml1-K3R*. (B) The lysine mutants described in (A) were YFP-tagged, grown up and compared to wild-type YFP-Sml1 levels in unbudded cells. Loss of the SUMO site resulted in reduction of YFP signal. (C) To confirm SUMO effect on Sml1, YFP-Sml1 was introduced into a *siz1*Δ *siz2*Δ *top1*Δ mutant, which shows reduced global sumoylation. Deletion of *TOP1* is to prevent Rad52 dependent damage. YFP-Sml1 levels were measured in unbudded mutant and wild-type cells. All bars represent Standard Error.

Figure 4-2:

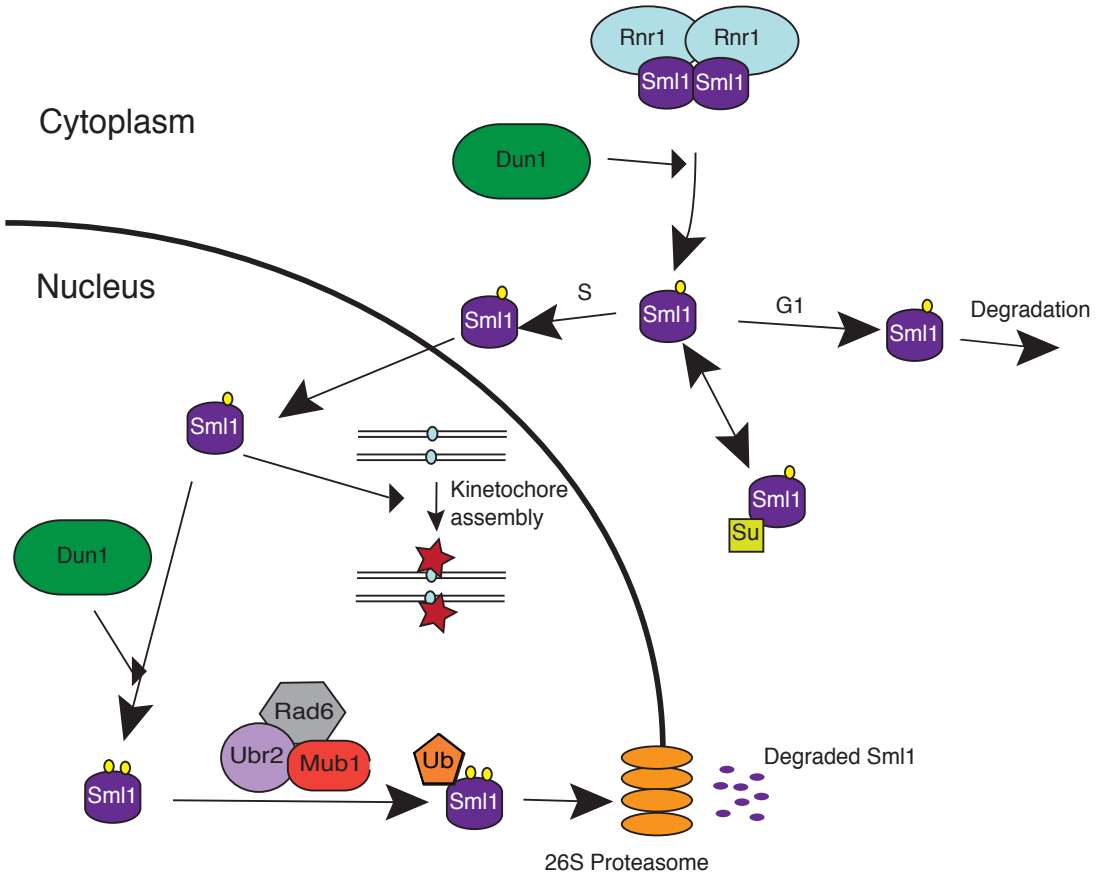

Figure 4-2: New Model for Sml1 cycle in the cell. Sml1 is phosphorylated by Dun1 and subsequently dissociates from Rnr1. If the dissociation is temporary, Sml1 is sumoylated to prevent degradation. Loss of sumoylation leads to degradation of Sml1. At the start of S-phase, dissociated Sml1 is translocated to the nucleus. In the nucleus, Sml1 plays a role in kinetochore assembly by recruitment of Scm3. This recruitment can be abrogated by phosphorylation of Sml1. The doubly phosphorylated Sml1 is ubiquitylated by the Rad6-Ubr2-Mub1 complex and degraded by the 26S proteasome.

REFERENCES:

Akiyoshi, B., Sarangapani, K.K., Powers, A.F., Nelson, C.R., Reichow, S.L., Arellano-Santoyo, H., Gonen, T., Ranish, J.A., Asbury, C.L., and Biggins, S. (2010). Tension directly stabilizes reconstituted kinetochore-microtubule attachments. Nature *468*, 576-579.

Alani, E., Thresher, R., Griffith, J.D., and Kolodner, R.D. (1992). Characterization of DNA-binding and strand-exchange stimulation properties of y-RPA, a yeast single-strand-DNA-binding protein. J Mol Biol *227*, 54-71.

Alvaro, D., Lisby, M., and Rothstein, R. (2007). Genome-wide analysis of Rad52 foci reveals diverse mechanisms impacting recombination. PLoS Genet *3*, e228.

Andreson, B.L., Gupta, A., Georgieva, B.P., and Rothstein, R. (2010). The ribonucleotide reductase inhibitor, Sml1, is sequentially phosphorylated, ubiquitylated and degraded in response to DNA damage. Nucleic acids research *38*, 6490-6501.

Armanios, M. (2009). Syndromes of telomere shortening. Annu Rev Genomics Hum Genet *10*, 45-61.

Arnerić, M., and Lingner, J. (2007). Tel1 kinase and subtelomere-bound Tbf1 mediate preferential elongation of short telomeres by telomerase in yeast. EMBO Rep *8*, 1080-1085.

Ball, H.L., Ehrhardt, M.R., Mordes, D.A., Glick, G.G., Chazin, W.J., and Cortez, D. (2007). Function of a conserved checkpoint recruitment domain in ATRIP proteins. Mol Cell Biol *27*, 3367-3377.

Barlow, J.H., Lisby, M., and Rothstein, R. (2008). Differential regulation of the cellular response to DNA double-strand breaks in G1. Molecular cell *30*, 73-85.

Barnhart, E.L., Dorer, R.K., Murray, A.W., and Schuyler, S.C. (2011a). Reduced Mad2 expression keeps relaxed kinetochores from arresting budding yeast in mitosis. Mol Biol Cell *22*, 2448-2457.

Barnhart, M.C., Kuich, P.H., Stellfox, M.E., Ward, J.A., Bassett, E.A., Black, B.E., and Foltz, D.R. (2011b). HJURP is a CENP-A chromatin assembly factor sufficient to form a functional de novo kinetochore. J Cell Biol *194*, 229-243.

Bashkirov, V.I., Bashkirova, E.V., Haghnazari, E., and Heyer, W.D. (2003). Direct kinase-to-kinase signaling mediated by the FHA phosphoprotein recognition domain of the Dun1 DNA damage checkpoint kinase. Mol Cell Biol *23*, 1441-1452.

Bermudez, V.P., Maniwa, Y., Tappin, I., Ozato, K., Yokomori, K., and Hurwitz, J. (2003). The alternative Ctf18-Dcc1-Ctf8-replication factor C complex required for sister chromatid cohesion loads proliferating cell nuclear antigen onto DNA. Proc Natl Acad Sci U S A *100*, 10237-10242.

Bernstein, K.A., Reid, R.J., Sunjevaric, I., Demuth, K., Burgess, R.C., and Rothstein, R. (2011). The Shu complex, which contains Rad51 paralogues, promotes DNA repair through inhibition of the Srs2 anti-recombinase. Mol Biol Cell *22*, 1599-1607.

Bosoy, D., and Lue, N.F. (2004). Yeast telomerase is capable of limited repeat addition processivity. Nucleic acids research *32*, 93-101.

Brachmann, C.B., Davies, A., Cost, G.J., Caputo, E., Li, J., Hieter, P., and Boeke, J.D. (1998). Designer deletion strains derived from *Saccharomyces cerevisiae* S288C: a useful set of strains and plasmids for PCR-mediated gene disruption and other applications. Yeast *14*, 115-132.

Burrack, L.S., and Berman, J. (2012). Flexibility of centromere and kinetochore structures. Trends Genet *28*, 204-212.

Camahort, R., Li, B., Florens, L., Swanson, S.K., Washburn, M.P., and Gerton, J.L. (2007). Scm3 is essential to recruit the histone h3 variant cse4 to centromeres and to maintain a functional kinetochore. Molecular cell *26*, 853-865.

Chabes, A., Domkin, V., Larsson, G., Liu, A., Graslund, A., Wijmenga, S., and Thelander, L. (2000). Yeast ribonucleotide reductase has a heterodimeric iron-radical-containing subunit. Proc Natl Acad Sci U S A *97*, 2474-2479.

Chabes, A., Domkin, V., and Thelander, L. (1999). Yeast Sml1, a protein inhibitor of ribonucleotide reductase. The Journal of biological chemistry *274*, 36679-36683.

Chabes, A., Georgieva, B., Domkin, V., Zhao, X., Rothstein, R., and Thelander, L. (2003a). Survival of DNA damage in yeast directly depends on increased dNTP levels allowed by relaxed feedback inhibition of ribonucleotide reductase. Cell *112*, 391-401.

Chabes, A., and Stillman, B. (2007). Constitutively high dNTP concentration inhibits cell cycle progression and the DNA damage checkpoint in yeast Saccharomyces cerevisiae. Proc Natl Acad Sci U S A *104*, 1183-1188.

Chabes, A.L., Pfleger, C.M., Kirschner, M.W., and Thelander, L. (2003b). Mouse ribonucleotide reductase R2 protein: a new target for anaphase-promoting complex-Cdh1-mediated proteolysis. Proc Natl Acad Sci U S A *100*, 3925-3929.

Chai, W., Sfeir, A.J., Hoshiyama, H., Shay, J.W., and Wright, W.E. (2006). The involvement of the Mre11/Rad50/Nbs1 complex in the generation of G-overhangs at human telomeres. EMBO Rep *7*, 225-230.

Chang, M., Arneric, M., and Lingner, J. (2007). Telomerase repeat addition processivity is increased at critically short telomeres in a Tel1-dependent manner in Saccharomyces cerevisiae. Genes & development *21*, 2485-2494.

Chen, S.H., Albuquerque, C.P., Liang, J., Suhandynata, R.T., and Zhou, H. (2010). A proteome-wide analysis of kinase-substrate network in the DNA damage response. The Journal of biological chemistry *285*, 12803-12812.

Chen, S.H., Smolka, M.B., and Zhou, H. (2007). Mechanism of Dun1 activation by Rad53 phosphorylation in Saccharomyces cerevisiae. The Journal of biological chemistry *282*, 986-995.

Chu, H.M., Yun, M., Anderson, D.E., Sage, H., Park, H.W., and Endow, S.A. (2005). Kar3 interaction with Cik1 alters motor structure and function. Embo J *24*, 3214-3223.

Ciosk, R., Shirayama, M., Shevchenko, A., Tanaka, T., Toth, A., and Nasmyth, K. (2000). Cohesin's binding to chromosomes depends on a separate complex consisting of Scc2 and Scc4 proteins. Molecular cell *5*, 243-254.

Clemenson, C., and Marsolier-Kergoat, M.C. (2006). The spindle assembly checkpoint regulates the phosphorylation state of a subset of DNA checkpoint proteins in Saccharomyces cerevisiae. Mol Cell Biol *26*, 9149-9161.

Cohn, M., and Blackburn, E.H. (1995). Telomerase in yeast. Science *269*, 396-400.

Collins, K. (2006). The biogenesis and regulation of telomerase holoenzymes. Nat Rev Mol Cell Biol *7*, 484-494.

Cottingham, F.R., Gheber, L., Miller, D.L., and Hoyt, M.A. (1999). Novel roles for saccharomyces cerevisiae mitotic spindle motors. J Cell Biol *147*, 335-350.

Cristofari, G., Reichenbach, P., Regamey, P.O., Banfi, D., Chambon, M., Turcatti, G., and Lingner, J. (2007). Low- to high-throughput analysis of telomerase modulators with Telospot. Nat Methods *4*, 851-853.

Cross, F.R. (1997). 'Marker swap' plasmids: convenient tools for budding yeast molecular genetics. Yeast *13*, 647-653.

Danielsson, J., Liljedahl, L., Barany-Wallje, E., Sonderby, P., Kristensen, L.H., Martinez-Yamout, M.A., Dyson, H.J., Wright, P.E., Poulsen, F.M., Maler, L.*, et al*. (2008). The intrinsically disordered RNR inhibitor Sml1 is a dynamic dimer. Biochemistry *47*, 13428-13437.

Davidson, M.B., Katou, Y., Keszthelyi, A., Sing, T.L., Xia, T., Ou, J., Vaisica, J.A., Thevakumaran, N., Marjavaara, L., Myers, C.L.*, et al*. (2012). Endogenous DNA replication stress results in expansion of dNTP pools and a mutator phenotype. Embo J *31*, 895-907.

de Bruin, R.A., Kalashnikova, T.I., Chahwan, C., McDonald, W.H., Wohlschlegel, J., Yates, J., 3rd, Russell, P., and Wittenberg, C. (2006). Constraining G1-specific transcription to late G1 phase: the MBF-associated corepressor Nrm1 acts via negative feedback. Molecular cell *23*, 483-496.

de Lange, T. (2009). How telomeres solve the end-protection problem. Science *326*, 948-952.

Desany, B.A., Alcasabas, A.A., Bachant, J.B., and Elledge, S.J. (1998). Recovery from DNA replicational stress is the essential function of the S-phase checkpoint pathway. Genes & development *12*, 2956-2970.

DeZwaan, D.C., and Freeman, B.C. (2010). Is there a telomere-bound 'EST' telomerase holoenzyme? Cell Cycle *9*, 1913-1917.

Diffley, J.F., and Labib, K. (2002). The chromosome replication cycle. J Cell Sci *115*, 869-872.

Domkin, V., Thelander, L., and Chabes, A. (2002). Yeast DNA damage-inducible Rnr3 has a very low catalytic activity strongly stimulated after the formation of a cross-talking Rnr1/Rnr3 complex. The Journal of biological chemistry *277*, 18574-18578.

Elledge, S.J., and Davis, R.W. (1987). Identification and isolation of the gene encoding the small subunit of ribonucleotide reductase from Saccharomyces cerevisiae: DNA damage-inducible gene required for mitotic viability. Mol Cell Biol *7*, 2783-2793.

Elledge, S.J., and Davis, R.W. (1990). Two genes differentially regulated in the cell cycle and by DNA-damaging agents encode alternative regulatory subunits of ribonucleotide reductase. Genes & development *4*, 740-751.

Emili, A. (1998). MEC1-dependent phosphorylation of Rad9p in response to DNA damage. Molecular cell *2*, 183-189.

Fasullo, M., Tsaponina, O., Sun, M., and Chabes, A. (2010). Elevated dNTP levels suppress hyper-recombination in Saccharomyces cerevisiae S-phase checkpoint mutants. Nucleic acids research *38*, 1195-1203.

Feng, J., Funk, W.D., Wang, S.S., Weinrich, S.L., Avilion, A.A., Chiu, C.P., Adams, R.R., Chang, E., Allsopp, R.C., Yu, J., *et al*. (1995). The RNA component of human telomerase. Science *269*, 1236-1241.

Finn, K., Lowndes, N.F., and Grenon, M. (2011). Eukaryotic DNA damage checkpoint activation in response to double-strand breaks. Cell Mol Life Sci.

Foltz, D.R., Jansen, L.E., Bailey, A.O., Yates, J.R., 3rd, Bassett, E.A., Wood, S., Black, B.E., and Cleveland, D.W. (2009). Centromere-specific assembly of CENP-a nucleosomes is mediated by HJURP. Cell *137*, 472-484.

Forstemann, K., Hoss, M., and Lingner, J. (2000). Telomerase-dependent repeat divergence at the 3' ends of yeast telomeres. Nucleic acids research *28*, 2690-2694.

Forstemann, K., and Lingner, J. (2001). Molecular basis for telomere repeat divergence in budding yeast. Mol Cell Biol *21*, 7277-7286.

Fraschini, R., Beretta, A., Sironi, L., Musacchio, A., Lucchini, G., and Piatti, S. (2001). Bub3 interaction with Mad2, Mad3 and Cdc20 is mediated by WD40 repeats and does not require intact kinetochores. Embo J *20*, 6648-6659.

Fujita, Y., Hayashi, T., Kiyomitsu, T., Toyoda, Y., Kokubu, A., Obuse, C., and Yanagida, M. (2007). Priming of centromere for CENP-A recruitment by human hMis18alpha, hMis18beta, and M18BP1. Dev Cell *12*, 17-30.

Fulton, T.B., and Blackburn, E.H. (1998). Identification of Kluyveromyces lactis telomerase: discontinuous synthesis along the 30-nucleotide-long templating domain. Mol Cell Biol *18*, 4961-4970.

Garber, P.M., and Rine, J. (2002). Overlapping roles of the spindle assembly and DNA damage checkpoints in the cell-cycle response to altered chromosomes in Saccharomyces cerevisiae. Genetics *161*, 521-534.

Gardner, M.K., Haase, J., Mythreye, K., Molk, J.N., Anderson, M., Joglekar, A.P., O'Toole, E.T., Winey, M., Salmon, E.D., Odde, D.J., *et al*. (2008). The microtubule-based motor Kar3 and plus end-binding protein Bim1 provide structural support for the anaphase spindle. J Cell Biol *180*, 91-100.

Gardner, R., Putnam, C.W., and Weinert, T. (1999). RAD53, DUN1 and PDS1 define two parallel G2/M checkpoint pathways in budding yeast. Embo J *18*, 3173-3185.

Garvik, B., Carson, M., and Hartwell, L. (1995). Single-stranded DNA arising at telomeres in cdc13 mutants may constitute a specific signal for the RAD9 checkpoint. Mol Cell Biol *15*, 6128-6138.

Gatbonton, T., Imbesi, M., Nelson, M., Akey, J.M., Ruderfer, D.M., Kruglyak, L., Simon, J.A., and Bedalov, A. (2006). Telomere length as a quantitative trait: genome-wide survey and genetic mapping of telomere length-control genes in yeast. PLoS Genet *2*, e35.

Ge, J., Perlstein, D.L., Nguyen, H.H., Bar, G., Griffin, R.G., and Stubbe, J. (2001). Why multiple small subunits (Y2 and Y4) for yeast ribonucleotide reductase? Toward understanding the role of Y4. Proc Natl Acad Sci U S A *98*, 10067-10072.

Giaever, G., Chu, A.M., Ni, L., Connelly, C., Riles, L., Veronneau, S., Dow, S., Lucau-Danila, A., Anderson, K., Andre, B., *et al*. (2002). Functional profiling of the Saccharomyces cerevisiae genome. Nature *418*, 387-391.

Gilbert, C.S., Green, C.M., and Lowndes, N.F. (2001). Budding yeast Rad9 is an ATP-dependent Rad53 activating machine. Molecular cell *8*, 129-136.

Greenwell, P.W., Kronmal, S.L., Porter, S.E., Gassenhuber, J., Obermaier, B., and Petes, T.D. (1995). *TEL1*, a gene involved in controlling telomere length in *S. cerevisiae*, is homologous to the human ataxia telangiectasia gene. Cell *82*, 823-829.

Greider, C.W. (1991). Telomerase is processive. Mol Cell Biol *11*, 4572-4580.

Greider, C.W. (1996). Telomere length regulation. Annual review of biochemistry *65*, 337-365.

Greider, C.W., and Blackburn, E.H. (1985). Identification of a specific telomere terminal transferase activity in Tetrahymena extracts. Cell *43*, 405-413.

Greider, C.W., and Blackburn, E.H. (1989). A telomeric sequence in the RNA of Tetrahymena telomerase required for telomere repeat synthesis. Nature *337*, 331-337.

Guacci, V., Koshland, D., and Strunnikov, A. (1997). A direct link between sister chromatid cohesion and chromosome condensation revealed through the analysis of MCD1 in S. cerevisiae. Cell *91*, 47-57.

Haering, C.H., Nakamura, T.M., Baumann, P., and Cech, T.R. (2000). Analysis of telomerase catalytic subunit mutants in vivo and in vitro in Schizosaccharomycespombe. Proc Natl Acad Sci U S A *97*, 6367-6372.

Hakansson, P., Hofer, A., and Thelander, L. (2006). Regulation of mammalian ribonucleotide reduction and dNTP pools after DNA damage and in resting cells. The Journal of biological chemistry *281*, 7834-7841.

Hammond, P.W., and Cech, T.R. (1997). dGTP-dependent processivity and possible template switching of *Euplotes* telomerase. Nucleic acids research *25*, 3698-3704.

Hammond, P.W., and Cech, T.R. (1998). Euplotes telomerase: evidence for limited base-pairing during primer elongation and dGTP as an effector of translocation. Biochemistry *37*, 5162-5172.

Hammond, P.W., Lively, T.N., and Cech, T.R. (1997). The anchor site of telomerase from Euplotes aediculatus revealed by photo-cross-linking to single- and double-stranded DNA primers. Mol Cell Biol *17*, 296-308.

Hardy, C.D., Schultz, C.S., and Collins, K. (2001). Requirements for the dGTP-dependent repeat addition processivity of recombinant Tetrahymena telomerase. The Journal of biological chemistry *276*, 4863-4871.

Harley, C.B., Futcher, A.B., and Greider, C.W. (1990). Telomeres shorten during ageing of human fibroblasts. Nature *345*, 458-460.

Harrington, L., Zhou, W., McPhail, T., Oulton, R., Yeung, D.S., Mar, V., Bass, M.B., and Robinson, M.O. (1997). Human telomerase contains evolutionarily conserved catalytic and structural subunits. Genes & development *11*, 3109-3115.

Harrison, J.C., and Haber, J.E. (2006). Surviving the breakup: the DNA damage checkpoint. Annu Rev Genet *40*, 209-235.

Hayashi, T., Fujita, Y., Iwasaki, O., Adachi, Y., Takahashi, K., and Yanagida, M. (2004). Mis16 and Mis18 are required for CENP-A loading and histone deacetylation at centromeres. Cell *118*, 715-729.

Hewawasam, G., Shivaraju, M., Mattingly, M., Venkatesh, S., Martin-Brown, S., Florens, L., Workman, J.L., and Gerton, J.L. (2010). Psh1 is an E3 ubiquitin ligase that targets the centromeric histone variant Cse4. Molecular cell *40*, 444-454.

Hoyt, M.A., Totis, L., and Roberts, B.T. (1991). S. cerevisiae genes required for cell cycle arrest in response to loss of microtubule function. Cell *66*, 507-517.

Huang, M., and Elledge, S.J. (1997). Identification of RNR4, encoding a second essential small subunit of ribonucleotide reductase in Saccharomyces cerevisiae. Mol Cell Biol *17*, 6105-6113.

Huang, M., Zhou, Z., and Elledge, S.J. (1998). The DNA replication and damage checkpoint pathways induce transcription by inhibition of the Crt1 repressor. Cell *94*, 595-605.

Hug, N., and Lingner, J. (2006). Telomere length homeostasis. Chromosoma *115*, 413-425.

Huh, W.K., Falvo, J.V., Gerke, L.C., Carroll, A.S., Howson, R.W., Weissman, J.S., and O'Shea, E.K. (2003). Global analysis of protein localization in budding yeast. Nature *425*, 686-691.

Indjeian, V.B., Stern, B.M., and Murray, A.W. (2005). The centromeric protein Sgo1 is required to sense lack of tension on mitotic chromosomes. Science *307*, 130-133.

Jacob, N.K., Kirk, K.E., and Price, C.M. (2003). Generation of telomeric G strand overhangs involves both G and C strand cleavage. Molecular cell *11*, 1021-1032.

Kim, C., Snyder, R.O., and Wold, M.S. (1992). Binding properties of replication protein A from human and yeast cells. Mol Cell Biol *12*, 3050-3059.

Kim, E.M., and Burke, D.J. (2008). DNA damage activates the SAC in an ATM/ATR-dependent manner, independently of the kinetochore. PLoS Genet *4*, e1000015.

Kim, W., Bennett, E.J., Huttlin, E.L., Guo, A., Li, J., Possemato, A., Sowa, M.E., Rad, R., Rush, J., Comb, M.J., *et al*. (2011). Systematic and quantitative assessment of the ubiquitin-modified proteome. Molecular cell *44*, 325-340.

Kitajima, T.S., Kawashima, S.A., and Watanabe, Y. (2004). The conserved kinetochore protein shugoshin protects centromeric cohesion during meiosis. Nature *427*, 510-517.

Kitamura, E., Tanaka, K., Kitamura, Y., and Tanaka, T.U. (2007). Kinetochore microtubule interaction during S phase in Saccharomyces cerevisiae. Genes & development *21*, 3319-3330.

Klinkenberg, L.G., Webb, T., and Zitomer, R.S. (2006). Synergy among differentially regulated repressors of the ribonucleotide diphosphate reductase genes of Saccharomyces cerevisiae. Eukaryot Cell *5*, 1007-1017.

Kondo, T., Matsumoto, K., and Sugimoto, K. (1999). Role of a complex containing Rad17, Mec3, and Ddc1 in the yeast DNA damage checkpoint pathway. Mol Cell Biol *19*, 1136-1143.

Kumar, D., Abdulovic, A.L., Viberg, J., Nilsson, A.K., Kunkel, T.A., and Chabes, A. (2011). Mechanisms of mutagenesis in vivo due to imbalanced dNTP pools. Nucleic acids research *39*, 1360-1371.

Kumar, D., Viberg, J., Nilsson, A.K., and Chabes, A. (2010). Highly mutagenic and severely imbalanced dNTP pools can escape detection by the S-phase checkpoint. Nucleic acids research *38*, 3975-3983.

Larrivee, M., LeBel, C., and Wellinger, R.J. (2004). The generation of proper constitutive G-tails on yeast telomeres is dependent on the MRX complex. Genes & development *18*, 1391-1396.

Larson, G.P., Castanotto, D., Rossi, J.J., and Malafa, M.P. (1994). Isolation and functional analysis of a Kluyveromyces lactis RAP1 homologue. Gene *150*, 35-41.

Lee, M.S., and Spencer, F.A. (2004). Bipolar orientation of chromosomes in Saccharomyces cerevisiae is monitored by Mad1 and Mad2, but not by Mad3. Proc Natl Acad Sci U S A *101*, 10655-10660.

Lee, Y.D., and Elledge, S.J. (2006). Control of ribonucleotide reductase localization through an anchoring mechanism involving Wtm1. Genes & development *20*, 334-344.

Lee, Y.D., Wang, J., Stubbe, J., and Elledge, S.J. (2008). Dif1 is a DNA-damage-regulated facilitator of nuclear import for ribonucleotide reductase. Molecular cell *32*, 70-80.

Lengronne, A., McIntyre, J., Katou, Y., Kanoh, Y., Hopfner, K.P., Shirahige, K., and Uhlmann, F. (2006). Establishment of sister chromatid cohesion at the S. cerevisiae replication fork. Molecular cell *23*, 787-799.

Lew, D.J., and Burke, D.J. (2003). The spindle assembly and spindle position checkpoints. Annu Rev Genet *37*, 251-282.

Li, J., Lee, G.I., Van Doren, S.R., and Walker, J.C. (2000). The FHA domain mediates phosphoprotein interactions. J Cell Sci *113 Pt 23*, 4143-4149.

Li, R., and Murray, A.W. (1991). Feedback control of mitosis in budding yeast. Cell *66*, 519-531.

Li, X., and Nicklas, R.B. (1995). Mitotic forces control a cell-cycle checkpoint. Nature *373*, 630-632.

Lingner, J., Cech, T.R., Hughes, T.R., and Lundblad, V. (1997a). Three Ever Shorter Telomere (EST) genes are dispensable for in vitro yeast telomerase activity. Proc Natl Acad Sci U S A *94*, 11190-11195.

Lingner, J., Hughes, T.R., Shevchenko, A., Mann, M., Lundblad, V., and Cech, T.R. (1997b). Reverse transcriptase motifs in the catalytic subunit of telomerase. Science *276*, 561-567.

Lisby, M., Barlow, J.H., Burgess, R.C., and Rothstein, R. (2004). Choreography of the DNA damage response: spatiotemporal relationships among checkpoint and repair proteins. Cell *118*, 699-713.

Lisby, M., Rothstein, R., and Mortensen, U.H. (2001). Rad52 forms DNA repair and recombination centers during S phase. Proc Natl Acad Sci U S A *98*, 8276-8282.

Liu, H., Jin, F., Liang, F., Tian, X., and Wang, Y. (2011). The Cik1/Kar3 motor complex is required for the proper kinetochore-microtubule interaction after stressful DNA replication. Genetics *187*, 397-407.

Lue, N.F. (2004). Adding to the ends: what makes telomerase processive and how important is it? Bioessays *26*, 955-962.

Lue, N.F., Lin, Y.C., and Mian, I.S. (2003). A conserved telomerase motif within the catalytic domain of telomerase reverse transcriptase is specifically required for repeat addition processivity. Mol Cell Biol *23*, 8440-8449.

Lue, N.F., and Peng, Y. (1997). Identification and characterization of a telomerase activity from Schizosaccharomyces pombe. Nucleic acids research *25*, 4331-4337.

Lundblad, V., and Szostak, J.W. (1989). A mutant with a defect in telomere elongation leads to senescence in yeast. Cell *57*, 633-643.

Lydall, D., and Weinert, T. (1995). Yeast checkpoint genes in DNA damage processing: implications for repair and arrest. Science *270*, 1488-1491.

Majka, J., Binz, S.K., Wold, M.S., and Burgers, P.M. (2006a). Replication protein A directs loading of the DNA damage checkpoint clamp to 5'-DNA junctions. The Journal of biological chemistry *281*, 27855-27861.

Majka, J., Niedziela-Majka, A., and Burgers, P.M. (2006b). The checkpoint clamp activates Mec1 kinase during initiation of the DNA damage checkpoint. Molecular cell *24*, 891-901.

Mason, M., Schuller, A., and Skordalakes, E. (2011). Telomerase structure function. Current opinion in structural biology *21*, 92-100.

Mayer, M.L., Gygi, S.P., Aebersold, R., and Hieter, P. (2001). Identification of RFC(Ctf18p, Ctf8p, Dcc1p): an alternative RFC complex required for sister chromatid cohesion in S. cerevisiae. Molecular cell *7*, 959-970.

Mayer, M.L., Pot, I., Chang, M., Xu, H., Aneliunas, V., Kwok, T., Newitt, R., Aebersold, R., Boone, C., Brown, G.W., *et al*. (2004). Identification of protein complexes required for efficient sister chromatid cohesion. Mol Biol Cell *15*, 1736-1745.

Melo, J.A., Cohen, J., and Toczyski, D.P. (2001). Two checkpoint complexes are independently recruited to sites of DNA damage in vivo. Genes & development *15*, 2809-2821.

Meluh, P.B., Yang, P., Glowczewski, L., Koshland, D., and Smith, M.M. (1998). Cse4p is a component of the core centromere of Saccharomyces cerevisiae. Cell *94*, 607-613.

Meyne, J., Ratliff, R.L., and Moyzis, R.K. (1989). Conservation of the human telomere sequence (TTAGGG)n among vertebrates. Proc Natl Acad Sci U S A *86*, 7049-7053.

Mimitou, E.P., and Symington, L.S. (2008). Sae2, Exo1 and Sgs1 collaborate in DNA double-strand break processing. Nature *455*, 770-774.

Mimitou, E.P., and Symington, L.S. (2011). DNA end resection--unraveling the tail. DNA Repair (Amst) *10*, 344-348.

Mishra, P.K., Au, W.C., Choy, J.S., Kuich, P.H., Baker, R.E., Foltz, D.R., and Basrai, M.A. (2011). Misregulation of Scm3p/HJURP causes chromosome instability in Saccharomyces cerevisiae and human cells. PLoS Genet *7*, e1002303.

Morin, G.B. (1989). The human telomere terminal transferase enzyme is a ribonucleoprotein that synthesizes TTAGGG repeats. Cell *59*, 521-529.

Musacchio, A., and Salmon, E.D. (2007). The spindle-assembly checkpoint in space and time. Nat Rev Mol Cell Biol *8*, 379-393.

Naiki, T., Kondo, T., Nakada, D., Matsumoto, K., and Sugimoto, K. (2001). Chl12 (Ctf18) forms a novel replication factor C-related complex and functions redundantly with Rad24 in the DNA replication checkpoint pathway. Mol Cell Biol *21*, 5838-5845.

Nakamura, T.M., Morin, G.B., Chapman, K.B., Weinrich, S.L., Andrews, W.H., Lingner, J., Harley, C.B., and Cech, T.R. (1997). Telomerase catalytic subunit homologs from fission yeast and human. Science *277*, 955-959.

Navadgi-Patil, V.M., and Burgers, P.M. (2009). A tale of two tails: activation of DNA damage checkpoint kinase Mec1/ATR by the 9-1-1 clamp and by Dpb11/TopBP1. DNA Repair (Amst) *8*, 996-1003.

Ng, T.M., Waples, W.G., Lavoie, B.D., and Biggins, S. (2009). Pericentromeric sister chromatid cohesion promotes kinetochore biorientation. Mol Biol Cell *20*, 3818-3827.

Nick McElhinny, S.A., Kumar, D., Clark, A.B., Watt, D.L., Watts, B.E., Lundstrom, E.B., Johansson, E., Chabes, A., and Kunkel, T.A. (2010a). Genome instability due to ribonucleotide incorporation into DNA. Nat Chem Biol *6*, 774-781.

Nick McElhinny, S.A., Watts, B.E., Kumar, D., Watt, D.L., Lundstrom, E.B., Burgers, P.M., Johansson, E., Chabes, A., and Kunkel, T.A. (2010b). Abundant ribonucleotide incorporation into DNA by yeast replicative polymerases. Proc Natl Acad Sci U S A *107*, 4949-4954.

Nicklas, R.B., Ward, S.C., and Gorbsky, G.J. (1995). Kinetochore chemistry is sensitive to tension and may link mitotic forces to a cell cycle checkpoint. J Cell Biol *130*, 929-939.

Okazaki, R., Okazaki, T., Sakabe, K., Sugimoto, K., and Sugino, A. (1968). Mechanism of DNA chain growth. I. Possible discontinuity and unusual secondary structure of newly synthesized chains. Proc Natl Acad Sci U S A *59*, 598-605.

Olovnikov, A.M. (1973). A theory of marginotomy. The incomplete copying of template margin in enzymic synthesis of polynucleotides and biological significance of the phenomenon. J Theor Biol *41*, 181-190.

Ortiz, J., Stemmann, O., Rank, S., and Lechner, J. (1999). A putative protein complex consisting of Ctf19, Mcm21, and Okp1 represents a missing link in the budding yeast kinetochore. Genes & development *13*, 1140-1155.

Paciotti, V., Clerici, M., Lucchini, G., and Longhese, M.P. (2000). The checkpoint protein Ddc2, functionally related to S. pombe Rad26, interacts with Mec1 and is regulated by Mec1-dependent phosphorylation in budding yeast. Genes & development *14*, 2046-2059.

Page, B.D., and Snyder, M. (1992). CIK1: a developmentally regulated spindle pole body-associated protein important for microtubule functions in Saccharomyces cerevisiae. Genes & development *6*, 1414-1429.

Papouli, E., Chen, S., Davies, A.A., Huttner, D., Krejci, L., Sung, P., and Ulrich, H.D. (2005). Crosstalk between SUMO and ubiquitin on PCNA is mediated by recruitment of the helicase Srs2p. Molecular cell *19*, 123-133.

Pardo, B., Ma, E., and Marcand, S. (2006). Mismatch tolerance by DNA polymerase Pol4 in the course of nonhomologous end joining in Saccharomyces cerevisiae. Genetics *172*, 2689-2694.

Paulovich, A.G., Toczyski, D.P., and Hartwell, L.H. (1997). When checkpoints fail. Cell *88*, 315-321.

Pellicioli, A., Lucca, C., Liberi, G., Marini, F., Lopes, M., Plevani, P., Romano, A., Di Fiore, P.P., and Foiani, M. (1999). Activation of Rad53 kinase in response to DNA damage and its effect in modulating phosphorylation of the lagging strand DNA polymerase. Embo J *18*, 6561-6572.

Peng, Y., Mian, I.S., and Lue, N.F. (2001). Analysis of telomerase processivity: mechanistic similarity to HIV-1 reverse transcriptase and role in telomere maintenance. Molecular cell *7*, 1201-1211.

Peter, M., Gartner, A., Horecka, J., Ammerer, G., and Herskowitz, I. (1993). *FAR1* links the signal transduction pathway to the cell cycle machinery in yeast. Cell *73*, 747-760.

Petronczki, M., Chwalla, B., Siomos, M.F., Yokobayashi, S., Helmhart, W., Deutschbauer, A.M., Davis, R.W., Watanabe, Y., and Nasmyth, K. (2004). Sister-chromatid cohesion mediated by the alternative RF-CCtf18/Dcc1/Ctf8, the helicase Chl1 and the polymerase-alpha-associated protein Ctf4 is essential for chromatid disjunction during meiosis II. J Cell Sci *117*, 3547-3559.

Pike, B.L., Hammet, A., and Heierhorst, J. (2001). Role of the N-terminal forkhead-associated domain in the cell cycle checkpoint function of the Rad53 kinase. The Journal of biological chemistry *276*, 14019-14026.

Pinsky, B.A., and Biggins, S. (2005). The spindle checkpoint: tension versus attachment. Trends Cell Biol *15*, 486-493.

Poddar, A., Stukenberg, P.T., and Burke, D.J. (2005). Two complexes of spindle checkpoint proteins containing Cdc20 and Mad2 assemble during mitosis independently of the kinetochore in Saccharomyces cerevisiae. Eukaryot Cell *4*, 867-878.

Poli, J., Tsaponina, O., Crabbe, L., Keszthelyi, A., Pantesco, V., Chabes, A., Lengronne, A., and Pasero, P. (2012). dNTP pools determine fork progression and origin usage under replication stress. Embo J *31*, 883-894.

Przewloka, M.R., and Glover, D.M. (2009). The kinetochore and the centromere: a working long distance relationship. Annu Rev Genet *43*, 439-465.

Ranjitkar, P., Press, M.O., Yi, X., Baker, R., MacCoss, M.J., and Biggins, S. (2010). An E3 ubiquitin ligase prevents ectopic localization of the centromeric histone H3 variant via the centromere targeting domain. Molecular cell *40*, 455-464.

Ray, A., and Runge, K.W. (1999). The yeast telomere length counting machinery is sensitive to sequences at the telomere-nontelomere junction. Mol Cell Biol *19*, 31-45.

Reichard, P. (1988). Interactions between deoxyribonucleotide and DNA synthesis. Annual review of biochemistry *57*, 349-374.

Reid, R.J., Gonzalez-Barrera, S., Sunjevaric, I., Alvaro, D., Ciccone, S., Wagner, M., and Rothstein, R. (2011). Selective ploidy ablation, a high-throughput plasmid transfer protocol, identifies new genes affecting topoisomerase I-induced DNA damage. Genome Res *21*, 477-486.

Reid, R.J., Lisby, M., and Rothstein, R. (2002). Cloning-free genome alterations in Saccharomyces cerevisiae using adaptamer-mediated PCR. Methods Enzymol *350*, 258-277.

Resnick, M.A., and Martin, P. (1976). The repair of double-strand breaks in the nuclear DNA of Saccharomyces cerevisiae and its genetic control. Mol Gen Genet *143*, 119-129.

Rieder, C.L., Cole, R.W., Khodjakov, A., and Sluder, G. (1995). The checkpoint delaying anaphase in response to chromosome monoorientation is mediated by an inhibitory signal produced by unattached kinetochores. J Cell Biol *130*, 941-948.

Ritchie, K.B., Mallory, J.C., and Petes, T.D. (1999). Interactions of TLC1 (which encodes the RNA subunit of telomerase), TEL1, and MEC1 in regulating telomere length in the yeast Saccharomyces cerevisiae. Mol Cell Biol *19*, 6065-6075.

Rolef Ben-Shahar, T., Heeger, S., Lehane, C., East, P., Flynn, H., Skehel, M., and Uhlmann, F. (2008). Eco1-dependent cohesin acetylation during establishment of sister chromatid cohesion. Science *321*, 563-566.

Sabouri, N., Viberg, J., Goyal, D.K., Johansson, E., and Chabes, A. (2008). Evidence for lesion bypass by yeast replicative DNA polymerases during DNA damage. Nucleic acids research *36*, 5660-5667.

Salguero, I., Guarino, E., Shepherd, M.E., Deegan, T.D., Havens, C.G., Macneill, S.A., Walter, J.C., and Kearsey, S.E. (2012). Ribonucleotide Reductase Activity Is Coupled to DNA Synthesis via Proliferating Cell Nuclear Antigen. Curr Biol *22*, 720-726.

Sanchez, Y., Desany, B.A., Jones, W.J., Liu, Q., Wang, B., and Elledge, S.J. (1996). Regulation of RAD53 by the ATM-like kinases MEC1 and TEL1 in yeast cell cycle checkpoint pathways. Science *271*, 357-360.

Sandrini, M.P., and Piskur, J. (2005). Deoxyribonucleoside kinases: two enzyme families catalyze the same reaction. Trends Biochem Sci *30*, 225-228.

Schatz, P.J., Pillus, L., Grisafi, P., Solomon, F., and Botstein, D. (1986). Two functional alpha-tubulin genes of the yeast Saccharomyces cerevisiae encode divergent proteins. Mol Cell Biol *6*, 3711-3721.

Schwartz, K., Richards, K., and Botstein, D. (1997). BIM1 encodes a microtubule-binding protein in yeast. Mol Biol Cell *8*, 2677-2691.

Schwartz, M.F., Duong, J.K., Sun, Z., Morrow, J.S., Pradhan, D., and Stern, D.F. (2002). Rad9 phosphorylation sites couple Rad53 to the Saccharomyces cerevisiae DNA damage checkpoint. Molecular cell *9*, 1055-1065.

Sfeir, A.J., Chai, W., Shay, J.W., and Wright, W.E. (2005). Telomere-end processing the terminal nucleotides of human chromosomes. Molecular cell *18*, 131-138.

Shay, J.W., and Bacchetti, S. (1997). A survey of telomerase activity in human cancer. Eur J Cancer *33*, 787-791.

Sherman, F. (1991). Getting started with yeast. Methods Enzymol *194*, 3-21.

Shim, E.Y., Chung, W.H., Nicolette, M.L., Zhang, Y., Davis, M., Zhu, Z., Paull, T.T., Ira, G., and Lee, S.E. (2010). Saccharomyces cerevisiae Mre11/Rad50/Xrs2 and Ku proteins regulate association of Exo1 and Dna2 with DNA breaks. Embo J *29*, 3370-3380.

Sikorski, R.S., and Hieter, P. (1989). A system of shuttle vectors and yeast host strains designed for efficient manipulation of DNA in Saccharomyces cerevisiae. Genetics *122*, 19-27.

Singer, M.S., and Gottschling, D.E. (1994). TLC1: template RNA component of Saccharomyces cerevisiae telomerase. Science *266*, 404-409.

Skibbens, R.V., Corson, L.B., Koshland, D., and Hieter, P. (1999). Ctf7p is essential for sister chromatid cohesion and links mitotic chromosome structure to the DNA replication machinery. Genes & development *13*, 307-319.

Smolka, M.B., Albuquerque, C.P., Chen, S.H., and Zhou, H. (2007). Proteome-wide identification of in vivo targets of DNA damage checkpoint kinases. Proc Natl Acad Sci U S A *104*, 10364-10369.

Spencer, F., Gerring, S.L., Connelly, C., and Hieter, P. (1990). Mitotic chromosome transmission fidelity mutants in Saccharomyces cerevisiae. Genetics *124*, 237-249.

Stark, C., Breitkreutz, B.J., Chatr-Aryamontri, A., Boucher, L., Oughtred, R., Livstone, M.S., Nixon, J., Van Auken, K., Wang, X., Shi, X., *et al*. (2011). The BioGRID Interaction Database: 2011 update. Nucleic acids research *39*, D698-704.

Stoler, S., Rogers, K., Weitze, S., Morey, L., Fitzgerald-Hayes, M., and Baker, R.E. (2007). Scm3, an essential Saccharomyces cerevisiae centromere protein required for G2/M progression and Cse4 localization. Proc Natl Acad Sci U S A *104*, 10571-10576.

Storchova, Z., Becker, J.S., Talarek, N., Kogelsberger, S., and Pellman, D. (2011). Bub1, Sgo1, and Mps1 mediate a distinct pathway for chromosome biorientation in budding yeast. Mol Biol Cell *22*, 1473-1485.

Strathern, J., Hicks, J., and Herskowitz, I. (1981). Control of cell type in yeast by the mating type locus. The alpha 1-alpha 2 hypothesis. J Mol Biol *147*, 357-372.

Sun, Z., Fay, D.S., Marini, F., Foiani, M., and Stern, D.F. (1996). Spk1/Rad53 is regulated by Mec1-dependent protein phosphorylation in DNA replication and damage checkpoint pathways. Genes & development *10*, 395-406.

Sweeney, F.D., Yang, F., Chi, A., Shabanowitz, J., Hunt, D.F., and Durocher, D. (2005). Saccharomyces cerevisiae Rad9 acts as a Mec1 adaptor to allow Rad53 activation. Curr Biol *15*, 1364-1375.

Tanaka, H., Arakawa, H., Yamaguchi, T., Shiraishi, K., Fukuda, S., Matsui, K., Takei, Y., and Nakamura, Y. (2000). A ribonucleotide reductase gene involved in a p53-dependent cell-cycle checkpoint for DNA damage. Nature *404*, 42-49.

Tanaka, T.U., Rachidi, N., Janke, C., Pereira, G., Galova, M., Schiebel, E., Stark, M.J., and Nasmyth, K. (2002). Evidence that the Ipl1-Sli15 (Aurora kinase-INCENP) complex promotes chromosome bi-orientation by altering kinetochore-spindle pole connections. Cell *108*, 317-329.

Tang, H.M., Siu, K.L., Wong, C.M., and Jin, D.Y. (2009). Loss of yeast peroxiredoxin Tsa1p induces genome instability through activation of the DNA damage checkpoint and elevation of dNTP levels. PLoS Genet *5*, e1000697.

Teixeira, M.T., Arneric, M., Sperisen, P., and Lingner, J. (2004). Telomere length homeostasis is achieved via a switch between telomerase- extendible and -nonextendible states. Cell *117*, 323-335.

Torres-Rosell, J., Sunjevaric, I., De Piccoli, G., Sacher, M., Eckert-Boulet, N., Reid, R., Jentsch, S., Rothstein, R., Aragon, L., and Lisby, M. (2007). The Smc5-Smc6 complex and SUMO modification of Rad52 regulates recombinational repair at the ribosomal gene locus. Nat Cell Biol *9*, 923-931.

Toussaint, M., Dionne, I., and Wellinger, R.J. (2005). Limited TTP supply affects telomere length regulation in a telomerase-independent fashion. Nucleic acids research *33*, 704-713.

Traut, T.W. (1994). Physiological concentrations of purines and pyrimidines. Mol Cell Biochem *140*, 1-22.

Tsaponina, O., Barsoum, E., Astrom, S.U., and Chabes, A. (2011). Ixr1 is required for the expression of the ribonucleotide reductase Rnr1 and maintenance of dNTP pools. PLoS Genet *7*, e1002061.

Uchiki, T., Dice, L.T., Hettich, R.L., and Dealwis, C. (2004). Identification of phosphorylation sites on the yeast ribonucleotide reductase inhibitor Sml1. The Journal of biological chemistry *279*, 11293-11303.

Uhlmann, F., Lottspeich, F., and Nasmyth, K. (1999). Sister-chromatid separation at anaphase onset is promoted by cleavage of the cohesin subunit Scc1. Nature *400*, 37-42.

Watson, J.D. (1972). Origin of concatemeric T7 DNA. Nat New Biol *239*, 197-201.

Weiss, E., and Winey, M. (1996). The Saccharomyces cerevisiae spindle pole body duplication gene MPS1 is part of a mitotic checkpoint. J Cell Biol *132*, 111-123.

Werner, J.N., Chen, E.Y., Guberman, J.M., Zippilli, A.R., Irgon, J.J., and Gitai, Z. (2009). Quantitative genome-scale analysis of protein localization in an asymmetric bacterium. Proc Natl Acad Sci U S A *106*, 7858-7863.

Winzeler, E.A., Shoemaker, D.D., Astromoff, A., Liang, H., Anderson, K., Andre, B., Bangham, R., Benito, R., Boeke, J.D., Bussey, H., *et al*. (1999). Functional characterization of the S. cerevisiae genome by gene deletion and parallel analysis. Science *285*, 901-906.

Wu, X., and Huang, M. (2008). Dif1 controls subcellular localization of ribonucleotide reductase by mediating nuclear import of the R2 subunit. Mol Cell Biol *28*, 7156-7167.

Xu, H., Faber, C., Uchiki, T., Fairman, J.W., Racca, J., and Dealwis, C. (2006a). Structures of eukaryotic ribonucleotide reductase I provide insights into dNTP regulation. Proc Natl Acad Sci U S A *103*, 4022-4027.

Xu, H., Faber, C., Uchiki, T., Racca, J., and Dealwis, C. (2006b). Structures of eukaryotic ribonucleotide reductase I define gemcitabine diphosphate binding and subunit assembly. Proc Natl Acad Sci U S A *103*, 4028-4033.

Yao, R., Zhang, Z., An, X., Bucci, B., Perlstein, D.L., Stubbe, J., and Huang, M. (2003). Subcellular localization of yeast ribonucleotide reductase regulated by the DNA replication and damage checkpoint pathways. Proc Natl Acad Sci U S A *100*, 6628-6633.

Yu, G.L., Bradley, J.D., Attardi, L.D., and Blackburn, E.H. (1990). In vivo alteration of telomere sequences and senescence caused by mutated Tetrahymena telomerase RNAs. Nature *344*, 126-132.

Zhang, Z., An, X., Yang, K., Perlstein, D.L., Hicks, L., Kelleher, N., Stubbe, J., and Huang, M. (2006). Nuclear localization of the Saccharomyces cerevisiae ribonucleotide reductase small subunit requires a karyopherin and a WD40 repeat protein. Proc Natl Acad Sci U S A *103*, 1422-1427.

Zhang, Z., and Reese, J.C. (2005). Molecular genetic analysis of the yeast repressor Rfx1/Crt1 reveals a novel two-step regulatory mechanism. Mol Cell Biol *25*, 7399-7411.

Zhang, Z., Yang, K., Chen, C.C., Feser, J., and Huang, M. (2007). Role of the C terminus of the ribonucleotide reductase large subunit in enzyme regeneration and its inhibition by Sml1. Proc Natl Acad Sci U S A *104*, 2217-2222.

Zhao, X., Chabes, A., Domkin, V., Thelander, L., and Rothstein, R. (2001). The ribonucleotide reductase inhibitor Sml1 is a new target of the Mec1/Rad53 kinase cascade during growth and in response to DNA damage. Embo J *20*, 3544-3553.

Zhao, X., Georgieva, B., Chabes, A., Domkin, V., Ippel, J.H., Schleucher, J., Wijmenga, S., Thelander, L., and Rothstein, R. (2000). Mutational and structural analyses of the ribonucleotide reductase inhibitor Sml1 define its Rnr1 interaction domain whose inactivation allows suppression of mec1 and rad53 lethality. Mol Cell Biol *20*, 9076-9083.

Zhao, X., Muller, E.G., and Rothstein, R. (1998). A suppressor of two essential checkpoint genes identifies a novel protein that negatively affects dNTP pools. Molecular cell *2*, 329-340.

Zhao, X., and Rothstein, R. (2002). The Dun1 checkpoint kinase phosphorylates and regulates the ribonucleotide reductase inhibitor Sml1. Proc Natl Acad Sci U S A *99*, 3746-3751.

Zhou, Z., and Elledge, S.J. (1993). DUN1 encodes a protein kinase that controls the DNA damage response in yeast. Cell *75*, 1119-1127.

Zou, L., Liu, D., and Elledge, S.J. (2003). Replication protein A-mediated recruitment and activation of Rad17 complexes. Proc Natl Acad Sci U S A *100*, 13827-13832.

APPENDIX:

The ribonucleotide reductase inhibitor, Sml1, is sequentially phosphorylated, ubiquitylated and degraded in response to DNA damage

I performed the experiments that appear in Figure 5 of the following paper. Furthermore, my contribution allowed us to construct the model shown in Figure 6. I also played a role in writing and editing the final drafts of the paper prior to submission

6490–6501 *Nucleic Acids Research, 2010, Vol. 38, No. 19* *Published online 21 June 2010*
doi:10.1093/nar/gkq552

The ribonucleotide reductase inhibitor, Sml1, is sequentially phosphorylated, ubiquitylated and degraded in response to DNA damage

Bethany L. Andreson[1], Amitabha Gupta[2], Bilyana P. Georgieva[3] and Rodney Rothstein[3,*]

[1]Department of Biological Sciences, Columbia University, New York, NY 10027, [2]Department of Cellular, Molecular and Biophysical Studies and [3]Department of Genetics and Development, Columbia University Medical School, New York, NY 10032, USA

Received May 10, 2010; Revised May 28, 2010; Accepted May 29, 2010

ABSTRACT

Regulation of ribonucleotide reductase (RNR) is important for cell survival and genome integrity in the face of genotoxic stress. The Mec1/Rad53/Dun1 DNA damage response kinase cascade exhibits multifaceted controls over RNR activity including the regulation of the RNR inhibitor, Sml1. After DNA damage, Sml1 is degraded leading to the up-regulation of dNTP pools by RNR. Here, we probe the requirements for Sml1 degradation and identify several sites required for *in vivo* phosphorylation and degradation of Sml1 in response to DNA damage. Further, in a strain containing a mutation in Rnr1, *rnr1-W688G*, mutation of these sites in Sml1 causes lethality. Degradation of Sml1 is dependent on the 26S proteasome. We also show that degradation of phosphorylated Sml1 is dependent on the E2 ubiquitin-conjugating enzyme, Rad6, the E3 ubiquitin ligase, Ubr2, and the E2/E3-interacting protein, Mub1, which form a complex previously only implicated in the ubiquitylation of Rpn4.

INTRODUCTION

DNA damage activates a checkpoint kinase cascade that both halts the cell cycle and concurrently activates factors that repair the damage. One consequence of checkpoint activation is to increase dNTP production, which causes about a 6- to 8-fold increase in dNTP pools after DNA damage treatment (1). Transient up-regulation of dNTP pools leads to increased resistance to DNA-damaging agents, but also increased mutation rates (1). Furthermore, constitutively high dNTP pools inhibit the entry into S phase by delaying replication initiation and also impair activation of the DNA damage checkpoint (2). Therefore, proper dNTP regulation is crucial for cell growth and DNA damage repair.

dNTP production is tightly controlled throughout the cell cycle and in response to DNA damage. This is accomplished through the regulation of ribonucleotide reductase (RNR), the enzyme that performs the rate-limiting step in *de novo* synthesis of dNTPs (3). In most eukaryotes, the RNR enzyme is a heterotetramer, comprised of one large homodimeric R1 subunit and one small homodimeric R2 subunit. In *Saccharomyces cerevisiae*, there are four genes (*RNR1-4*) that encode RNR polypeptides, but only *RNR1, RNR2* and *RNR4* are essential (4–6). The yeast enzyme is comprised of one homodimeric Rnr1 subunit, as well as a heterodimeric Rnr2/Rnr4 subunit. Although protein levels of the second large polypeptide, Rnr3, increase dramatically in response to DNA damage, there is no detectable growth or DNA repair defect for *rnr3Δ* (7). However, Rnr3 is important for cell survival in response to genotoxic stress when the target of rapamycin (TOR) pathway is inhibited by Rapamycin treatment (8).

The regulation of RNR is multifaceted and includes both allosteric regulation (9) and checkpoint-dependent regulation controlled by the Mec1/Rad53/Dun1 kinases. Following damage, Mec1, the ataxia telangiectasia-related (ATR) homolog in yeast, is activated and initiates a kinase cascade that controls many aspects of the DNA damage response including cell-cycle progression, expression of transcriptional targets, replication fork stability and late-replication origin firing (10). Additionally, all of the

*To whom correspondence should be addressed. Tel: +1 212 305 1733; Fax: +1 212 923 2090; Email: rothstein@cancercenter.columbia.edu
Present address:
Bilyana P. Georgieva, Wilmer Cutler Pickering Hale and Dorr LLP, New York, NY 10022, USA.

The authors wish it to be known that, in their opinion, the first three authors should be regarded as joint First Authors.

RNR genes are transcriptionally induced in a Dun1-dependent manner following checkpoint activation, varying from about 3-fold for *RNR1* to more than 100-fold for *RNR3* (4–6,11). The RNR proteins are also regulated by changes in their subcellular localization (12). At all stages of the cell cycle, Rnr1 and Rnr3 are found in the cytoplasm, where dNTP synthesis is thought to occur. In contrast, Rnr2 and Rnr4, the small subunits, are localized to the nucleus during G1 and are co-transported to the cytoplasm during S phase and after DNA damage treatment (13). Wtm1, a WD40-containing protein, is involved in anchoring Rnr2 and Rnr4 to the nucleus in G1 (14,15), while the cytoplasmic protein, Dif1, is required for nuclear import of Rnr2 (16,17). In response to DNA damage, Wtm1 releases the small RNR heterodimeric subunit from the nucleus and Dif1 is degraded, allowing Rnr2 and Rnr4 to remain in the cytoplasm (14–17).

In budding yeast, RNR is also regulated by the protein inhibitor Sml1, which was first identified as a suppressor of the lethality of *mec1* and *rad53* mutations (18). A *sml1Δ* mutation leads to increased levels of all four dNTPs compared to wild type (18) and Sml1 binds to Rnr1 and inhibits RNR activity *in vitro* (19,20). The Sml1 protein is degraded in response to DNA damage and this regulation is dependent on the Mec1, Rad53 and Dun1 checkpoint kinases, mutations of which completely stabilize Sml1 (21). This degradation correlates with the appearance of Dun1-dependent phosphorylated forms of Sml1 (21); however, it was not shown directly whether this phosphorylation is required for the degradation of the protein. Purified Dun1 from yeast directly phosphorylates recombinant Sml1 *in vitro* and Sml1 physically interacts with Dun1 in a two-hybrid assay (22). Additionally, three serines in the Sml1 protein (56, 58 and 60) can be phosphorylated by Dun1 *in vitro* (23). Recently, Sml1 degradation was shown to be a very sensitive indicator of DNA damage checkpoint activation (24) and its degradation occurs even when Rad53 phosphorylation is undetectable (25).

Ubiquitylation, an important post-translational modification, commonly targets proteins for degradation by the 26S proteasome [for review see Refs (26) and (27)]. Protein ubiquitylation is controlled by a sequence of reactions carried out by three types of conjugating enzymes: E1 (ubiquitin-activating enzyme), E2 (ubiquitin-conjugating enzyme) and E3s (ubiquitin-protein ligases) as well as by deubiquitylation enzymes. The E3 enzymes determine specificity for the target protein, and also regulate where the ubiquitin will be added (28).

An E2 that is involved in the DNA damage response, Rad6, associates with several E3 enzymes, including Ubr1, Bre1 and Rad18 (29–31) and is known to ubiquitylate the proliferating cell nuclear antigen (PCNA) and 9-1-1 clamps, among other targets (32,33). Rad6 has also been shown to associate with the E3 Ubr2, which was discovered due to its sequence homology to Ubr1 (34) and was later shown to have a role in the ubiquitylation and degradation of the proteasomal regulator Rpn4 (35). Mub1 is an additional factor required for the ubiquitylation of Rpn4 *in vivo* and *in vitro* (36).

In the present study, site-directed mutagenesis was used to identify the *in vivo* phospho-acceptors important for Sml1 degradation. Changing four serines (56, 58, 60 and 61) to alanines, *sml1-4SA*, prevents the degradation of the protein by blocking its *in vivo* and *in vitro* Dun1 phosphorylation. Endogenous expression of the *sml1-4SA* gene alone does not affect cell growth or DNA damage repair since other forms of RNR regulation are still intact. However, when sml-4SA is overexpressed, it slows S phase progression. Additionally, failure to degrade Sml1 is toxic when Rnr1 function is compromised (*rnr1-W688G*). Sml1 phosphorylation is required for its degradation in response to DNA damage. The degradation of Sml1 following DNA damage treatment also depends on the Rad6–Ubr2–Mub1 E2/E3 ubiquitin complex. Our results suggest a model whereby DNA damage-induced phosphorylation and ubiquitylation of Sml1 occur sequentially triggering degradation of Sml1 by the 26S proteasome.

MATERIALS AND METHODS

Strains and media

The strains used in this study are listed in Supplementary Table S1. Sml1 phosphorylation was detected in strains that have increased levels of Sml1 due to overexpression of *RNR1*, which does not affect the regulation or function of Sml1 (21). In Figure 1D and Supplementary Figure S1, strains were transformed with pWJ841, a 2-μ plasmid that carries *RNR1* (21). All mutations were generated by polymerase chain reaction (PCR). Integrations at the respective chromosomal loci were done by the cloning-free PCR-based allele replacement method (37). The correct integration was verified through sequencing of an amplified segment from the respective genomic region. To distinguish between the different alleles, mutations were engineered to either introduce or delete a restriction site: *sml1-4SA* is detected by loss of an MboII site; *rnr1-W688G* has a new SfcI site. The chromosomal *GAL-SML1* locus described previously (21) was used to make the *GAL-sml1-4SA* strain (W3332-5C). Media and growth conditions used in all experiments are standard (38) with the addition of twice the amount of leucine (60 μg/ml) in all synthetic complete (SC)-based media. Cultures were grown in Yeast extract, peptone, dextrose (YPD), SC or SC-dropout for plasmid selection. YPD or Yeast extract, peptone, galactose (YPGal) contains 1% yeast extract, 2% peptone and 2% glucose or 2% galactose, respectively. YPGly (2% peptone, 1% yeast extract, 3% glycerol and 3% D-lactic acid) or YPRaffinose (1% yeast extract, 2% peptone and 2% raffinose) medium was used in experiments where galactose induction was required. For the experiments in Figures 2 and 4D, cells were grown in YPGly medium, pH 4.5, to facilitate the induction of *GAL-sml1* constructs. To synchronize cells in G1, 3.4 μg/ml α-factor was added for 2.5 h. Galactose (2%) induction was initiated in the last 30 min of this treatment and continued after the cells were released from α-mating factor by rapid filtration into YPGal medium. S-phase progression was monitored by analysis of the DNA content through flow cytometry.

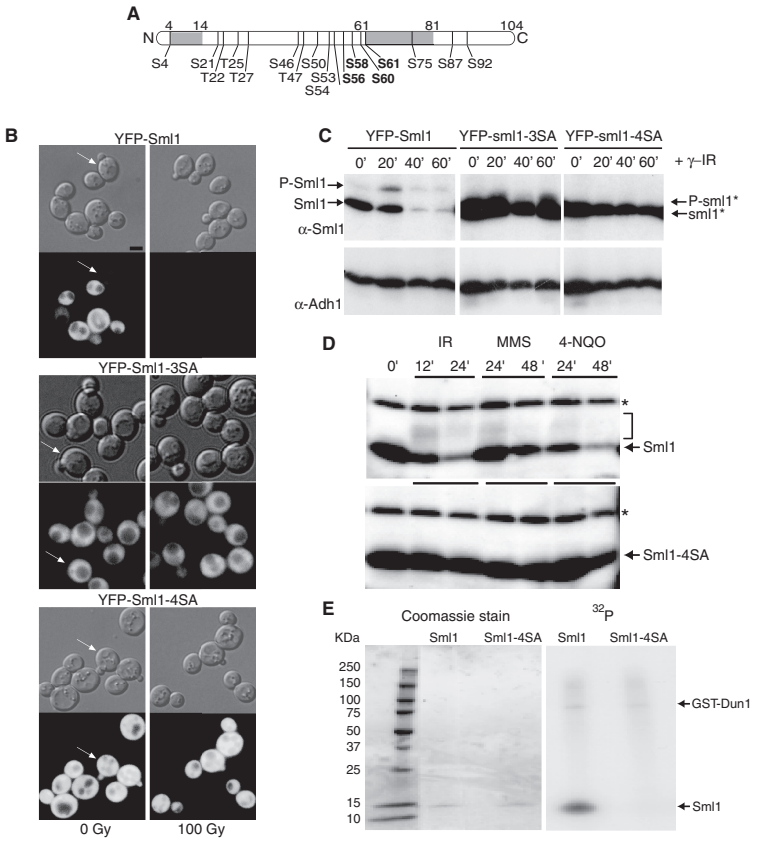

Figure 1. Mutations that eliminate putative phosphorylation sites in Sml1 stabilize the protein after DNA damage treatment and prevent *in vivo* and *in vitro* phosphorylation. (**A**) Depiction of the Sml1 protein with the positions of all serine and threonine residues that are potential phosphorylation sites. The shaded regions indicate the positions of two α helices, including the C-terminal helix, which is important for Sml1 binding to Rnr1. The four serines changed in the *sml1-4SA* mutant are shown in bold type. (**B**) Mid-log phase cultures of cells expressing YFP-Sml1 (W4622-14B), YFP-sml1-3SA (W6976-4A) or YFP-sml1-4SA (W4748-4D) fusion proteins were treated with 100 Gy of γ-irradiation. Protein stability was examined by visualizing YFP fluorescence before and after treatment. White arrows indicate cells that are in S phase (small buds). The scale bar is equal to 3 μm. (**C**) Total yeast extracts of the strains shown in (**B**) were probed with anti-Sml1 antibody to examine stability and *in vivo* phosphorylation, as determined by mobility shift of immunoblot, of the fusion proteins in logarithmically growing cultures. To control for loading, the membrane was stripped and re-probed using anti-Adh1 antibody. (**D**) Total yeast extracts from wild-type (W1588-4C) and *sml1-4SA* (W3329-7D) strains were examined for Sml1 *in vivo* phosphorylation in response to treatment with γ-irradiation (300 Gy), 0.05% MMS and 4-NQO (0.25 mg/l). The arrow indicates the position of Sml1 proteins. The slower migrating bands (indicated by a bracket) are due to phosphorylation (21). Immunoblots were probed with anti-Sml1 serum. The top band, labeled with an asterisk, is a Sml1-independent cross-reacting band used as a loading control. (**E**) Recombinant purified Sml1 and sml1-4SA were incubated with GST-Dun1 fusion protein purified from yeast. A portion of the reaction was resolved on a 4–20% SDS–PAGE gradient gel, stained with Coomassie blue and subsequently visualized by autoradiography for ^{32}P incorporation. Both reactions contained the same amount of recombinant protein (left) and exhibited the same level of kinase activity as observed by GST-Dun1 autophosphorylation (right).

Protein extracts and immunoblots

Several methods of protein extraction were used to detect protein levels. For the experiments in Figures 1C, 5A, C and D; Supplementary Figure S1, extracts were made by the 'boiling method' as described in ref. (21). For the experiment in Figure 3C, protein extracts were prepared by the trichloroacetic acid (TCA) method (39), and for the experiments in Figure 1D, a variation of this experiment using NP-40 extraction buffer (1% NP-40, 150 mM NaCl, 50 mM Tris, pH 8.0) was performed. Immediately before use, this buffer was supplemented with a protease inhibitor cocktail (Roche, as per manufacturer's

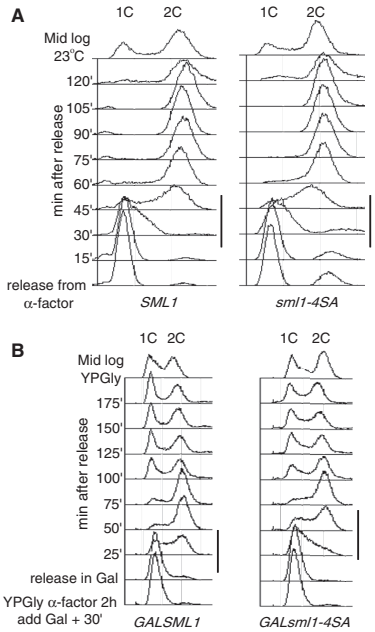

Figure 2. Overexpression of *sml1-4SA*, but not *SML1,* slows S phase progression in wild-type cells. (**A**) Wild-type and sml1-4SA strains were analyzed for cell-cycle progression. There is no significant difference in the duration of S phase between the two strains when the proteins are expressed endogenously (black lines to the right of the panels). (**B**) Overexpression of *sml1-4SA* (W3332-5C), but not *SML1* (W2056-8A), driven by a strong galactose promoter slows S phase progression in wild-type cells. Black lines to the right of the panels indicate S-phase.

instructions), 1 μM pepstatin, 1 mM PMSF, 30 mM NaF and 1 mM DTT. Proteins were separated by SDS–PAGE, transferred to polyvinylidene fluoride membranes and blots were probed with anti-Sml1 serum (21), anti-Rad53 antibody (Santa Cruz) or anti-Adh1 (alcohol dehydrogenase) antibody (Chemicon International, AB1202). Sml1 bands were detected using ECL+ (Amersham).

In vitro kinase assays

The ORFs of *SML1* and *sml1-4SA* were PCR amplified and cloned in the pET3a expression vector (Stratagene) to generate plasmids pWJ1265 and pWJ1266, respectively (primer sequences available on request). Recombinant proteins were expressed in BL21(DE3)pLYS(S) bacteria and purified as described previously (19). Expression of pWJ772, a GST-Dun1 fusion protein (22), was induced for 5 h with 4% galactose in a *pep4Δ* strain exponentially growing in SC-Ura medium with 2% raffinose. Preparation of GST-Dun1 extracts and *in vitro* kinase assays were carried out essentially as described previously (22). A portion of the reaction was resolved on a 4–20% SDS–PAGE gradient gel (Bio-Rad) then stained with Coomassie blue R-250 (Bio-Rad) and subsequently autoradiographed.

DNA damage sensitivity experiments

Exponential cultures were sonicated and plated at the appropriate dilutions on YPD plates with methyl methane sulfonate (MMS) or 4-nitroquinoline 1-oxide (4-NQO), prepared 24 h before the experiment. Cells were grown at 30°C and viable colonies were counted after 4 days. DNA damage sensitivity experiments were repeated at least three times and a minimum of two strains for each genotype were tested.

YFP fusions, construction and fluorescence microscopy

Yellow fluorescent protein (YFP) and cyan fluorescent protein (CFP) fusions of the proteins (Sml1 variants, Rnr1, Rnr2 and Rnr3) were made by the cloning-free PCR-based allele replacement method and are at the corresponding chromosomal loci (40). All fusions are to the N-terminal end of the proteins and are separated by an eight-alanine linker. Cells were processed for differential interference contrast (DIC) and fluorescence microscopy as described previously (41) and fluorescence was quantified using Openlab software (Improvision).

Two-hybrid construction and testing

Sml1 was cloned using primers BamHI_Sml1 and Sml1_PstI. Ubr2 was cloned using SmaI_Ubr2 and Ubr2_PstI. Mub1 was cloned using SmaI_Mub1 and Mub1_PstI. All primer sequences are available upon request. PCR products from the Sml1 PCR were cut with BamHI and PstI as inserted into pGAD-C2 and pGBD-C2 (42). Ubr2 and Mub1 PCR products were digested with SmaI and PstI and inserted into pGAD-C1 and pGBD-C1 (42). All pGAD derived plasmids, including pGAD-C1, were transformed into PJ69-4A and all pGBD-derived plasmids, including pGBD-C1, were transformed into PJ69-4α (42). Strains containing pGBD-Sml1 and pGBD-Ubr2 were not further tested due to autoactivation of the reporters. Strains containing pGBD-C1, and pGBD-Mub1 were mated with strains containing pGAD-C1, pGAD-Sml1 and pGAD-Ubr2. Diploids were grown up overnight in medium lacking LEU and TRP to select for plasmids. Strains were diluted to an optical density (OD_{600}) = 1.0, were serially diluted 5-fold and spotted on to -LEU–TRP, and -LEU–TRP–HIS plates. Plates were scanned after 4 days of growth.

RESULTS

Multiple serine to alanine changes in Sml1 stabilize the protein after DNA damage treatment and prevent *in vivo* and *in vitro* phosphorylation

Previously, we showed that the degradation of Sml1 after DNA damage treatment depends on the *MEC1*/*RAD53*/*DUN1* checkpoint pathway and correlates with the

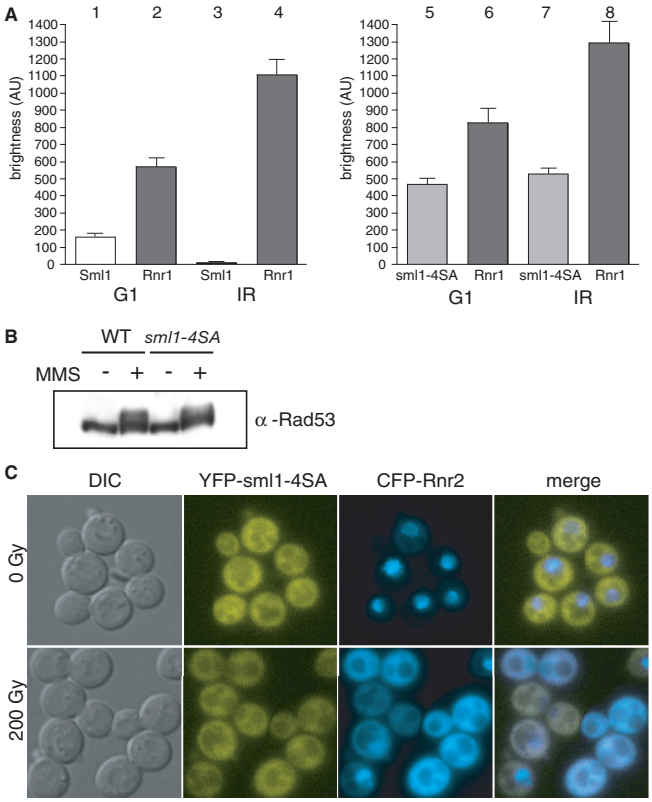

Figure 3. RNR regulation and checkpoint activation are normal in a *sml1-4SA* strain. (**A**) Cells expressing YFP-Sml1 (W5530-6C) or YFP-sml1-4SA (W5755-2A) along with CFP-Rnr1 were visualized by fluorescent microscopy before and an hour after 200 Gy of γ-irradiation. Live cell images were captured identically and YFP levels are depicted on the graphs. Cells without buds are G1 cells and were used for subsequent analyses. (**B**) Protein extracts were taken from wild-type (W1588-4C) and *sml1-4SA* (W3329-7D) cells before and an hour after 0.03% MMS treatment and analyzed by immunoblot using a Rad53 antibody. (**C**) Cells expressing both YFP-sml1-4SA and CFP-Rnr2 proteins (W5766-1D) were visualized by fluorescent microscopy before and an hour after 200 Gy of γ-irradiation. WT, wild-type strain.

phosphorylation of Sml1 (21). In addition, Dun1, a serine/threonine kinase (43), phosphorylates Sml1 *in vitro* (22). Since there are 13 serines and 4 threonines in the 104 amino acids Sml1 protein (Figure 1A), we used site-directed mutagenesis to identify potential phosphorylation sites in Sml1 that would prevent Sml1 degradation following DNA damage treatment. Notably, three serines (56, 58 and 60) were found by Dealwis and colleagues (23) to be phosphorylated by Dun1 *in vitro*. Although mutation of these three serines to alanines, referred to as sml1-3SA, results in a stable protein as determined by fluorescent microscopy (Figure 1B), this protein still undergoes a mobility shift following DNA damage treatment, likely resulting from phosphorylation (Figure 1C). Therefore, Sml1 mutants containing different combinations of serine to alanine changes were examined by fluorescence microscopy and immunoblot for their stability and phosphorylation state following γ-irradiation (data not shown). While many of the mutants are stable, it was necessary to change four serines (56, 58, 60 and 61) to alanines to block any detectable phosphorylation of the protein, indicated by a mobility shift on the gel (Figure 1C). Henceforth, we call this mutant sml1-4SA because four serines were changed to alanines.

Protein levels and localization of Sml1 and sml1-4SA were analyzed by visualizing the fluorescence of YFP-tagged fusion proteins. In unirradiated cells, wild-type Sml1 levels are lower during S phase, while sml1-4SA levels remain unaltered throughout the cell cycle (Figure 1B, arrows). Furthermore, as shown in the right panel of Figure 1B and in Figure 1C, wild-type Sml1 protein is completely degraded within an hour after

γ-irradiation, while the sml1-4SA mutant protein is stable. A similar result was observed on immunoblots of untagged proteins using anti-Sml1 serum (Figure 1D). YFP-Sml1 and YFP-sml1-4SA show the same dispersed cytoplasmic localization. Using anti-GFP antibody as well as fluorescence intensity for quantification, we find that the levels of YFP-sml1-4SA are 2- to 2.5-fold higher compared to the levels of YFP-Sml1 in exponentially growing cultures, indicating that YFP-sml1-4SA is present at higher levels in the cell.

Next, we analyzed the *in vivo* phosphorylation state of untagged sml1-4SA in response to a variety of DNA damaging agents in the presence of *RNR1* overexpression, which facilitates detection of phosphorylated Sml1 on an immunoblot (21). In wild-type cells, DNA damage treatment results in the appearance of phosphorylated species of Sml1 observed as a band or bands with reduced electrophoretic mobility (Figure 1D, top) (21). No such bands are seen in the *sml1-4SA* mutant, demonstrating the absence of any detectable *in vivo* phosphorylation of the sml1-4SA protein (Figure 1D, bottom).

The increased stability and undetectable phosphorylated protein in the *sml1-4SA* strain following DNA damage is reminiscent of Sml1 behavior in a *dun1Δ* mutant. Therefore, we measured the phosphorylation of the sml1-4SA mutant protein by Dun1 *in vitro*. While GST-Dun1 purified from total yeast extracts phosphorylates wild-type Sml1 *in vitro* (22), it does not detectably phosphorylate sml1-4SA mutant protein (Figure 1E). The *in vitro* phosphorylation experiment is consistent with the *in vivo* phosphorylation data suggesting that the mutations in *sml1-4SA* prevent phosphorylation by Dun1.

Since we find no detectable growth defect in a *sml1-4SA* strain (Figure 2A), we investigated the effect of overexpressing the non-degradable sml1-4SA protein on the cell cycle after release from G1 arrest. We confirmed that overexpression of wild-type Sml1 does not affect entry into or progression through the cell cycle (Figure 2B, first panel and ref. (21)). In contrast, overexpression of sml1-4SA delays the start of and extends the progression of S phase (Figure 2B, second panel). At 25 min post-release, most of the cells in the *GAL-SML1* strain have started DNA replication and by 50 min the majority of the DNA is replicated. Comparing the same time points in the GAL-sml1-4SA strain shows that while some DNA replication has initiated at 25 min, the majority is delayed ~25 min and initiation occurs at the 50-min time point.

Taken together, these results show that changing the four serines identified in our analyses to alanines likely abolishes Sml1 phosphorylation by Dun1 both *in vivo* and *in vitro*. Furthermore, the stability of the non-phosphorylatable mutant sml1-4SA indicates that phosphorylation of Sml1 is essential to target the protein for degradation after DNA damage.

Other aspects of dNTP regulation and checkpoint activation are functional in *sml1-4SA*

While there are many facets to RNR regulation, their relationships are not well understood. Therefore, we investigated the induction of Rnr1 as well as the relocalization of the small Rnr2 subunit from the nucleus to the cytoplasm when Sml1 phosphorylation is blocked. Using fluorescently tagged proteins, Sml1 and Rnr1 levels were analyzed before and after γ-irradiation. Both Sml1 and Rnr1 levels fluctuate throughout the cell cycle in unirradiated cells. After irradiation, all of the cells are comparably arrested in G2/M. To eliminate the variability that occurs between different cell-cycle stages in the unirradiated samples, we only measured fluorescence in G1 cells. As previously shown in Figure 1B, YFP-Sml1 disappears after γ-irradiation while YFP-sml1-4SA remains stable (Figure 3A). It was previously reported that Rnr1 protein levels increase about 2-fold following DNA damage treatment (7). We also see a 2-fold increase in endogenously tagged CFP-Rnr1 levels in wild-type cells treated with γ-irradiation (Figure 3A; bars 2 and 4). Similarly, Rnr1 levels increase following DNA damage treatment in *sml1-4SA* cells (Figure 2A; bars 6 and 8). These results suggest that Rnr1 transcriptional regulation is still intact in the *sml1-4SA* strain. Furthermore, in unirradiated G1 cells, Rnr1 levels are increased in the *sml1-4SA* strain compared to wild type (Figure 3A; bars 2 and 6; $P < 0.001$). We suggest that this increase compensates for the higher Sml1 levels in this strain during unperturbed growth and after DNA damage treatment.

In response to DNA damage treatment, Rad53 is phosphorylated (44) and Rnr2 and Rnr4 move from the nucleus to the cytoplasm (12). We examined these upstream and downstream events in both wild-type and *sml1-4SA* cells after γ-irradiation. In contrast to untreated cells, Rad53 is phosphorylated following MMS treatment in both wild-type and *sml1-4SA* cells (Figure 3B). Thus, checkpoint activation appears normal even in the absence of Sml1 degradation. Additionally, when we examine a downstream event, we find that CFP-tagged Rnr2 moves from the nucleus to the cytoplasm in both wild-type and *sml1-4SA* cells after γ-irradiation (data not shown and Figure 3C). This result demonstrates that blocking phosphorylation and degradation of Sml1 does not affect RNR relocalization. Altogether, these experiments indicate that the relative stability of the Sml1 protein does not affect these other aspects of the DNA damage response.

Sml1 protein down-regulation is necessary for survival of mutants compromised in dNTP regulation

Unlike a *dun1Δ* strain, which is also defective in Sml1 degradation, a *sml1-4SA* strain is not sensitive to DNA damaging agents (data not shown). We suspect that the *sml1-4SA* mutant does not show increased DNA damage sensitivity because other aspects of the DNA damage response and of RNR regulation remain functional as shown in Figure 3. To explore this question further, *sml1-4SA* was combined with a mutation that is defective in dNTP regulation: *rnr1-W688G*. We chose the *rnr1-W688G* strain because it is particularly sensitive to Sml1 regulation. This allele was isolated based on its ability to physically interact with *sml1* mutants that do not bind to wild-type Rnr1 (45). Since rnr1-W688G can also interact with wild-type Sml1, the mutation may cause

a stronger interaction between Sml1 and Rnr1. In support to this view, rnr1-W688G causes increased sensitivity to DNA damaging agents, which can be suppressed by deleting *SML1* (Figure 4A). In addition, rnr1-W688G most likely leads to endogenous DNA damage, indicated by the constitutive expression of YFP-Rnr3 in these cells (Figure 4B).

Next, we analyzed the spores from a cross between an *rnr1-W688G* strain and a *sml1-4SA* strain to test the genetic interaction between stabilized Sml1 and this sensitizing mutation. Genetic analysis of this diploid shows that spores of the genotype *rnr1-W688G sml1-4SA* are synthetic lethal (Figure 4C, left). This interaction is identical to that seen when the *rnr1-W688G* allele is combined with *dun1Δ* (Figure 4C, right), which is also defective for Sml1 degradation (22) as well as RNR regulation (12,43). Furthermore, deletion of *SML1* suppresses the synthetic lethality between *rnr1-W688G* and *dun1Δ* (Figure 4C, right). Interestingly, the levels of YFP-Sml1 fluorescent protein in an unperturbed *rnr1-W688G* strain are undetectable (data not shown), also indicating that there is a constitutively active checkpoint in this strain. However, even the low levels of Sml1 in an *rnr1-W688G* strain must account for some dNTP inhibition, as deletion of *SML1* rescues the severe petite phenotype, indicative of low dNTP pools (18) observed in an *rnr1-W688G* strain (data not shown). Taken together, these results show that the degradation of Sml1 becomes essential in the *rnr1-W688G* strain, likely due to the aberrant regulation of this sensitized RNR subunit.

To more closely inspect the effects of expressing Sml1 and sml1-4SA in the *rnr1-W688G* strain, both genes were

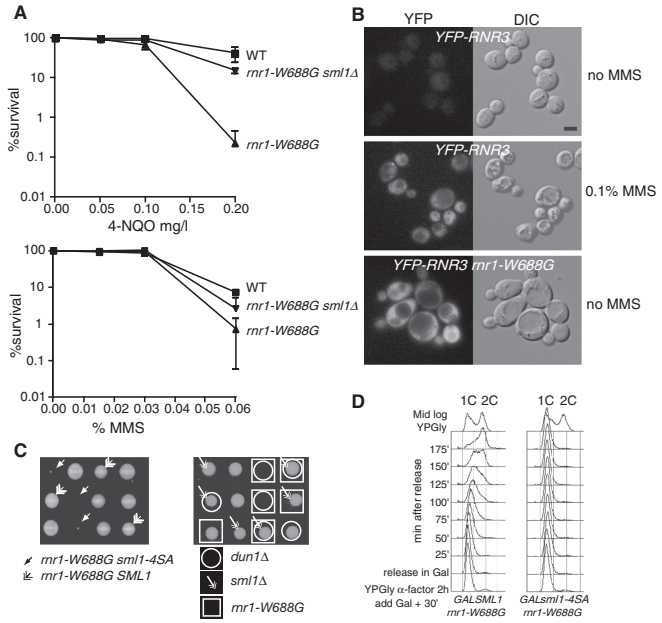

Figure 4. sml1-4SA sensitizes cells that are defective in dNTP regulation. (**A**) *rnr1-W688G* is sensitive to genotoxic stress. The DNA damage sensitivities of the strains [wild type (W1588-4C), *rnr1-W688G* (W4383-1B) and *rnr1-W688G sml1Δ* (W4383-10C)] were examined in a quantitative survival assay used to determine the LD_{50} values after 4-NQO (mg/l) and MMS (%) treatments. Mid-log phase cultures were sonicated and appropriate dilutions were plated on YPD for viability, or on YPD plates containing 4NQO (top) and MMS (bottom) at various concentrations. The reported value is the mean of three experiments and the error bars represent the standard error of the mean. (**B**) *rnr1-W688G* induces Rnr3 expression in the absence of exogenous damage. The activation of the DNA damage checkpoint was monitored through the induction of a YFP-Rnr3 fusion protein (W6986-1B). Rnr3 is induced in response to DNA damage and the induction depends on checkpoint signaling (55). In the absence of DNA damage, YFP-Rnr3 is not expressed in wild-type cells (top). To induce YFP-Rnr3 expression, mid-log phase cells were treated with 0.1% MMS for 5 h (middle). The *rnr1-W688G* mutation causes YFP-Rnr3 to be expressed without any exogenous DNA damage treatment (bottom). (**C**) Dissection of heterozygous diploid *SML1/sml1-4SA rnr1-W688G/RNR1* (W4383) and *SML1/sml1Δ DUN1/dun1Δ RNR1/rnr1-W688G* (W4384) strains shows a genetic interaction between *rnr1-W688G* and the *sml1-4SA* and *dun1Δ* alleles. Deletion of *sml1Δ* suppresses the synthetic lethality between *rnr1-W688G* and *dun1Δ*. The four spores of each tetrad are positioned in the three rows shown. (**D**) Yeast cells (W3755-14D: *GAL-SML1 rnr1-W688G* and W3756-3B: *GAL-sml1-4SA rnr1-W688G*) growing in YPGly at 30°C were synchronized at G1 with α-factor for 2 h. Galactose was added 30 min into the treatment. The pheromone was removed through rapid filtration and cells were released in fresh YPGal without α-factor. At each time point, samples were fixed in 70% ethanol for DNA content analysis by FACS. WT, wild-type strain.

placed under the control of a conditional galactose promoter. Transient overexpression of either Sml1 or sml1-4SA in the *rnr1-W688G* mutant has a dramatic effect on growth. For example, the *rnr1-W688G* strain is sensitive to increased levels of wild-type Sml1 since entry into S phase is significantly delayed (Figure 4D, first panel; Figure 2B). However, these cells do resume the cell cycle and continue to grow. On the other hand, overexpression of sml1-4SA in the *rnr1-W688G* strain completely blocks entry into S phase after release from G1 (Figure 4D, second panel). This result provides an explanation for the lethality of the *rnr1-W688G sml1-4SA* double mutant shown in Figure 4C, namely, it is unable to progress through S phase.

Sml1 degradation is dependent on the 26S proteasome as well as the *RAD6–UBR2–MUB1* ubiquitin ligase complex

Phosphorylation is often a signal for substrates targeted for degradation by the 26S proteasome via ubiquitylation (46,47). To determine whether Sml1 degradation is dependent on the 26S proteasome, Sml1 stability after DNA damage treatment was examined following inactivation of two essential genes of the proteasome (48,49). Figure 5A shows that Sml1 protein degradation is impaired in the temperature-sensitive mutants, *pre1-1* or *pre2-2*, at the restrictive temperature (50).

To determine the ubiquitin ligase(s) responsible for the ubiquitylation of Sml1, we introduced a YFP-Sml1 plasmid into all 36 of the known non-essential E3 ubiquitin ligases (Supplementary Table S2). Sml1 stability was examined by fluorescent microscopy following 100 Gy of γ-irradiation and YFP-Sml1 was only stable in the *ubr2Δ* strain (data not shown). Ubr2 has previously been shown to interact with the Rad6 E2 ubiquitin conjugating enzyme and with Mub1, an E2/E3 interacting protein (35,36). This complex ubiquitylates Rpn4, a transcription factor involved in the biosynthesis of proteasome components (35,36). Therefore, we introduced a YFP-Sml1 plasmid into *rad6Δ* and *mub1Δ* strains and found that YFP-Sml1 is also stable following DNA damage treatment. Notably, stabilization of YFP-Sml1 following 100 Gy of γ-irradiation is not seen in deletions of any of the other six known non-essential E2s (Supplementary Table S2) (data not shown).

To avoid potential problems associated with plasmid-based expression of YFP-Sml1, a genomic copy of YFP-Sml1 was introduced into the *rad6Δ*, *ubr2Δ* and *mub1Δ* genetic backgrounds. In addition, Ubr1 is a known interactor with Rad6 (30) and shows homology with Ubr2 (34). Therefore, we also introduced a genomic copy of YFP-Sml1 into a *ubr1Δ* strain. Fluorescent protein levels were examined in all strains before and after DNA damage treatment. As shown in Figure 5B, YFP-Sml1 is degraded within 40 min following treatment with 100 Gy of γ-irradiation in both wild-type and *ubr1Δ* strains, but is stable in *rad6Δ*, *ubr2Δ*, and *mub1Δ* strains. Furthermore, endogenous levels of Sml1 are higher in the *rad6Δ*, *ubr2Δ*, and *mub1Δ* mutants, even in the absence of DNA damage. Next, YFP-Sml1 protein from these strains was examined by immunoblot following γ-irradiation (Figure 5C). In wild-type cells at 20 min post damage, a slower migrating band appears, which is consistent with phosphorylation of the protein (Figure 1C) and this band is degraded at 45 min post-irradiation. Similar results are also observed in a *ubr1Δ* mutant. Interestingly, in *rad6Δ*, *ubr2Δ* and *mub1Δ* mutants, this slower migrating band is seen even in the absence of DNA damage treatment and accumulates post-DNA damage with no noticeable degradation. Next, the non-phosphorylatable YFP-*sml1-4SA* was introduced into the *rad6Δ*, *ubr2Δ*, *mub1Δ*, *ubr1Δ* mutants and a wild-type strain and immunoblots were performed following DNA damage treatment. As seen in Figure 5D, the slower migrating band observed in Figure 5C is absent, consistent with the notion that this is the phosphorylated form of Sml1. In addition, as expected (Figure 1D), the YFP-sml1-4SA protein is stable following DNA damage treatment in all strains. Finally, untagged Sml1 is more stable in *rad6Δ*, *ubr2Δ* and *mub1Δ* strains following 100 Gy of γ-irradiation compared to wild-type and *ubr1Δ* strains (Supplementary Figure S1).

Mub1 has been implicated in the substrate specificity of the E2/E3 complex during the ubiquitylation of Rpn4 (36). Using a two-hybrid approach, we investigated the interactions between Ubr2, Mub1 and Sml1. Unfortunately, GBD-Sml1 and GBD-Ubr2 show non-specific interactions with an empty GAD construct and could not be tested further (data not shown). On the other hand, GBD-Mub1 shows an interaction with GAD-Ubr2 confirming results found previously (36). Interestingly, GBD-Mub1 also interacts with GAD-Sml1 indicating a direct link between these two proteins (Figure 5E).

DISCUSSION

Sml1, a regulator of RNR, is phosphorylated and degraded in response to DNA damage treatment (22). Although the precise serine residue(s) that is/are phosphorylated is not known, we show that it is necessary to change four serines to alanines in the Sml1 protein to eliminate any detectable phosphorylation *in vivo* (Figure 1C and data not shown). There are numerous examples of phosphorylation at multiple sites to control protein stability. The detailed analysis of Sic1, a cell-cycle regulator and a substrate of the SCF ^{Cdc4} complex, showed that phosphorylation at any six, but not five, of the nine possible phosphorylation sites, targets it for ubiquitylation and degradation (51). In another example, mutation of six phospho-acceptor residues in FANCI is necessary to abolish its phosphorylation, monoubiquitylation, focus formation and DNA repair activity (52). Thus, the number of phosphorylated residues, rather than their position, is often more important for targeting a protein for degradation. Furthermore, the amino acid sequence at the site that we identified in Sml1 contains multiple serines in close proximity (SASASS), making it unlikely that phosphorylation at a particular site is important. Recently, a small cytoplasmic protein, Dif1, was shown to be required for Rnr2 import into the nucleus (16,17). Interestingly, Dif1 shares

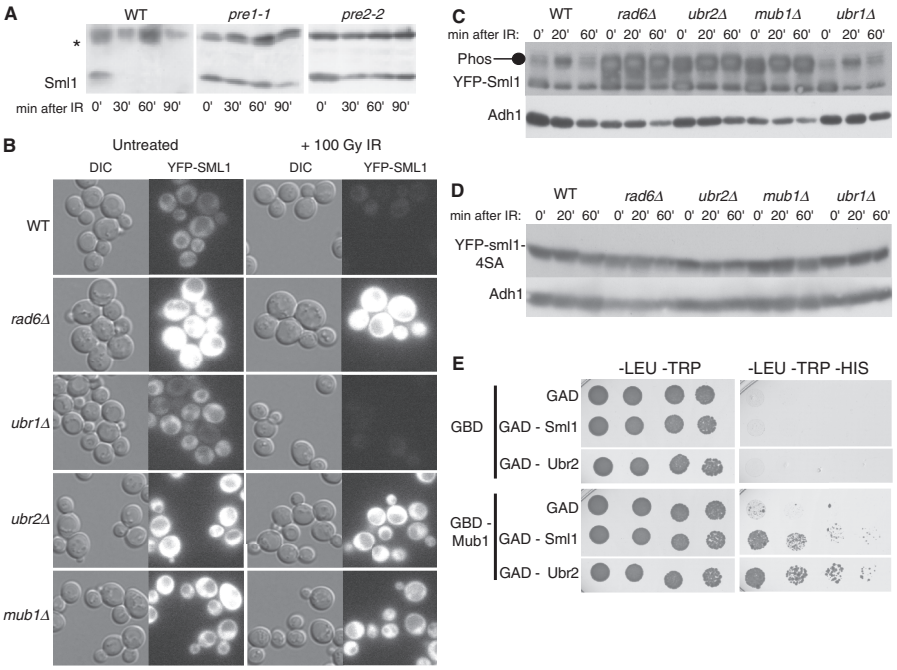

Figure 5. Sml1 is degraded by the 26S proteasome and the degradation is dependent on Rad6, Ubr2 and Mub1. (**A**) Wild-type (MHY686) or mutant cells were shifted to 37°C for 3 h to inactivate the proteasome in the *pre1-1* (MHY687) and *pre2-2* (MHY689) mutants, and treated with 0.03% MMS. Samples were run on a 15% SDS–PAGE gel. Using anti-Sml1 serum, total yeast extracts were examined for Sml1 protein levels at the indicated time points after MMS treatment. In both immunoblots, the top band, labeled with an asterisk, is a Sml1-independent cross-reacting band used as a loading control. (**B**) Mid-log cultures of WT, *rad6*Δ, *ubr1*Δ, *ubr2*Δ and *mub1* strains containing a genomic copy of YFP-Sml1 (W9174-5D, W9174-10C, W9177-8B, W9175-7C and W9176-4D, respectively) were treated with 100 Gy of γ-irradiation. Protein stability was examined by visualizing YFP fluorescence before and after treatment. (**C**) (Top panel) Total yeast extracts from logarithmically growing cultures of the strains shown in (**B**) were immunoblotted and probed with anti-Sml1 antibody to examine stability and *in vivo* phosphorylation. To control for loading, the membrane was stripped and re-probed using anti-Adh1 antibody. (**D**) Total yeast extracts of mid-log cultures of WT, *rad6*Δ, *ubr1*Δ, *ubr2*Δ and *mub1* strains containing a genomic copy of YFP-*sml1-4SA* (W9261-7D, W9261-11B, W9264-11C, W9262-2D and W9263-7B, respectively) were treated with 100 Gy of γ-irradiation, immunoblotted and probed with anti-Sml1 antibody. To control for loading, the membrane was stripped and re-probed using anti-Adh1 antibody. (**E**) Diploids containing different combinations of GBD or GBD-Mub1 with GAD, GAD-Sml1 or GAD-Ubr2 (as indicated) were spotted in 5-fold serial dilutions onto -LEU–TRP and -LEU–TRP–HIS media. The -LEU–TRP medium selects for diploids containing a GBD and GAD plasmids. Growth on medium lacking histidine indicates a two-hybrid interaction and was observed for GBD-Mub1 and GAD-Sml1 as well as GBD-Mub1 and GAD-Ubr2. Plates were scanned after 4 days of growth. WT, wild-type strain.

homology with Sml1 at three of the four serines that are mutated in sml1-4SA (56, 60 and 61). Since Dif1 is also phosphorylated and degraded in a Dun1-dependent manner, perhaps it shares a similar mechanism for degradation with Sml1.

The serine to alanine mutations in sml1-4SA completely block detectable phosphorylation and degradation of the protein. However, the non-degradable protein does not alter cell survival or resistance to DNA damage unless *sml1-4SA* is combined with a mutation that further impairs RNR activity (Figure 3C). Our results confirm that dNTP regulation is robust and there is a discernible biological effect only when multiple components of this regulation are eliminated. For example, a *dun1Δ* strain is DNA damage sensitive, since it affects dNTP regulation not only by preventing Sml1 degradation, but also by affecting induction of the *RNR* genes, as well as the relocalization of the R2 subunit. However, in a *sml1-4SA* strain, only sml1-4SA stability is affected, while other aspects of RNR regulation are normal (Figure 3). In addition, there is a small but significant increase in Rnr1 levels in a *sml1-4SA* strain compared to wild type (Figure 3A, bars 2 and 6; $P < 0.001$). We suggest that cells expressing the non-degradable sml1-4SA compensate for low dNTP pools by increasing *RNR1* transcription.

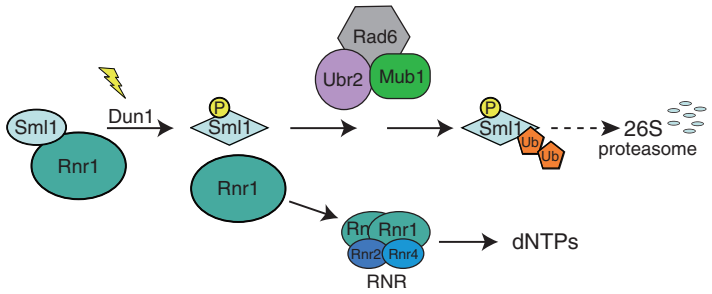

Figure 6. A model for Sml1 regulation in response to DNA damage. Prior to modification, Sml1 is bound to Rnr1 and inhibits RNR activity. Following DNA damage, Dun1 is activated and phosphorylates Sml1 on serines 56, 58, 60 and/or 61. Phosphorylation promotes ubiquitylation of Sml1 by the Rad6–Ubr2–Mub1 complex, targeting Sml1 for degradation by the 26S proteasome. The released Rnr1 associates with Rnr2 and Rnr4 to form an active RNR enzyme allowing the production of dNTPs.

We show that the Sml1 protein is degraded via the 26S proteasome (Figure 5A). Screening the 36 known non-essential E3 enzymes, we found that Ubr2 is required for Sml1 degradation (Figure 5B). Ubr2 ubiquitylates the transcription factor, Rpn4, in concert with the Rad6 E2 ligase and the Mub1 proteins (35,36), and both of these proteins are also important for Sml1 degradation (Figure 5). Since Rpn4 is involved in the regulation of proteasomal genes (53), its stability in *ubr2Δ*, *rad6Δ* and/or *mub1Δ* mutants could potentially lead to an increase in proteasomes. Up-regulation of proteasomal subunits due to increased Rpn4 levels would in fact destabilize Sml1, making it unlikely that these mutants are having an indirect effect on Sml1 stability. Furthermore, the two-hybrid experiment demonstrates a direct interaction between Mub1 and Sml1 (Figure 5D). Therefore, Ubr2, Rad6 and Mub1 likely ubiquitylate Sml1 directly, leading to its degradation in response to DNA damage. This E2/E3 complex may also be involved in the turnover of Sml1 protein during S phase, since increased levels of phosphorylated Sml are observed in *ubr2Δ*, *rad6Δ* and *mub1Δ* strains even without DNA damage treatment (Figure 5C).

Although Rad6, in conjunction with several E3 ubiquitin ligases, has many targets in the DNA damage pathway including PCNA and members of the 9-1-1 complex (29–33), this is the first interaction, to our knowledge, that also requires the Ubr2/Mub1 proteins. Sml1 protein localizes to the cytoplasm where it is bound to Rnr1 (Figure 1B and (12)). Ubr2 is also found in the cytoplasm (54), perhaps facilitating Sml1 ubiquitylation. It will be important to determine whether the Rad6–Ubr2–Mub1 complex ubiquitylates other DNA damage-regulated proteins. Of particular interest is Dif1, another cytoplasmically localized protein, which shares homology with Sml1 and is involved in dNTP regulation (16,17).

Taken together, our results can be summarized in a model describing Sml1 modifications that target the protein for degradation in response to DNA damage (Figure 6). In this model, before DNA damage, Sml1 is bound to Rnr1, inhibiting RNR activity. Following DNA damage, the Mec1/Rad53/Dun1 kinase cascade is activated and phosphorylates Sml1. This phosphorylation triggers a conformational change in Sml1 leading to its dissociation from Rnr1. Phosphorylated Sml1 is recognized by the Rad6–Ubr2–Mub1 E2/E3 ligase complex, which ubiquitylates Sml1 targeting it for degradation by the 26S proteasome. In the end, loss of Rnr1 inhibition after Sml1 degradation allows the formation of an active RNR enzyme leading to an increase in the production of dNTPs to facilitate DNA damage repair.

SUPPLEMENTARY DATA

Supplementary Data are available at NAR Online.

ACKNOWLEDGEMENTS

We are grateful to Kara Bernstein, Rebecca Burgess, Michael Lisby, Peter Thorpe and Xiaolan Zhao for thoughtful comments on the manuscript. We also thank Mark Hochstrasser for strains.

FUNDING

Funding for open access charge: National Institutes of Health (GM50237).

Conflict of interest statement. None declared.

REFERENCES

1. Chabes,A., Georgieva,B., Domkin,V., Zhao,X., Rothstein,R. and Thelander,L. (2003) Survival of DNA damage in yeast directly depends on increased dNTP levels allowed by relaxed feedback inhibition of ribonucleotide reductase. *Cell*, **112**, 391–401.
2. Chabes,A. and Stillman,B. (2007) Constitutively high dNTP concentration inhibits cell cycle progression and the DNA damage checkpoint in yeast Saccharomyces cerevisiae. *Proc. Natl Acad. Sci. USA*, **104**, 1183–1188.
3. Reichard,P. (1988) Interactions between deoxyribonucleotide and DNA synthesis. *Annu. Rev. Biochem.*, **57**, 349–374.
4. Elledge,S.J. and Davis,R.W. (1990) Two genes differentially regulated in the cell cycle and by DNA-damaging agents encode

alternative regulatory subunits of ribonucleotide reductase. *Genes Dev.*, **4**, 740–751.
5. Elledge,S.J. and Davis,R.W. (1987) Identification and isolation of the gene encoding the small subunit of ribonucleotide reductase from Saccharomyces cerevisiae: DNA damage-inducible gene required for mitotic viability. *Mol. Cell. Biol.*, **7**, 2783–2793.
6. Huang,M. and Elledge,S.J. (1997) Identification of RNR4, encoding a second essential small subunit of ribonucleotide reductase in Saccharomyces cerevisiae. *Mol. Cell. Biol.*, **17**, 6105–6113.
7. Domkin,V., Thelander,L. and Chabes,A. (2002) Yeast DNA damage-inducible Rnr3 has a very low catalytic activity strongly stimulated after the formation of a cross-talking Rnr1/Rnr3 complex. *J. Biol. Chem.*, **277**, 18574–18578.
8. Shen,C., Lancaster,C.S., Shi,B., Guo,H., Thimmaiah,P. and Bjornsti,M.A. (2007) TOR signaling is a determinant of cell survival in response to DNA damage. *Mol. Cell. Biol.*, **27**, 7007–7017.
9. Thelander,L. and Reichard,P. (1979) Reduction of ribonucleotides. *Annu. Rev. Biochem.*, **48**, 133–158.
10. Nyberg,K.A., Michelson,R.J., Putnam,C.W. and Weinert,T.A. (2002) Toward maintaining the genome: DNA damage and replication checkpoints. *Annu. Rev. Genet.*, **36**, 617–656.
11. Wang,P.J., Chabes,A., Casagrande,R., Tian,X.C., Thelander,L. and Huffaker,T.C. (1997) Rnr4p, a novel ribonucleotide reductase small-subunit protein. *Mol. Cell. Biol.*, **17**, 6114–6121.
12. Yao,R., Zhang,Z., An,X., Bucci,B., Perlstein,D.L., Stubbe,J. and Huang,M. (2003) Subcellular localization of yeast ribonucleotide reductase regulated by the DNA replication and damage checkpoint pathways. *Proc. Natl Acad. Sci. USA*, **100**, 6628–6633.
13. An,X., Zhang,Z., Yang,K. and Huang,M. (2006) Cotransport of the heterodimeric small subunit of the Saccharomyces cerevisiae ribonucleotide reductase between the nucleus and the cytoplasm. *Genetics*, **173**, 63–73.
14. Lee,Y.D. and Elledge,S.J. (2006) Control of ribonucleotide reductase localization through an anchoring mechanism involving Wtm1. *Genes Dev.*, **20**, 334–344.
15. Zhang,Z., An,X., Yang,K., Perlstein,D.L., Hicks,L., Kelleher,N., Stubbe,J. and Huang,M. (2006) Nuclear localization of the Saccharomyces cerevisiae ribonucleotide reductase small subunit requires a karyopherin and a WD40 repeat protein. *Proc. Natl Acad. Sci. USA*, **103**, 1422–1427.
16. Lee,Y.D., Wang,J., Stubbe,J. and Elledge,S.J. (2008) Dif1 is a DNA-damage-regulated facilitator of nuclear import for ribonucleotide reductase. *Mol. Cell*, **32**, 70–80.
17. Wu,X. and Huang,M. (2008) Dif1 controls subcellular localization of ribonucleotide reductase by mediating nuclear import of the R2 subunit. *Mol. Cell. Biol.*, **28**, 7156–7167.
18. Zhao,X., Muller,E.G. and Rothstein,R. (1998) A suppressor of two essential checkpoint genes identifies a novel protein that negatively affects dNTP pools. *Mol. Cell*, **2**, 329–340.
19. Chabes,A., Domkin,V. and Thelander,L. (1999) Yeast Sml1, a protein inhibitor of ribonucleotide reductase. *J. Biol. Chem.*, **274**, 36679–36683.
20. Zhao,X., Georgieva,B., Chabes,A., Domkin,V., Ippel,J.H., Schleucher,J., Wijmenga,S., Thelander,L. and Rothstein,R. (2000) Mutational and structural analyses of the ribonucleotide reductase inhibitor Sml1 define its Rnr1 interaction domain whose inactivation allows suppression of mec1 and rad53 lethality. *Mol. Cell. Biol.*, **20**, 9076–9083.
21. Zhao,X., Chabes,A., Domkin,V., Thelander,L. and Rothstein,R. (2001) The ribonucleotide reductase inhibitor Sml1 is a new target of the Mec1/Rad53 kinase cascade during growth and in response to DNA damage. *EMBO J.*, **20**, 3544–3553.
22. Zhao,X. and Rothstein,R. (2002) The Dun1 checkpoint kinase phosphorylates and regulates the ribonucleotide reductase inhibitor Sml1. *Proc. Natl Acad. Sci. USA*, **99**, 3746–3751.
23. Uchiki,T., Dice,L.T., Hettich,R.L. and Dealwis,C. (2004) Identification of phosphorylation sites on the yeast ribonucleotide reductase inhibitor Sml1. *J. Biol. Chem.*, **279**, 11293–11303.
24. Torres-Rosell,J., Sunjevaric,I., De Piccoli,G., Sacher,M., Eckert-Boulet,N., Reid,R., Jentsch,S., Rothstein,R., Aragon,L. and Lisby,M. (2007) The Smc5-Smc6 complex and SUMO modification of Rad52 regulates recombinational repair at the ribosomal gene locus. *Nat. Cell Biol.*, **9**, 923–931.
25. Barlow,J.H., Lisby,M. and Rothstein,R. (2008) Differential regulation of the cellular response to DNA double-strand breaks in G1. *Mol. Cell*, **30**, 73–85.
26. Hofmann,K. (2009) Ubiquitin-binding domains and their role in the DNA damage response. *DNA Repair*, **8**, 544–556.
27. Xu,P. and Peng,J. (2006) Dissecting the ubiquitin pathway by mass spectrometry. *Biochim. Biophys. Acta*, **1764**, 1940–1947.
28. Pickart,C.M. and Eddins,M.J. (2004) Ubiquitin: structures, functions, mechanisms. *Biochim. Biophys. Acta*, **1695**, 55–72.
29. Bailly,V., Lamb,J., Sung,P., Prakash,S. and Prakash,L. (1994) Specific complex formation between yeast RAD6 and RAD18 proteins: a potential mechanism for targeting RAD6 ubiquitin-conjugating activity to DNA damage sites. *Genes Dev.*, **8**, 811–820.
30. Dohmen,R.J., Madura,K., Bartel,B. and Varshavsky,A. (1991) The N-end rule is mediated by the UBC2(RAD6) ubiquitin-conjugating enzyme. *Proc. Natl Acad. Sci. USA*, **88**, 7351–7355.
31. Wood,A., Krogan,N.J., Dover,J., Schneider,J., Heidt,J., Boateng,M.A., Dean,K., Golshani,A., Zhang,Y., Greenblatt,J.F. *et al.* (2003) Bre1, an E3 ubiquitin ligase required for recruitment and substrate selection of Rad6 at a promoter. *Mol. Cell*, **11**, 267–274.
32. Hoege,C., Pfander,B., Moldovan,G.L., Pyrowolakis,G. and Jentsch,S. (2002) RAD6-dependent DNA repair is linked to modification of PCNA by ubiquitin and SUMO. *Nature*, **419**, 135–141.
33. Fu,Y., Zhu,Y., Zhang,K., Yeung,M., Durocher,D. and Xiao,W. (2008) Rad6-Rad18 mediates a eukaryotic SOS response by ubiquitinating the 9-1-1 checkpoint clamp. *Cell*, **133**, 601–611.
34. Hochstrasser,M. (1996) Ubiquitin-dependent protein degradation. *Annu. Rev. Genet.*, **30**, 405–439.
35. Wang,L., Mao,X., Ju,D. and Xie,Y. (2004) Rpn4 is a physiological substrate of the Ubr2 ubiquitin ligase. *J. Biol. Chem.*, **279**, 55218–55223.
36. Ju,D., Wang,X., Xu,H. and Xie,Y. (2008) Genome-wide analysis identifies MYND-domain protein Mub1 as an essential factor for Rpn4 ubiquitylation. *Mol. Cell. Biol.*, **28**, 1404–1412.
37. Erdeniz,N., Mortensen,U.H. and Rothstein,R. (1997) Cloning-free PCR-based allele replacement methods. *Genome Res.*, **7**, 1174–1183.
38. Adams,A., Gottschling,D., Kaiser,C. and Stearns,T. (1997) *Methods in Yeast Genetics*. Cold Spring Harbor Press, Cold Spring Harbor, NY.
39. Sambrook,J., Fritsch,E.F. and Maniatis,T. (1989) *Molecular Cloning: A Laboratory Manual*, 2nd edn. Cold Spring Harbor Laboratory Press, Cold Spring Harbor, NY.
40. Reid,R.J.D., Lisby,M. and Rothstein,R. (2002) Cloning-free genome alterations in Saccharomyces cerevisiae using adaptamer-mediated PCR. *Meth. Enzymol.*, **350**, 258–277.
41. Lisby,M., Rothstein,R. and Mortensen,U.H. (2001) Rad52 forms DNA repair and recombination centers during S phase. *Proc. Natl Acad. Sci. USA*, **98**, 8276–8282.
42. James,P., Halladay,J. and Craig,E.A. (1996) Genomic libraries and a host strain designed for highly efficient two-hybrid selection in yeast. *Genetics*, **144**, 1425–1436.
43. Zhou,Z. and Elledge,S.J. (1993) DUN1 encodes a protein kinase that controls the DNA damage response in yeast. *Cell*, **75**, 1119–1127.
44. Pellicioli,A., Lucca,C., Liberi,G., Marini,F., Lopes,M., Plevani,P., Romano,A., Di Fiore,P.P. and Foiani,M. (1999) Activation of Rad53 kinase in response to DNA damage and its effect in modulating phosphorylation of the lagging strand DNA polymerase. *EMBO J.*, **18**, 6561–6572.
45. Georgieva,B., Zhao,X. and Rothstein,R. (2000) Damage response and dNTP regulation: the interaction between ribonucleotide reductase and its inhibitor, Sml1. *Cold Spring Harb. Symp. Quant. Biol.*, **65**, 343–346.
46. Ciechanover,A., Finley,D. and Varshavsky,A. (1984) The ubiquitin-mediated proteolytic pathway and mechanisms of

energy-dependent intracellular protein degradation. *J. Cell. Biochem.*, **24**, 27–53.
47. Hershko,A. and Ciechanover,A. (1998) The ubiquitin system. *Annu. Rev. Biochem.*, **67**, 425–479.
48. Heinemeyer,W., Simeon,A., Hirsch,H.H., Schiffer,H.H., Teichert,U. and Wolf,D.H. (1991) Lysosomal and non-lysosomal proteolysis in the eukaryotic cell: studies on yeast. *Biochem. Soc. Trans.*, **19**, 724–725.
49. Heinemeyer,W., Gruhler,A., Mohrle,V., Mahe,Y. and Wolf,D.H. (1993) PRE2, highly homologous to the human major histocompatibility complex-linked RING10 gene, codes for a yeast proteasome subunit necessary for chrymotryptic activity and degradation of ubiquitinated proteins. *J. Biol. Chem.*, **268**, 5115–5120.
50. Richter-Ruoff,B., Wolf,D.H. and Hochstrasser,M. (1994) Degradation of the yeast MAT alpha 2 transcriptional regulator is mediated by the proteasome. *FEBS Lett.*, **354**, 50–52.
51. Nash,P., Tang,X., Orlicky,S., Chen,Q., Gertler,F.B., Mendenhall,M.D., Sicheri,F., Pawson,T. and Tyers,M. (2001) Multisite phosphorylation of a CDK inhibitor sets a threshold for the onset of DNA replication. *Nature*, **414**, 514–521.
52. Ishiai,M., Kitao,H., Smogorzewska,A., Tomida,J., Kinomura,A., Uchida,E., Saberi,A., Kinoshita,E., Kinoshita-Kikuta,E., Koike,T. *et al.* (2008) FANCI phosphorylation functions as a molecular switch to turn on the Fanconi anemia pathway. *Nat. Struct. Mol. Biol.*, **15**, 1138–1146.
53. Mannhaupt,G., Schnall,R., Karpov,V., Vetter,I. and Feldmann,H. (1999) Rpn4p acts as a transcription factor by binding to PACE, a nonamer box found upstream of 26S proteasomal and other genes in yeast. *FEBS Lett.*, **450**, 27–34.
54. Huh,W.K., Falvo,J.V., Gerke,L.C., Carroll,A.S., Howson,R.W., Weissman,J.S. and O'Shea,E.K. (2003) Global analysis of protein localization in budding yeast. *Nature*, **425**, 686–691.
55. Allen,J.B., Zhou,Z., Siede,W., Friedberg,E.C. and Elledge,S.J. (1994) The SAD1/RAD53 protein kinase controls multiple checkpoints and DNA damage-induced transcription in yeast. *Genes Dev.*, **8**, 2401–2415.